Technical challenges with the development of small scale LNG terminals and fuelling stations

Rossios Konstantinos

SID: 3302130003

SCHOOL OF SCIENCE & TECHNOLOGY

A thesis submitted for the degree of

Master of Science (MSc) in Energy Systems

NOVEMBER 2014

THESSALONIKI – GREECE

Abstract

This dissertation was written as a part of the MSc in Energy Systems at the International Hellenic University. The completion of this thesis was co-funded by the Act "SSF (State Scholarships Foundation) scholarships Program for first cycle postgraduate studies (Master)" - Horizontal Act, from funds of the OP "Education and Lifelong Learning", of the European Social Fund (ESF) under the NSRF 2007-2013.

During the past few years we have witnessed a huge increase in interest for delivering Liquefied Natural Gas (LNG) directly to the customer. It is expected this trend to continue taking into account European Union's policy on alternative fuel infrastructure. As a consequence, the subject of this work is small scale LNG chain with a special focus on road transport and semi-trailer trucks.

Challenges related to the development of small scale LNG infrastructure could be technical and non-technical. The former are under our sphere of interest and especially the formation of the so called "boil-off gas" inside the LNG trailer truck. The commercial CFD software ANSYS FLUENT is used to simulate the development of the LNG evaporation inside the truck.

The successful integration of this work is facilitated by some people who helped me overcome the emerged difficulties. First of all, I would like to thank SSF for the economic support at such difficult times. In addition, I am also very grateful to my supervisor A. Sardi for her valuable guidance throughout the entire time of this work and for her advices concerning the use of FLUENT.

Rossios Konstantinos

22/11/2014

Contents

1 Introduction

The importance of LNG infrastructure emerging from European Union policy is discussed in this chapter. Afterwards, LNG properties are presented and there is a description of large and small scale LNG chain. Next, a comparison among available insulation technologies and semi-trailer trucks is introduced. Finally, previous related works are displayed at the end of this chapter.

1.1 EU Clean Fuel Strategy

The Trans-European network policy aims to implement the transport infrastructure and interconnections that underpin the Single European Market, to secure the free-flow of goods and people and to support growth, jobs and EU competitiveness. The result of this policy is the unified trans-European transport network (TEN-T), which connects east to west and comprises nine major corridors[1].

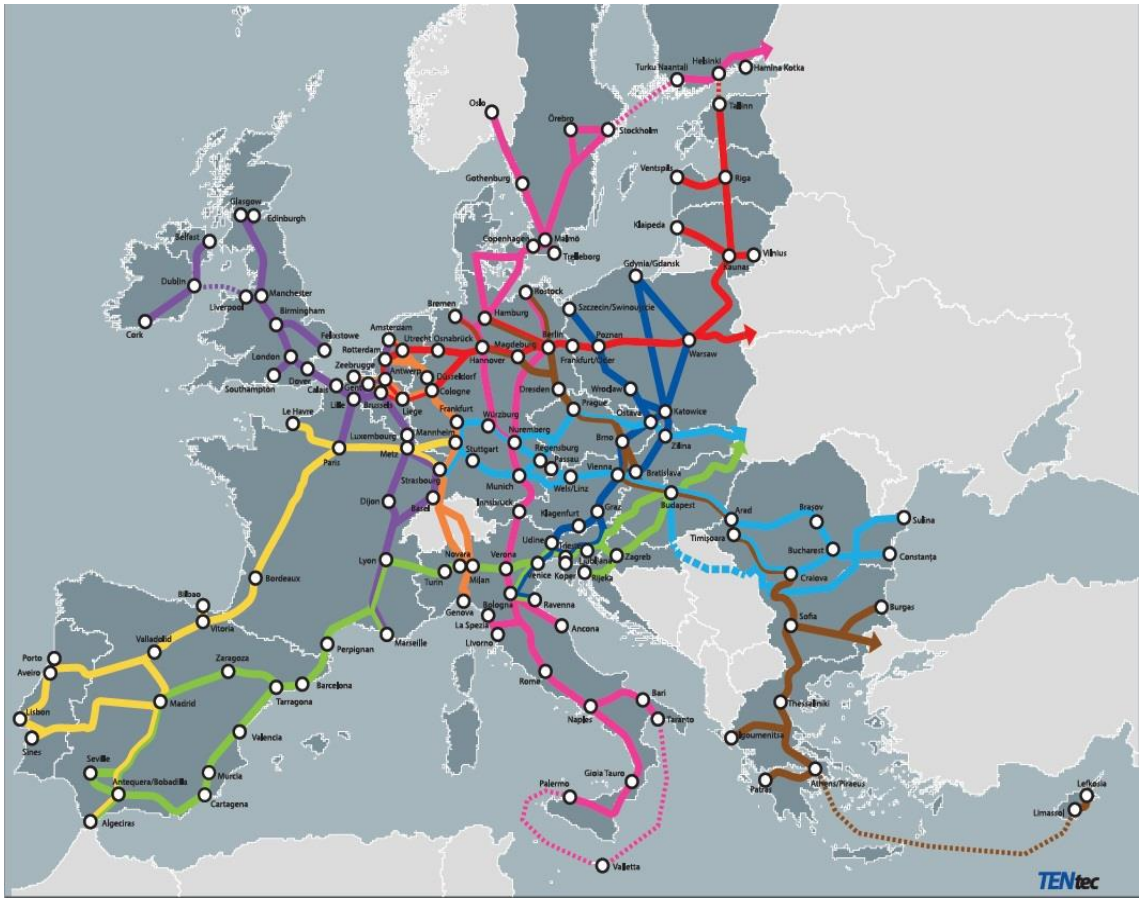

1.1 Trans-European transport network (roads, rail, ports)

According to the European Commission's proposal for a Directive on the deployment of alternative fuel infrastructure, the main goal of the proposal is to facilitate the development of alternative fuel infrastructure and the implementation of common technical specifications for this infrastructure in the Union. The main alternative fuels include electricity, hydrogen, biofuels, natural gas (in the forms of Compressed Natural Gas (CNG), Liquefied Natural Gas (LNG), or Gas-To-Liquid (GTL)) , and Liquefied Petroleum Gas (LPG).

Under the regime of Article 6 of the above proposal, all Member States are responsible for the existence of publicly accessible LNG refueling points for maritime and inland waterway transport in all maritime ports of the Trans-European Transport (TEN-T) Core Network by 31 December 2020 at the latest. In addition, Member States shall cooperate to ensure that heavy duty motor vehicles running on LNG can travel all along the roads on the TEN-T Core Network. For this purposes, publicly accessible refueling points for LNG shall be established *within distances not exceeding 400 km* (distances of 150km for CNG vehicles) by 31 December 2020 at the latest. Moreover, all LNG refueling points for maritime, inland waterway transport and motor vehicle should conform to the corresponding technical specifications under the European Norm (EN) schemes by 31 December 2015 at the latest[2].

Taking into consideration the above proposal of the European Commission, it is clear that natural gas is expected to play a vital role to transport in the upcoming years due to its long-term prospective in terms of security of supply and its environmental benefits. In addition, natural gas in liquefied form (LNG) with high energy density offers a cost-efficient alternative to diesel for waterborne activities (transport, offshore services, and fisheries), trucks and rail, with lower pollutant and CO2 emissions and higher energy efficiency. LNG is particularly suited for long-distance road freight transport for which alternatives to diesel are extremely limited. Trucks burning LNG might be able to meet the more stringent pollutant emission limits of future EURO VI standards cost-efficiently. LNG is also an attractive fuel option for vessels in particular to meet the new limits for sulfur content in marine fuels. As a consequence, the development of appropriate infrastructure is considered as a necessity.

1.2 LNG properties

Liquefied Natural gas is an odorless, colorless, noncorrosive and non-toxic cryogenic liquid, lighter than water, at normal atmospheric pressure. LNG is a liquid form of Natural Gas. The changes of phase from gas to liquid at boiling temperature of -163^0C will reduce the volume to about 600th times make it suitable to be transported in liquid phase. It is a mixture of light hydrocarbons primarily composed of methane (CH4, 85-98% by volume), with smaller quantities of ethane (C2H6), propane (C3H8), higher hydrocarbons (C4+) and nitrogen as an inert component. The composition of LNG depends on the reservoir source of the natural gas source and the treatment of gas at the liquefaction facility, i.e. the liquefaction pre-treatment and the liquefaction process. It can also vary with storage conditions and customer requirements.

LNG can be characterized according to its density, its methane or nitrogen composition, its heating heat value etc. The most commonly used parameter is its density. Accordingly, we differentiate between light, medium and heavy LNG. The table below presents the typical composition and the density of the three LNG classifications. Typical LNG thermo-physical properties are presented in Table 1.2. Figure 1.2 presents the LNG phase diagram and figure 1.3 presents the phase envelope for the nitrogen, methane, ethane, propane and n-butane system (where blue line stands for experimental results and the other two for calculated results with different methods)[3][4].

Composition(%)	LNG Light	LNG Medium	LNG Heavy
Methane	98	92	87
Propane	1.4	6	9.5
Butane	0.1	0	0.5
Nintogen	0.1	1	0.5
Density (kg/m^3)	427.74	445.69	464.83

Table 1.1 LNG classifications

Parameter	Value
Boiling Point	-160 ^{0}C to -162 ^{0}C
Molecular weight	16-19 g/mol
Density	425-482 kg/m^3
Specific heat capacity	2,2-3,7 kJ/kg/C
Viscosity	0,11-0,18 mPa · s
Higher heat value	38-44 MJ/m^3
Heat of vaporization	51,03 · 10^5 J/kg
Heat of Fusion	58,62 · 10^3 J/kg
Vapor density	1,826 kg/m^3

Table 1.2 LNG properties

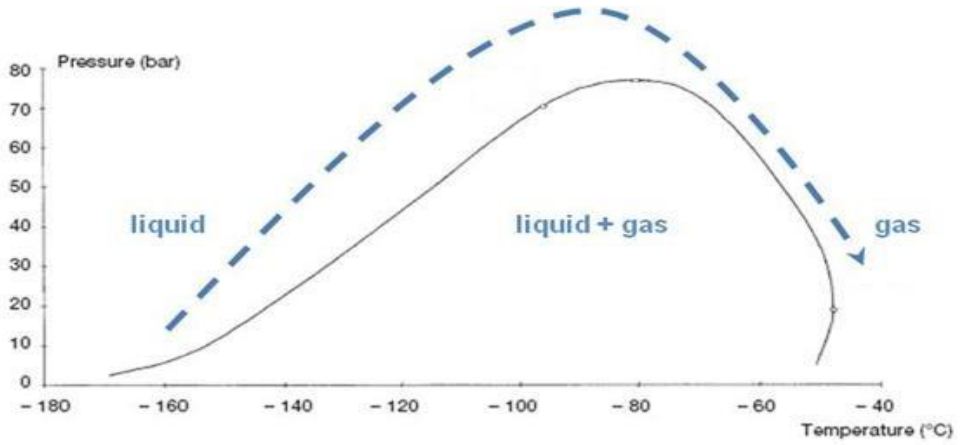

1.2 LNG phase envelope

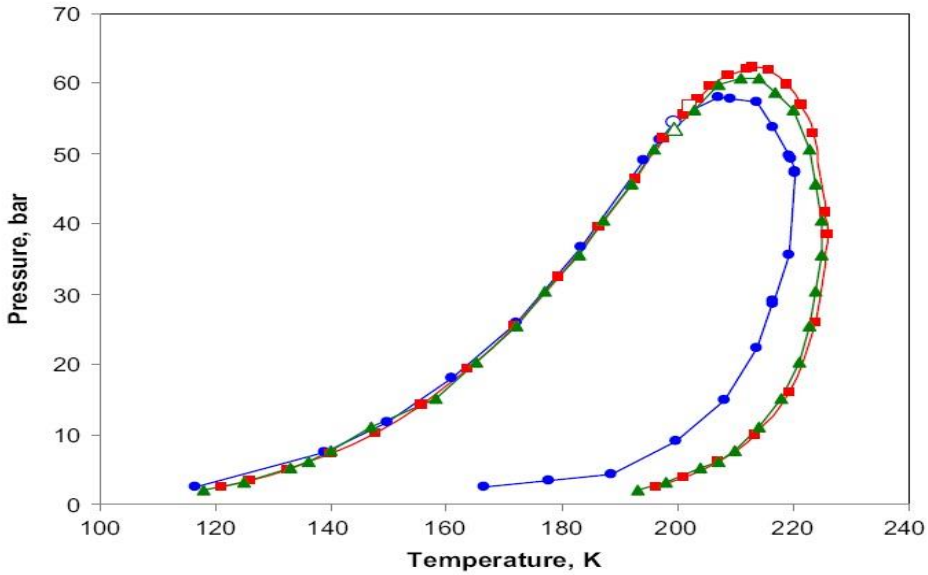

1.3 Nitrogen, methane, ethane, propane and n-butane system phase envelope[3][4]

1.3 LNG Supply Chain

The delivery of LNG to final consumer consists of different processes, each one interlinked with the next, forming a chain known as the LNG supply chain. These processes include *extraction and production, liquefaction, transportation, storage, regasification and delivery to consumers.*

The first process at the LNG chain is the extraction of natural gas from the resources. The extracted gas could be from a gas field (non-associated gas), which is also called "raw gas", or along with oil (associated gas). This distinction is important because associated gas has liquefied petroleum gas components (i.e. propane and butane) that must be extracted to meet LNG standards.

The produced natural gas is transported by pipelines from gas fields to a liquefaction facility. One of the primary purposes of liquefaction plants is to ensure the consistent composition and combustion characteristics by cooling and condensing natural gas to allow its loading as LNG and delivery to the end user. Therefore, their design must include several parallel processing modules (trains) for the preparation and liquefaction of natural gas, LNG storage tanks, facilities for loading LNG tankers, general purpose facilities, i.e. sea water pumping stations, electricity generation plants, nitrogen production plants, compressor stations, workshops and system security.

Preparation trains are used for the purification of gas from harmful components and liquefaction. The components that should be removed prior to liquefaction include carbon dioxide-CO_2, water and heavy hydrocarbons that would freeze at cryogenic process temperatures, hydrogen Sulfide-H_2S that must be removed to meet the LNG product specifications, corrosive and erosive components (mercury), inert components (helium and nitrogen) and oil.

After the removal of most contaminants and heavy hydrocarbons from the feed gas, the natural gas is subjected to the liquefaction process. Natural gas is converted to its liquefied form by the application of refrigeration technology making it possible to cool the gas down to approximately -163°C when it becomes a liquid. Cryogenic tanks are used to store the produced LNG until its transportation.

Special designed ships, LNG carriers, with special insulated tanks inside the hull are used to transfer LNG to the receiving terminal. The majority of existing LNG tankers has the cargo capacity ranging between 120.000 m^3 and 150.000 m^3, with some ships having the storage capacity of up to 264.000 m^3. This kind of transportation is used for long distance LNG distribution.

On the other hand, it is possible to deliver lower quantities of LNG by road using semi-trailer trucks or ISO containers, directly to end user forming a small scale LNG chain. This kind of direct on shore distribution could substitute a real pipeline; this is why **Virtual Pipeline** is a commonly used term for such transportation. At this case, specialized, double-skinned vacuum insulated tank trucks transfer LNG from the receiving terminals to "satellite" stations, where it is unloaded into insulated pressurized storage tanks.

The receiving terminal (sometimes called a re-gasification facility) is the last component of the LNG large scale supply chain. Its basic task is to receive and unload

liquefied natural gas from LNG tankers, store, vaporize LNG and distribute the gas into the distribution network. The receiving terminal is designed to deliver the specified quantity of gas into the distribution pipeline and maintain a reserve quantity of LNG[3][5][6][7][8].

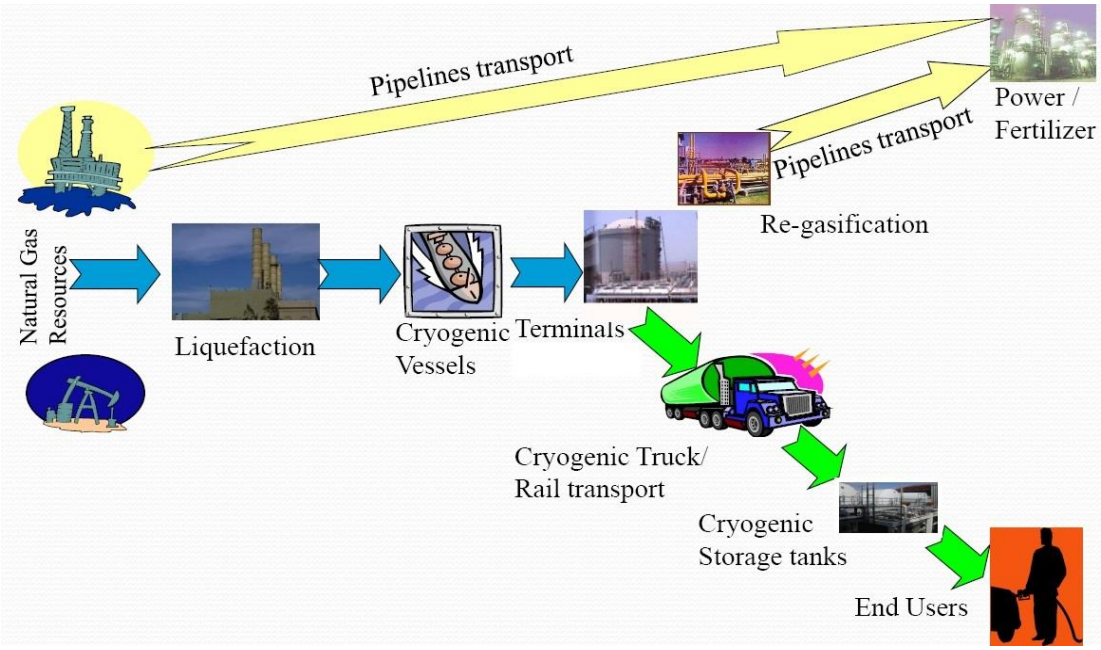

1.4 LNG supply chain[5]

1.4 Semi-trailer trucks and tanks specifications

As mentioned in the previous section, direct LNG distribution by road is possible using semi-trailer trucks or mobile tanks which can be transported either by railways or by trucks. In the next paragraphs we are going to present mobile and semi-trailer tank characteristics. Although, this thesis focuses on the operational characteristics of semi-trailer tanks, it is worth to note that mobile tanks share common design issues and are used for the same purpose (i.e. the small scale transportation of LNG), thus these are also presented in the paragraph below.

1.4.1 Mobile tanks

Mobile tanks can have the form of a standard ISO TC 104 container or a free style construction. The permitted transverse dimensions of a container are 2438×2591mm according to European regulations, while in case of a tank transported as a common load dimensions cannot exceed 3000×3000mm. Considering the above specifications, four design versions of cryogenic tanks were developed:

- type I – tank installed in a standard ISO TC 104 container frame with outer tank diameter D=2350 mm, length L=5946 mm, volume V=19 m^3 and operating pressure p=7 bar
- type II – tank as in type I, with decreased dimensions of inner supports because only empty tanks can be transported
- type III – tank with the outer diameter D=3000 mm and length L=6058 mm, volume V=32 m^3; operating pressure p=7 bar
- type IV – tank as in type III, but operating pressure increased to 12,5 bar

Type I, II tanks consist of an inner tank made of stainless steel (point 1 at figure 1.5) and an outer tank made of carbon steel (point 3). At the space between the tanks there are inner plastic supports (point 2), multilayer insulation material (point 4) and radiation shields (point 5). The air has been removed from this space creating a medium-level vacuum (point 6). In order to form the container frame (point 8) external supports are used (point 7). Finally, other fittings (point 9) are attached to the structure.

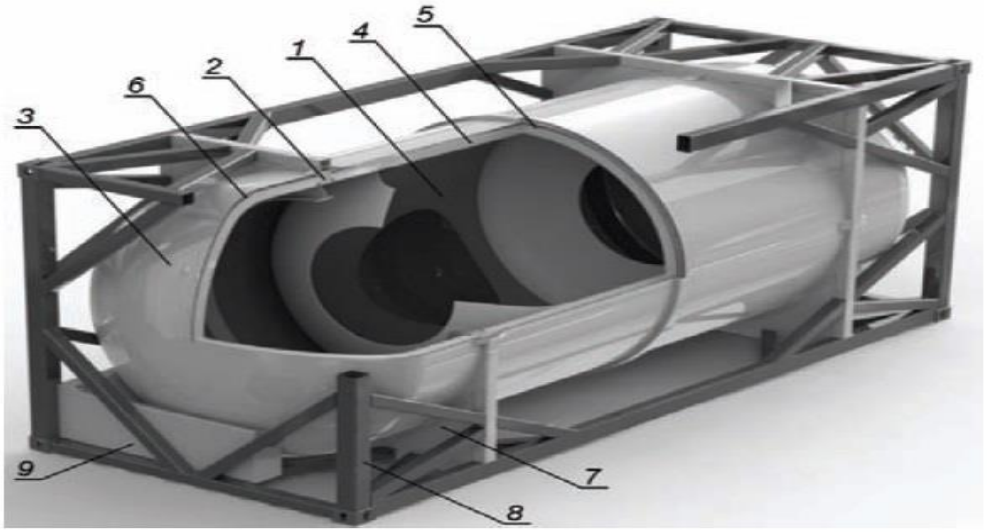

1.5 Tank type I, II tanks design

Type III, IV tanks are designed in almost the same way with the exception that there is no need to form the container frame. Similarly, these tanks are composed of an inner tank made (point 1 at figure 1.6) and an outer tank (point 2). At the space between the tanks there are inner plastic supports (point 3), multilayer insulation material (point 5) and radiation shields (point 6). The air has been removed from this space creating a medium-level vacuum (point 7). Outer supports (point 4) are used to hold up the tank, while extra fittings (point 8) integrate the whole structure. The main advantage of this structure is the higher capacity of its load due to less strict requirements[9].

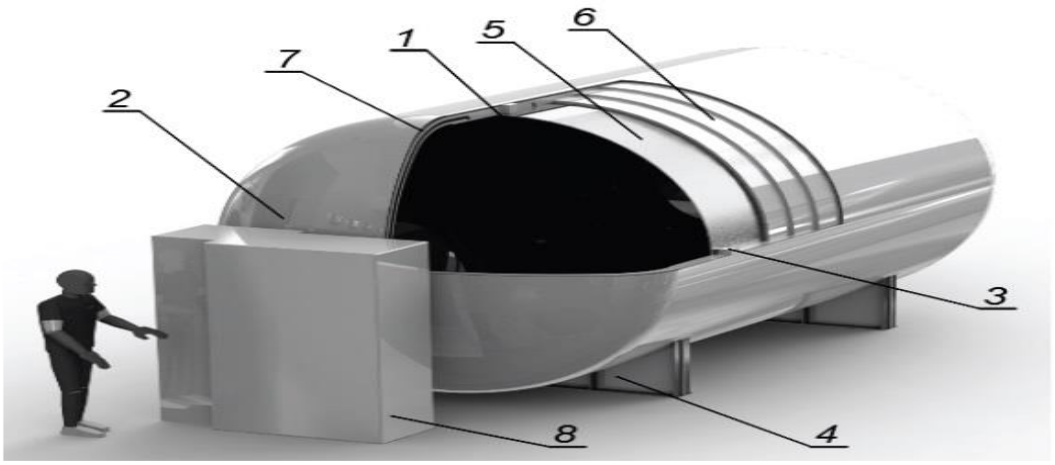

1.6 Type III, IV tanks design

1.4.2 Semi-trailer tanks

There are many different LNG semi-trailer suppliers, who manufacture trailers according to local regulations. As a consequence, there is a variety of available trailers designed with different criteria. However, despite the differentiated trailer capacities and dimensions there is a common plan behind the design of them. The concept includes an inner and an outer vessel, and a vacuum-insulated gap between them. Most trailers are tri-axle and the working pressure of the inner vessel fluctuates from 4 to 12 bar. In addition, all trailers are equipped with additional pipework and operational fittings for safety and regulation reasons. In the next paragraphs, some of them are presented coupled with their specifications.

Chart Inc.:

ST-12700 and ST-16300 are the two LNG trailers offered by Chart. The trailers consist of an inner pressure vessel at 4,83bar made of stainless steel and a structural vacuum vessel outer jacket made of lightweight, thin-gauge carbon and stainless steel. Control piping and instruments are located at the end of the trailer, in a rear piping cabinet easy to be accessed and maintained. ST-12700 is a 14,6m long and 3,74m high tandem-axle trailer capable to transport 17.815kg LNG at 4,83bar. On the other hand, ST-16300 is a 16,2m long and 3,91m high tri-axle trailer capable to transport 22.861kg LNG at 4,83bar. The drawings and specifications of each trailer are presented in figure 1.7[10].

SPECIFICATIONS

Model	ST-12700	ST-16300
Gross Capacity	12,700 gal / 48075 ltrs	16,300 gal / 61,702 ltrs
LNG Capacity (at 70 psig / 4.826 barg)	39,276 lbs / 17,815 kg	50,400 lbs / 22,861 kg
Maximum Allowable Working Pressure	70 psig / 4.83 barg	70 psig / 4.83 barg
Length (overall)	48 ft / 14.6 m	53 ft / 16.2 m
Width (overall)	8 ft 6 in / 2.6 m	8 ft 6 in / 2.6 m
Height	12 ft 5 in / 3.74 m	12 ft 10 in / 3.91 m
Weight	25,200 lbs / 11,431 kg	33,000 lbs / 14,966 kg
Design Codes	ASME Section VIII Division 1	ASME Section VIII Division 1
Axle Configuration	Tandem	Tri

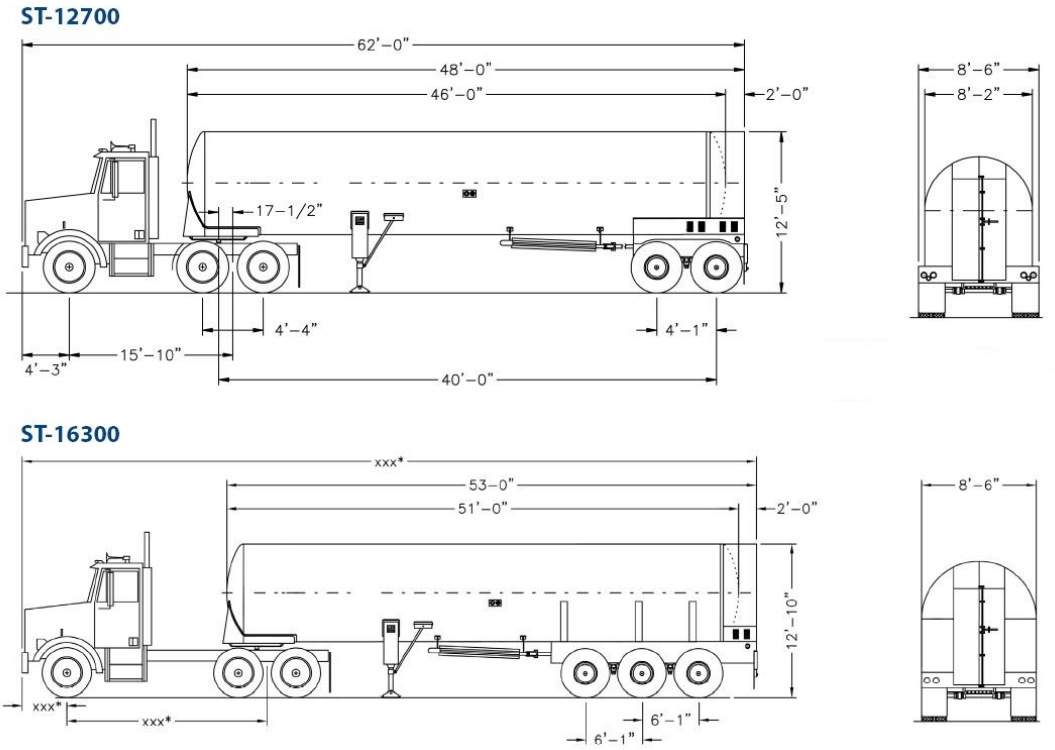

1.7 Chart trailers specifications

CRYOLOR:

SR-50000 is the LNG trailer offered by Cryolor. Although the vehicle structure is not given, it is clear that piping system and instruments are place at the back view. The tri-axle trailer, with 13,2m length and 3,78m height, is capable to transport 18.265kg (42.476lt) LNG at maximum working pressure of 7bar. Figure 1.8 presents SR-50000 drawing and specifications[11].

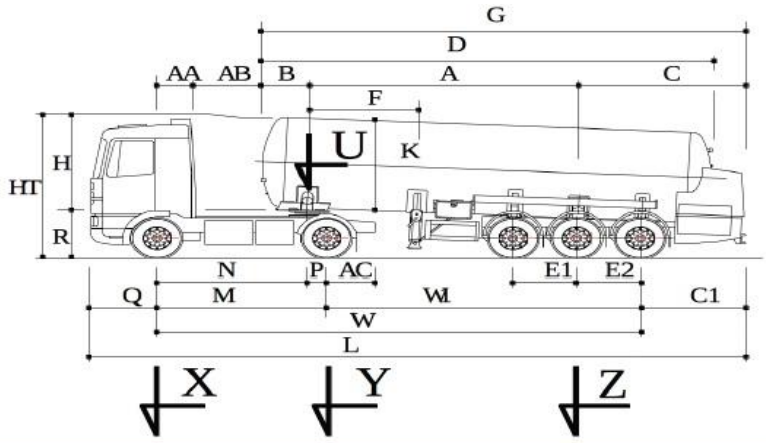

DIMENSIONS OF TRACTOR & SEMI-TRAILER (in mm)									
A	7 092	**E1**	1 320	**HT**	3 781	**P**	540	**R**	1 200
B	1 237	**E2**	1 320	**K**	Ø 2 520	**Q**	1 315	**W**	11 472
C	4 897	**F**	2 500	**L**	16 364	**AA**	895	**W1**	7 872
C1	3 577	**G**	13 226	**M**	3 600	**AB**	927		
D	12 218	**H**	2 581	**N**	3 060	**AC**	970	**Width**	2 550

1.8 CRYOLOR trailer specifications

Applied Cryo Technologies:

The dragon model ACT-LNG-1370 is a vacuum-insulated, cryogenic pressure transfer semi-trailer designed by Applied Cryo Technologies. It consists of an inner vessel made of stainless steel, an outer vessel made of carbon steel and SI super insulation system designed to work under high vacuum. This tandem-axle trailer is equipped with piping control cabinet in the same way as the previous trailers. In addition, this 14,53m long and 3,37m high trailer can transfer 42.457lt LNG at pressure of 4.83bar. Figure 1.9 presents dragon model specifications (drawing is not available)[12].

EQUIPMENT SPECIFICATIONS:	
PRODUCT SERVICE:	LNG
MAWP:	70 PSIG (4.83 BAR))
WARM WATER CAPACITY:	12,570 gal (47,582 liters)
VOLUME AT 70 PSI FILL DENSITY	11,216 gal (42,457 liters)
TARE WEIGHT:	25,100 lbs. (11, 385kg)
LENGTH:	47 ft. 8 in (14.53 m)
WIDTH:	102in (2.59 m)
HEIGHT:	11 ft. 11-.75"
DESIGN CODES:	ASME SEC VIII, DIV 1 USDOT SPECIFICATION MC-338 COMPRESSED GAS ASSOCIATION (CGA) 341 ASME/ANSI B31.3
DESIGN TEMPERATURE	-320° F / +100° F
NORMAL EVAPORATION RATE (NER):	0.4% LN2

1.9 ACT trailer specifications

Oilfield Hire & Services:

OHS offers two options for LNG trailers; one of 53.000 liters and another of 58.000 liters at 8bar. The maximum allowable working pressure is 11.7bar. The 53.000 liters tri-axle trailer is a perlite and vacuum-insulated unit suitable for the transportation of up to 20.000 kg of LNG. The total length of this trailer is 13,7m and it is 3,75m high. This trailer is the one only that provides information about the thickness of the insulation (in accordance to the drawing provided, figure 1.10) and as a result it is suitable for this work.

On the other hand, the 58.000 liters tri-axle LNG trailer, manufactured by GOFA, is a super-insulated vacuum unit suitable for the transportation of up to 21.000 kg of LNG. Both the inner and the outer vessel are made of stainless steel, while insulation consists of Cryotherm multilayer-insulation with reflective foils. The total length of the trailer is 13,9m[13][14].

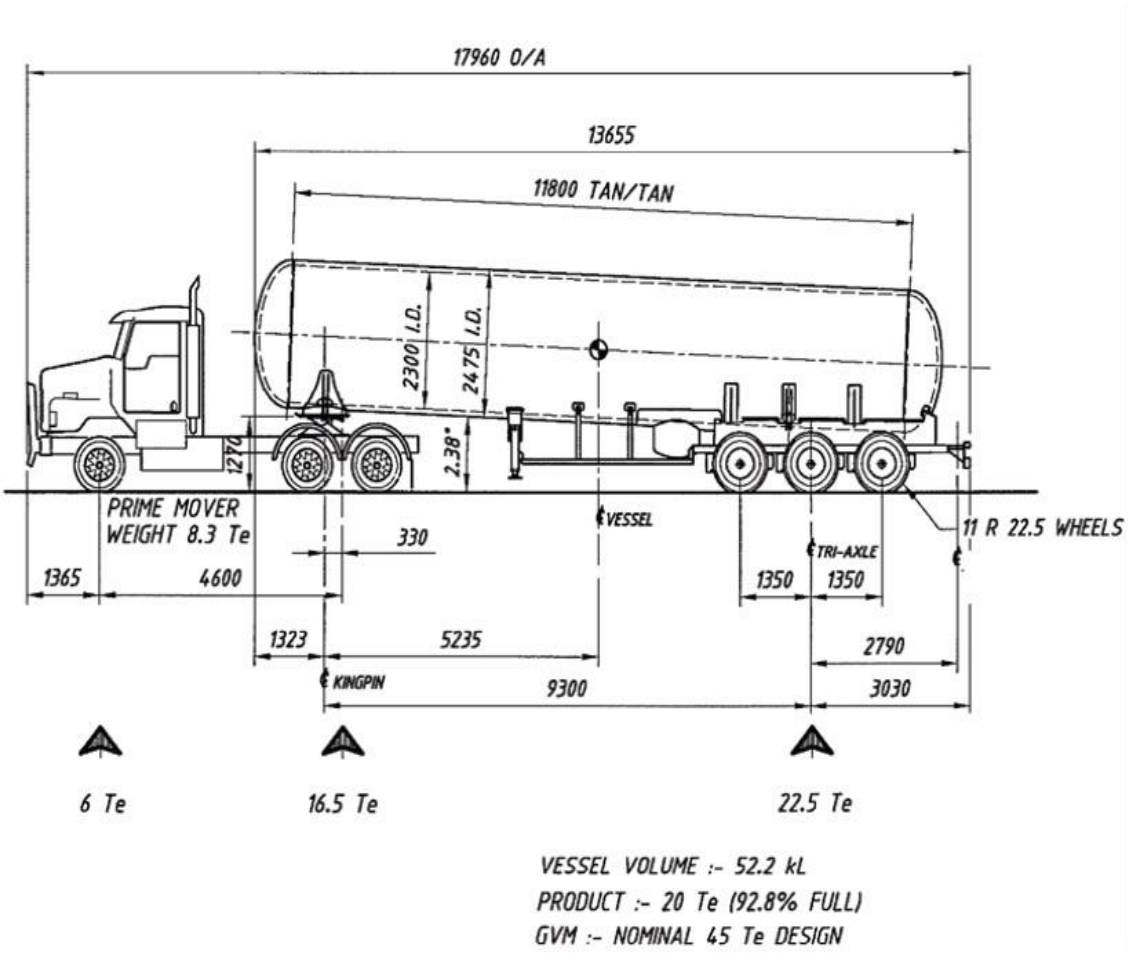

1.10 OHS trailer drawing

Table 1.3 summarizes the basic characteristics of the LNG trailers presented according to each supplier. It is clear that Chart manufactures the longest LNG trailers with the highest capacity among the others. However, maximum allowable pressure is offered by OHS trailers.

	Model	Capacity (lts)	Length (m)	Pressure (bar)	Axle
CHART	ST-12700	48.075	14,6	4,83	Tadem
	ST-16300	61.702	16,2	4,83	Tri
CRYOLOR	SR-50000	42.476	13,2	7	Tri
ACT Applied Cryo Technologies	ACT-LNG-1370	42.457	14,5	4,83	Tadem
OHS	53.000 LNG	53.000	13,7	8	Tri
	58.000 LNG	58.000	13,9	8	Tri

Table 1.3 LNG trailers summary

1.4.3 Insulation Materials

Polyurethane (PU) and Polyisocyanurate (PIR) foams are widely used at Cryogenic Insulation Systems. Foam insulation requires no vacuum. Other types of cryogenic insulation systems include those where the evacuated annular spaces (spaces between an inner and outer vessel) contain bulk filled materials, e.g., glass fiber, silica aerogel, or composites. However, LNG trailers use either perlite or Multilayer insulation (known also as super insulation) under vacuum in order to achieve high thermal performance and low temperatures, as mentioned in the previous section. As a consequence, these two materials are under the sphere of our interest. Multilayer insulation is used for special applications where high performances are required (liquid hydrogen and liquid helium), while perlite is greatly qualified for practical applications.

Vessel structures are typically surrounded by an outer vessel with a separating space that is vacuum evacuated. The pressure inside vacuum is settled in 10^{-4}torr range, eliminating convective heat transfer. Selecting materials with low conductivity, such as fiberglass and/or low density ceramics, prevent convective heat transfer. However, radiated heat transfer is another problem which is controlled by the barrier placed around the inner vessel. One common radiation barrier used in cryogenic applications is known as multilayer insulation (MLI), or super insulation.

The MLI generally contains multiple layers of reflective material separated by spacers having low conductivity. These radiation shields are stacked in parallel as close as possible without getting in touch. MLI will normally consist of 60 layers per inch. MLI is anisotropic by nature and very sensitive to mechanical compressions and edge effects resulting in careful treatment during installation.

Polyester, nylon or Mylar could be used as spacer material, placed between the layers, in order to isolate each layer from the other to completely prevent the separate coverings of foil from contacting. In such case, a thermal short circuit will occur and increase the heat transfer. The entire surface of the inner vessel is covered by aluminum foil.

The unique properties of perlite, a loose granular inorganic material of volcanic origin blown up at high temperatures, make it a useful tool in various insulation applications including cryogenic low-temperature storage and transportation. Low thermal conductivity and excellent thermal properties could be considered among perlite advantages. In addition, perlite is cheap, non-combustible, vermin and rot resistant and easy to handle and install. Furthermore, it does not shrink, swell, warp, or slump and does not retain moisture[15].

For cryogenic applications, evacuated perlite provides a superior insulation with thermal conductivity up to 40 times less than 0.029 W/m·K depending on vacuum and temperature. Thermal conductivity depends on temperature, density and the interstitial pressure. The value of it at -107 ^{0}C temperature, 139 kg/m^{3} density and

1.33mPa is calculated at 0.0007 W/m·K[16]. Hofmann suggested the following empirical equation to relate thermal conductivity with temperature $\lambda=a+bT^c$, where a, b, c calculated parameters. According to his work, these parameters for perlite-vacuum and Multilayer insulation (Linde-system consisting of dimpled aluminum foils as reflector and fiberglass paper as a spacer) are calculated respectively (a = $1{,}9112\cdot10^{-4}$; b = $3{,}4757\cdot10^{-12}$; c = 3,6783) for 50 kg/m^3 perlite density and (a = $1.6918\cdot10^{-5}$; b = $1.2268\cdot10^{-13}$; c = 3.6457) for 40 layers of MLI[17].

1.5 Boil-off gas and previous works

One of the challenges in transporting and storing LNG is maintaining the liquid phase of natural gas inside tanks. The major problem is the heat leakage to LNG through the tank shell results in LNG evaporation inside the tank. The created vapor phase, which is usually called Boil off Gas (BOG), is a significant problem considering that no external refrigeration action takes place. The boil off LNG can cause excessive pressure buildup inside tanks, and therefore we have to find methods to reduce pressure and prevent evaporation. One possible solution would be the release of the vapor phase. However, this is economically forbidden. Proposals for handling BOG include burning it up to power steam turbines or using re-liquefaction procedures.

It is clear that BOG rate estimation is a crucial process for the design of LNG infrastructure, considering that heat leakage can occur through the whole LNG chain. Most of the previous works consider maritime transportation, LNG terminals and mobile tanks. There is no work for trailer tanks and that could be a novelty for this work. In addition, the interactive simulation of ambient environment with the tank could be another novelty. Previous works assume evaporation of liquid on its surface without any visible bubbles. In contrast, multiphase evaporation flow simulation is our concern in this work. In the next paragraphs, most related past works are presented.

Rafal Sedlaczek described the whole large and small scale LNG chain considering BOG for large-scale LNG receiving terminal and LNG storage tank[18]. He highlighted the higher importance of LNG evaporation in small-scale chain compared to large scale. In the same mood, [6] examined the large scale chain BOG during storage, loading/unloading and ship voyage. They assumed evaporation of the liquid on its surface, while they suggested the boil-off gas rate (BOR) formula (extensively used in other works) $BOR = \frac{Q\cdot 3600\cdot 24}{\Delta H\cdot V_{LNG}\cdot\rho}\cdot 100$ (1), where BOR is in %/day, V_{LNG} volume of LNG in cargo tanks in m^3, ρ LNG density in kg/m^3, Q heat exchange in W and ΔH latent heat of evaporation in J/kg.

Energy balance at the liquid-vapor interface was also used by [19], who calculated BOR based on $\dot{m}_{BOG} = \frac{q_{\text{int},liq}\cdot A_{\text{int}}}{h_{fg}}$, where A_{int} is the liquid-vapor interface area and q_{int} is the averaged heat flux transferred to the interface from the bulk liquid. This is a two dimension work where all of the fluid properties except density were taken to be constant. The density variation due to temperature was described by the Boussinesq approximation. [20] used the thermodynamic and heat transfer methods to analyze the

pressure and temperature changes in LNG tanks. Based on (1) and after analyzing the tank shell properties, they got interesting results about BOR and insulation thickness.

Another interesting work was presented by [4], where ANSYS Fluent was used to estimate BOR inside LNG tanker. Authors instead of using (1), they based their results on: $MassTransferRate = \frac{r \cdot VF_l \cdot \rho_l \cdot (T_l - T_{sat})}{T_{sat}}$ (2), where r is under relaxation factor, VF_l is Liquid volume fraction, ρ_l is Liquid density, T_l is Liquid temperature and T_{sat} is saturated temperature. The implementation of User Define Function in ANSYS FLUENT enabled them to use fundamental equations of fluid flow. The schiller-naumann drag law for the phase interaction was used to describe the drag between the spherical vapor particle and surrounding LNG liquid condition, tracking the movement of gas phase inside tank. On the other hand, [21] estimated BOR inside an LNG tanker based on equation (1), where q was read directly from ANSYS FLUENT. This model is easy to understand, solve and implement because it is an estimation of BOR without taking into consideration the vapor movement inside the tank.

Another work of LNG BOG inside tankers was presented by [22], where Lee-Kesler-Plocker (LKP) and the Starling modified Benedict-Webb-Rubin (BWRS) empirical models were used to analyze the vapor-liquid phases of multi-component fluid mixtures. These iterative models are equations of state used for the calculation of LNG density and enthalpy. The BOR calculation was based again on equation (1). The results from BWRS model gave the reference for the relationship between compositions of LNG and BOG, while the results from LKP model revealed the relationship between operating pressure and BOG. Work by [23] examined the BOG on Spanish LNG terminals. They calculated the BOG's properties and heat of vaporization using Aspen Plus for different LNG compositions. Relying on this data and the absorbed heat of each terminal in Spain they showed the dependency of BOG on LNG composition at each Spanish terminal. Finally, [9] presented thermal calculations for transport and storage of LNG. Different types of mobile tanks were described, while distributions of temperature and heat flux were obtained for each one of them.

2 Basic Theory

ANSYS FLUENT provides comprehensive modeling capabilities for a wide range of fluid flow problems (incompressible and compressible, laminar and turbulent, steady-state or transient).This chapter describes the theoretical background for some of the basic physical models provided by FLUENT. However, only the models used in this work are going to be presented in this section. Hence, conservation equations for mass and momentum, turbulence models, models for heat transfer (including radiation) and multiphase flows are some of the topics discussed in this chapter and applied beyond in this work.

2.1 Continuity and Momentum equations

For all flows, ANSYS FLUENT solves conservation equations for mass and momentum. For flows involving heat transfer or compressibility, an additional equation for energy conservation is solved. Additional transport equations are also solved when the flow is turbulent. In this section, the conservation equations for laminar flow in an inertial (non-accelerating) reference frame are presented.

The equation for conservation of mass, or continuity equation, can be written as follows:

$$\frac{\partial \rho}{\partial t} + \nabla \cdot (\rho \vec{\upsilon}) = S_m \quad (1)$$

Equation (1) is the general form of the mass conservation equation and is valid for incompressible as well as compressible flows. The source S_m is the mass added to the continuous phase from the dispersed second phase (e.g., due to vaporization of liquid droplets) and any user-defined sources.

For 2D axisymmetric geometries, the continuity equation is given by:

$$\frac{\partial \rho}{\partial t} + \frac{\partial}{\partial x}(\rho \upsilon_x) + \frac{\partial}{\partial r}(\rho \upsilon_r) + \frac{\rho \upsilon_r}{\upsilon_r} = S_m \quad (2)$$

, where x is the axial coordinate, r is the radial coordinate, υ_x is the axial velocity, and υ_r is the radial velocity.

Conservation of momentum in an inertial (non-accelerating) reference frame is described by:

$$\frac{\partial}{\partial t}(\rho \vec{\upsilon}) + \nabla \cdot (\rho \vec{\upsilon} \vec{\upsilon}) = -\nabla p + \nabla \cdot (\bar{\bar{\tau}}) + \rho \vec{g} + \vec{F} \quad (3)$$

, where p is the static pressure, $\bar{\bar{\tau}}$ is the stress tensor (described below), $\rho \vec{g}$ and $\vec{F}$ are the gravitational body force and external body forces (e.g., that arise from interaction with the dispersed phase), respectively. $\vec{F}$ also contains other model-dependent source terms such as porous-media and user-defined sources.

The stress tensor $\bar{\bar{\tau}}$ is given by:

$$\bar{\bar{\tau}} = \mu\left[(\nabla\vec{\upsilon} + \nabla\vec{\upsilon}^{T}) - \frac{2}{3}\nabla\cdot\vec{\upsilon}I\right] \quad (4)$$

, where μ is the molecular viscosity, I is the unit tensor, and the second term on the right hand side is the effect of volume dilation.

For 2D axisymmetric geometries, the axial and radial momentum conservation equations are given by:

$$\frac{\partial}{\partial t}(\rho\upsilon_x) + \frac{1}{r}\frac{\partial}{\partial x}(\rho\upsilon_x\upsilon_r) + \frac{1}{r}\frac{\partial}{\partial r}(\rho\upsilon_x\upsilon_r) = -\frac{\partial p}{\partial x} + \frac{1}{r}\frac{\partial}{\partial x}\left[r\mu(2\frac{\partial\upsilon_x}{\partial x} - \frac{2}{3}(\nabla\cdot\vec{\upsilon})\right] \quad (5)$$
$$+\frac{1}{r}\frac{\partial}{\partial r}\left[r\mu(\frac{\partial\upsilon_x}{\partial r} + \frac{\partial\upsilon_r}{\partial x})\right] + F_x$$

and

$$\frac{\partial}{\partial t}(\rho\upsilon_r) + \frac{1}{r}\frac{\partial}{\partial x}(r\rho\upsilon_x\upsilon_r) + \frac{1}{r}\frac{\partial}{\partial r}(r\rho\upsilon_x\upsilon_r) = -\frac{\partial p}{\partial r} + \frac{1}{r}\frac{\partial}{\partial r}\left[r\mu(2\frac{\partial\upsilon_r}{\partial r} - \frac{2}{3}(\nabla\cdot\vec{\upsilon})\right] \quad (6)$$
$$+\frac{1}{r}\frac{\partial}{\partial x}\left[r\mu(\frac{\partial\upsilon_r}{\partial x} + \frac{\partial\upsilon_x}{\partial r})\right] + F_r - 2\mu\frac{\upsilon_r}{r^2} + \frac{2}{3}\frac{\mu}{r}(\nabla\cdot\vec{\upsilon}) + \rho\frac{\upsilon_z^{\,2}}{r}$$

, where $\nabla\cdot\vec{\upsilon} = \frac{\partial\upsilon_x}{\partial x} + \frac{\partial\upsilon_r}{\partial r} + \frac{u_r}{r}$ and υ_z the swirl velocity[24].

2.2 Turbulence

Turbulent flows are characterized by fluctuating velocity fields. These fluctuations mix transported quantities such as momentum, energy, and species concentration, and cause the transported quantities to fluctuate as well. Since these fluctuations can be of small scale and high frequency, they are too computationally expensive to simulate directly in practical engineering calculations. Instead, the instantaneous (exact) governing equations can be time-averaged, ensemble-averaged, or otherwise manipulated to remove the resolution of small scales, resulting in a modified set of equations that are computationally less expensive to solve. However, the modified equations contain additional unknown variables, and turbulence models are needed to determine these variables in terms of known quantities.

It is an unfortunate fact that no single turbulence model is universally accepted as being superior for all classes of problems. The choice of turbulence model will depend on considerations such as the physics encompassed in the flow, the established practice for a specific class of problem, the level of accuracy required, the available computational resources, and the amount of time available for the simulation. To make the most appropriate choice of model for your application, you need to understand the capabilities and limitations of the various options.

Time-dependent solutions of the Navier-Stokes equations for high Reynolds-number turbulent flows in complex geometries which set out to resolve all the way down to the smallest scales of the motions are unlikely to be attainable for some time to come. Two alternative methods can be employed to render the Navier-Stokes equations

tractable so that the small-scale turbulent fluctuations do not have to be directly simulated: Reynolds-averaging (or ensemble-averaging) and filtering. Both methods introduce additional terms in the governing equations that need to be modeled in order to achieve a "closure" for the unknowns.

The Reynolds-averaged Navier-Stokes (RANS) equations govern the transport of the averaged flow quantities, with the whole range of the scales of turbulence being modeled. The RANS-based modeling approach therefore greatly reduces the required computational effort and resources, and is widely adopted for practical engineering applications. An entire hierarchy of closure models is available in ANSYS FLUENT including Spalart-Allmaras, k-e and its variants, k-ω and its variants, and the RSM.

In Reynolds averaging, the solution variables in the instantaneous (exact) Navier-Stokes equations are decomposed into the mean (ensemble-averaged or time-averaged) and fluctuating components. For the velocity components:

$$u_i = \bar{u}_i + u_i' \quad (7)$$

, where $\bar{u}_i$ and u_i' are the mean and fluctuating velocity components (i = 1, 2, 3).

Likewise, for pressure and other scalar quantities:

$$\phi = \bar{\phi} + \phi'$$

, where φ denotes a scalar such as pressure, energy, or species concentration.

Substituting expressions of this form for the flow variables into the instantaneous continuity and momentum equations and taking a time (or ensemble) average (and dropping the over bar on the mean velocity, $\bar{u}$) yields the ensemble-averaged momentum equations. They can be written in Cartesian tensor form as:

$$\frac{\partial \rho}{\partial t} + \frac{\partial}{\partial x_i}(\rho \upsilon_i) = 0 \quad (8)$$

$$\frac{\partial}{\partial t}(\rho u_i) + \frac{\partial}{\partial x_j}(\rho u_i u_j) = -\frac{\partial p}{\partial x_i} + \frac{\partial}{\partial x_j}\left[\mu\left(\frac{\partial u_i}{\partial x_j} + \frac{\partial u_j}{\partial x_i} - \frac{2}{3}\delta_{ij}\frac{\partial u_l}{\partial x_l}\right)\right] + \frac{\partial}{\partial x_j}(-\rho\overline{u_i' u_j'}) \quad (9)$$

Equations (8) and (9) are called Reynolds-averaged Navier-Stokes (RANS) equations. They have the same general form as the instantaneous Navier-Stokes equations, with the velocities and other solution variables now representing ensemble-averaged (or time-averaged) values. Additional terms now appear that represent the effects of turbulence. These Reynolds stresses, $-\rho\overline{u_i' u_j'}$, must be modeled in order to close Equation (9).

The Reynolds-averaged approach to turbulence modeling requires that the Reynolds stresses in Equation (7)-(9) are appropriately modeled. A common method employs the Boussinesq hypothesis to relate the Reynolds stresses to the mean velocity gradients:

$$-\rho\overline{u_i'u_j'} = \mu_t(\frac{\partial u_i}{\partial x_j}+\frac{\partial u_j}{\partial x_i})-\frac{2}{3}(\rho k+\mu_t\frac{\partial u_k}{\partial x_k})\delta_{ij} \quad (10)$$

The Boussinesq hypothesis is the k-ε models and the k-ω models. The advantage of this approach is the relatively low computational cost associated with the computation of the turbulent viscosity, μ_t . In the case of the k-ε and k-ω models, two additional transport equations (for the turbulence kinetic energy, k, and either the turbulence dissipation rate, ε, or the specific dissipation rate, ω) are solved, and μ_t is computed as a function of k and ε or k and ω. The disadvantage of the Boussinesq hypothesis as presented is that it assumes μ_t is an isotropic scalar quantity, which is not strictly true.

Standard k-ε model

The simplest "complete models" of turbulence are the two-equation models in which the solution of two separate transport equations allows the turbulent velocity and length scales to be independently determined. The standard k-ε model in ANSYS FLUENT falls within this class of models and has become the workhorse of practical engineering flow calculations in the time since it was proposed by Launder and Spalding. Robustness, economy, and reasonable accuracy for a wide range of turbulent flows explain its popularity in industrial flow and heat transfer simulations. It is a semi-empirical model, and the derivation of the model equations relies on phenomenological considerations and empiricism.

The standard k-ε model is a model based on transport equations for the turbulence kinetic energy (k) and its dissipation rate (ε). The model transport equation for k is derived from the exact equation, while the model transport equation for ε was obtained using physical reasoning and bears little resemblance to its mathematically exact counterpart.

In the derivation of the k-ε model, the assumption is that the flow is fully turbulent, and the effects of molecular viscosity are negligible. The standard k-ε model is therefore valid only for fully turbulent flows. The turbulence kinetic energy, k, and its rate of dissipation, ε, are obtained from the following transport equations:

$$\frac{\partial}{\partial t}(\rho k)+\frac{\partial}{\partial x_i}(\rho k u_i)=\frac{\partial}{\partial x_j}\left[(\mu+\frac{\mu_t}{\sigma_k})\frac{\partial k}{\partial x_j}\right]+G_k+G_b-\rho\varepsilon-Y_M+S_k \quad (11)$$

And

$$\frac{\partial}{\partial t}(\rho \varepsilon)+\frac{\partial}{\partial x_i}(\rho \varepsilon u_i)=\frac{\partial}{\partial x_j}\left[(\mu+\frac{\mu_t}{\sigma_\varepsilon})\frac{\partial \varepsilon}{\partial x_j}\right]+C_{1\varepsilon}\frac{\varepsilon}{k}(G_k+C_{3\varepsilon}G_b)-C_{2\varepsilon}\rho\frac{\varepsilon^2}{k}+S_\varepsilon \quad (12)$$

In these equations, G_k represents the generation of turbulence kinetic energy due to the mean velocity gradients, G_b the generation of turbulence kinetic energy due to buoyancy, Y_M the contribution of the fluctuating dilatation in compressible turbulence to the overall dissipation rate. $C_{1\varepsilon}$, $C_{2\varepsilon}$, $C_{3\varepsilon}$ are constants, σ_k and σ_ε are the turbulent Prandtl numbers for k and ε, respectively, while S_k and S_ε are user-defined source terms. The turbulent (or eddy) viscosity, μ_t, is computed by combining k and ε as follows:

$$\mu_t = \rho C_\mu \frac{k^2}{\varepsilon}$$

The model constants $C_{1\varepsilon}$, $C_{2\varepsilon}$, C_μ, σ_k and σ_ε have the following default values:

$C_{1\varepsilon}$=1.44, $C_{2\varepsilon}$=1.92, C_μ=0.09, σ_k=1, σ_ε=1.3

These default values have been determined from experiments with air and water for fundamental turbulent shear flows including homogeneous shear flows and decaying isotropic grid turbulence. They have been found to work fairly well for a wide range of wall-bounded and free shear flows[24].

2.3 Heat transfer

The flow of thermal energy from matter occupying one region in space to matter occupying a different region in space is known as heat transfer. Heat transfer can occur by three main methods: conduction, convection, and radiation. Physical models involving conduction and/or convection only are the simplest, while buoyancy-driven flow or natural convection, and radiation models are more complex. Depending on your problem, ANSYS FLUENT will solve a variation of the energy equation that takes into account the heat transfer methods you have specified.

ANSYS FLUENT solves the energy equation in the following form:

$$\frac{\partial}{\partial t}(\rho E) + \nabla \cdot (\vec{\upsilon}(\rho E + p)) = \nabla \cdot (k_{eff} \nabla T - \sum_j h_j \overrightarrow{J_j} + (\overline{\overline{\tau}}_{eff} \cdot \vec{\upsilon})) + S_h \quad (13)$$

, where k_{eff} is the effective conductivity (k + k_t, where k_t is the turbulent thermal conductivity, defined according to the turbulence model being used), and J_j is the diffusion flux of species j. The first three terms on the right-hand side of Equation (13) represent energy transfer due to conduction, species diffusion, and viscous dissipation, respectively. S_h includes the heat of chemical reaction, and any other volumetric heat sources you have defined. In equation (13):

$$E = h - \frac{p}{\rho} + \frac{\upsilon^2}{2}$$

, where sensible enthalpy h is defined for ideal gases as:

$$h = \sum_j Y_j h_j$$

, and for incompressible flows as:

$$h = \sum_j Y_j h_j + \frac{p}{\rho}$$

, where Y_j is the mass fraction of species j

$$h_j = \int_{Tref}^{T} c_{p,j} dT$$

, where T_{ref} is 298,15K

Natural Convection and Buoyancy-Driven Flows

When heat is added to a fluid and the fluid density varies with temperature, a flow can be induced due to the force of gravity acting on the density variations. Such buoyancy-driven flows are termed natural-convection (or mixed-convection) flows and can be modeled by ANSYS FLUENT. The importance of buoyancy forces in a mixed convection flow can be measured by the ratio of the Grashof and Reynolds numbers:

$$\frac{Gr}{\mathrm{Re}^2} = \frac{g\beta\Delta TL}{\upsilon^2}$$

When this number approaches or exceeds unity, you should expect strong buoyancy contributions to the flow. Conversely, if it is very small, buoyancy forces may be ignored in your simulation. In pure natural convection, the strength of the buoyancy-induced flow is measured by the Rayleigh number:

$$Ra = \frac{g\beta\Delta TL^3\rho}{\mu\alpha}$$

, where β is the thermal expansion coefficient:

$$\beta = -\frac{1}{\rho}\left(\frac{\partial\rho}{\partial T}\right)_p$$

, and α is the thermal diffusivity:

$$a = \frac{k}{\rho c_p}$$

Rayleigh numbers less than 10^8 indicate a buoyancy-induced laminar flow, with transition to turbulence occurring over the range of $10^8 < \mathrm{Ra} < 10^{10}$.

Boussinesq approximation assumes incompressible flow due to low variations in density that makes small difference in the governing equations. However, the effect on the gravitational force term is important and thus is considered in this approximation. This approximation is rather popular in buoyancy driven flow where temperature differences are not very high. This approximation is described as follows: Constant reference density ρ_0 in all the governing equations except in the buoyancy term. Approximation of the density change for the buoyancy term with a constant thermal expansion coefficient:

$$\rho \approx \rho_0(1-\beta\Delta T) \quad (14)$$

The buoyancy term entered in the equations is, thus:

$$-\rho_0 \beta \Delta T = -\rho_0 \beta (T - T_0) \quad (15)$$

, with T_0 the reference temperature where $\rho=\rho_0$.

Surface-to-Surface (S2S) Radiation Model

The surface-to-surface radiation model can be used to account for the radiation exchange in an enclosure of gray-diffuse surfaces. The energy exchange between two surfaces depends in part on their size, separation distance, and orientation. These parameters are accounted for by a geometric function called a "view factor". The main assumption of the S2S model is that any absorption, emission, or scattering of radiation can be ignored; therefore, only "surface-to-surface" radiation need be considered for analysis.

ANSYS FLUENT's S2S radiation model assumes the surfaces to be gray and diffuse. Emissivity and absorptivity of a gray surface are independent of the wavelength. Also, by Kirchhoff's law, the emissivity equals the absorptivity ($\varepsilon=\alpha$). For a diffuse surface, the reflectivity is independent of the outgoing (or incoming) directions.

The gray-diffuse model is what is used in ANSYS FLUENT. Also, as stated earlier, for applications of interest, the exchange of radiative energy between surfaces is virtually unaffected by the medium that separates them. Thus, according to the gray-body model, if a certain amount of radiant energy (E) is incident on a surface, a fraction (ρE) is reflected, a fraction (αE) is absorbed, and a fraction (τE) is transmitted. Since for most applications the surfaces in question are opaque to thermal radiation (in the infrared spectrum), the surfaces can be considered opaque. The transmissivity, therefore, can be neglected. It follows, from the conservation of energy, that $\alpha+\rho=1$, since $\alpha=\varepsilon$ (emissivity), and $\rho=1-\varepsilon$.

The energy flux leaving a given surface is composed of directly emitted and reflected energy. The reflected energy flux is dependent on the incident energy flux from the surroundings, which then can be expressed in terms of the energy flux leaving all other surfaces. The energy reflected from surface k is:

$$q_{out,k} = \varepsilon_k \sigma T_k^4 + \rho_k q_{in.k}$$

, where $q_{out,k}$ is the energy flux leaving the surface, ε_k is the emissivity, σ is Boltzmann's constant, and $q_{in,k}$ is the energy flux incident on the surface from the surroundings.

The amount of incident energy upon a surface from another surface is a direct function of the surface-to-surface "view factor," F_{jk}. The view factor F_{jk} is the fraction of energy leaving surface k that is incident on surface j. The incident energy flux $q_{in,k}$ can be expressed in terms of the energy flux leaving all other surfaces as:

$$A_k q_{in,k} = \sum_{j=1}^{N} A_j q_{out,j} F_{jk}$$

, where A_k is the area of surface k and F_{jk} is the view factor between surface k and surface j. For N surfaces, using the view factor reciprocity relationship give

$$A_j F_{jk} = A_k F_{kj} \text{ for } j = 1, 2, 3...N$$

so that,

$$q_{in,k} = \sum_{j=1}^{N} F_{kj} q_{out,j}$$

Therefore,

$$q_{out,k} = \varepsilon_k \sigma T_k^4 + \rho_k \sum_{j=1}^{N} F_{kj} q_{out,j}$$

, which can be written:

$$J_k = E_k + \rho_k \sum_{j=1}^{N} F_{kj} J_k$$

, where J_k represents the energy that is given off of surface k, and E_k represents the emissive power of surface k. This represents N equations, which can be recast into matrix form as:

$$KJ = E$$

, where K is an N x N matrix, J is the radiosity vector, and E is the emissive power vector.

The view factor between two finite surfaces i and j is given by:

$$F_{ij} = \frac{1}{A_i} \int_{A_i} \int_{A_j} \frac{\cos \vartheta_i \cos \theta_j}{\pi r^2} \delta_{i,j} dA_i dA_j$$

, where δ_{ij} is determined by the visibility of dA_j to dA_i (δ_{ij}=1 if dA_j is visible to dA_i and 0 otherwise)[24].

2.4 Multiphase flows

A large number of flows encountered in nature and technology are a mixture of phases. Physical phases of matter are gas, liquid, and solid, but the concept of phase in a multiphase flow system is applied in a broader sense. In multiphase flow, a phase can be defined as an identifiable class of material that has a particular inertial response to and interaction with the flow and the potential field in which it is immersed. For example, different-sized solid particles of the same material can be treated as different phases because each collection of particles with the same size will have a similar dynamical response to the flow field.

The following regimes are gas-liquid or liquid-liquid flows:

- Bubbly flow: This is the flow of discrete gaseous or fluid bubbles in a continuous fluid.

- Droplet flow: This is the flow of discrete fluid droplets in a continuous gas.

- Slug flow: This is the flow of large bubbles in a continuous fluid.

- Stratified/free-surface flow: This is the flow of immiscible fluids separated by a clearly-defined interface.

The Volume of fluid (VOF) model

The VOF formulation in ANSYS FLUENT is generally used to compute a time-dependent solution, but for problems in which you are concerned only with a steady-state solution, it is possible to perform a steady-state calculation. The VOF formulation relies on the fact that two or more fluids (or phases) are not interpenetrating. For each additional phase that you add to your model, a variable is introduced: the volume fraction of the phase in the computational cell. In each control volume, the volume fractions of all phases sum to unity. The fields for all variables and properties are shared by the phases and represent volume-averaged values, as long as the volume fraction of each of the phases is known at each location. Thus the variables and properties in any given cell are either purely representative of one of the phases, or representative of a mixture of the phases, depending upon the volume fraction values. In other words, if the q^{th} fluid's volume fraction in the cell is denoted as a_q, then the following three conditions are possible:

- a_q=0 The cell is empty (of the q^{th} fluid)
- a_q=1 The cell is full (of the qth fluid)
- $0<a_q<1$ The cell contains the interface between the q^{th} fluid and one or more other fluids.

Based on the local value of a_q, the appropriate properties and variables will be assigned to each control volume within the domain.

The tracking of the interface(s) between the phases is accomplished by the solution of a continuity equation for the volume fraction of one (or more) of the phases. For the q^{th} phase, this equation has the following form:

$$\frac{1}{\rho_q}\left[\frac{\partial}{\partial t}(a_q\rho_q)+\nabla\cdot(a_q\rho_q\vec{\upsilon_q})=S_{aq}+\sum_{p=1}^{n}(\dot{m}_{pq}-\dot{m}_{qp})\right]$$

, where $\dot{m}_{qp}$ is the mass transfer from phase q to phase p and $\dot{m}_{pq}$ is the mass transfer from phase p to phase q. The volume fraction equation may be solved either through implicit or explicit time discretization.

When the implicit scheme is used for time discretization, ANSYS FLUENT's standard finite-difference interpolation schemes, QUICK, Second Order Upwind and First Order Upwind, and the Modified HRIC schemes, are used to obtain the face fluxes for all cells, including those near the interface. Since this equation requires the volume fraction values at the current time step (rather than at the previous step, as for

the explicit scheme), a standard scalar transport equation is solved iteratively for each of the secondary-phase volume fractions at each time step.

In the explicit approach, ANSYS FLUENT's standard finite-difference interpolation schemes are applied to the volume fraction values that were computed at the previous time step. When the explicit scheme is used, a time-dependent solution must be computed. The face fluxes can be interpolated either using interface reconstruction or using a finite volume discretization scheme. The reconstruction based schemes available in ANSYS FLUENT are Geo-Reconstruct and Donor-Acceptor. The discretization schemes available with explicit scheme for VOF are First Order Upwind, Second Order Upwind, CICSAM, Modified HRIC, and QUICK.

A single momentum equation is solved throughout the domain, and the resulting velocity field is shared among the phases. The momentum equation, shown below, is dependent on the volume fractions of all phases through the properties ρ and μ.

$$\frac{\partial}{\partial t}(\rho\vec{\upsilon}) + \nabla\cdot(\rho\vec{\upsilon}\vec{\upsilon}) = -\nabla p + \nabla\cdot\left[\mu(\nabla\vec{\upsilon} + \nabla\vec{\upsilon}^{T})\right] + \rho\vec{g} + \vec{F}$$

The energy equation, also shared among the phases, is shown below.

$$\frac{\partial}{\partial t}(\rho E) + \nabla\cdot(\vec{\upsilon}(\rho E + p)) = \nabla\cdot(k_{eff}\nabla T) + S_h$$

The VOF model treats energy, E, and temperature, T, as mass-averaged variables:

$$E = \frac{\sum_{q=1}^{n} a_q \rho_q E_q}{\sum_{q=1}^{n} a_q \rho_q}$$

, where E_q for each phase is based on the specific heat of that phase and the shared temperature. The properties ρ and k_{eff} (effective thermal conductivity) are shared by the phases. The source term, S_h, contains contributions from radiation, as well as any other volumetric heat sources.

The Mixture model

The mixture model is a simplified multiphase model that can be used in different ways. It can be used to model multiphase flows where the phases move at different velocities, but assume local equilibrium over short spatial length scales. It can be used to model homogeneous multiphase flows with very strong coupling and phases moving at the same velocity and lastly, the mixture models are used to calculate non-Newtonian viscosity.

The mixture model can model n phases (fluid or particulate) by solving the momentum, continuity, and energy equations for the mixture, the volume fraction equations for the secondary phases, and algebraic expressions for the relative velocities. Typical applications include sedimentation, cyclone separators, particle-

laden flows with low loading, and bubbly flows where the gas volume fraction remains low.

The mixture model is a good substitute for the full Eulerian multiphase model in several cases. A full multiphase model may not be feasible when there is a wide distribution of the particulate phase or when the interphase laws are unknown or their reliability can be questioned. A simpler model like the mixture model can perform as well as a full multiphase model while solving a smaller number of variables than the full multiphase model.

The mixture model, like the VOF model, uses a single-fluid approach. It differs from the VOF model in two respects:

- The mixture model allows the phases to be interpenetrating. The volume fractions a_q and a_p for a control volume can therefore be equal to any value between 0 and 1, depending on the space occupied by phase q and phase p.
- The mixture model allows the phases to move at different velocities, using the concept of slip velocities. (Note that the phases can also be assumed to move at the same velocity, and the mixture model is then reduced to a homogeneous multiphase model.)

The continuity equation for the mixture is:

$$\frac{\partial}{\partial t}(\rho_m) + \nabla \cdot (\rho_m \overrightarrow{\upsilon_m}) = 0$$

, where $\overrightarrow{\upsilon_m}$ is the mass-averaged velocity:

$$\overrightarrow{\upsilon_m} = \frac{\sum_{k=1}^{n} a_k \rho_k \overrightarrow{u_k}}{\rho_m}$$

And ρ_m is the mixture density:

$$\rho_m = \sum_{k=1}^{n} a_k \rho_k$$

a_k is the volume fraction phase k.

The momentum equation for the mixture can be obtained by summing the individual momentum equations for all phases. It can be expressed as:

$$\frac{\partial}{\partial t}(\rho_m \vec{\upsilon}_m) + \nabla \cdot (\rho_m \vec{\upsilon}_m \vec{\upsilon}_m) = -\nabla p + \nabla \cdot \left[\mu_m (\nabla \vec{\upsilon}_m + \nabla \overrightarrow{\upsilon_m}^T) \right] + \rho_m \vec{g} + \vec{F} + \nabla \cdot (\sum_{k=1}^{n} a_k \rho_k \vec{u}_{dr,k} \vec{u}_{dr,k})$$

, where n is the number of phases, F is a body force, and μ_m is the viscosity of the mixture:

$$\mu_m = \sum_{k=1}^{n} a_k \mu_k$$

And $\vec{u}_{dr,k}$ is the drift velocity for secondary phase k:

$$\vec{u}_{dr,k} = \vec{u}_k - \vec{u}_m$$

The energy equation for the mixture takes the following form:

$$\frac{\partial}{\partial t}(a_k \rho_k E_k) + \nabla \cdot \sum_{k=1}^{n} (a_k \vec{\upsilon}_k (\rho_k E_k + p)) = \nabla \cdot (k_{eff} \nabla T) + S_E$$

, where k_{eff} is the effective conductivity ($\Sigma\ a_k(k_k + k_t)$), where k_t is the turbulent thermal conductivity, defined according to the turbulence model being used). The first term on the right-hand side of the above equation represents energy transfer due to conduction. S_E includes any other volumetric heat sources.

From the continuity equation for secondary phase p, the volume fraction equation for secondary phase p can be obtained:

$$\frac{\partial}{\partial t}(a_p \rho_p) + \nabla \cdot (a_p \rho_p \overrightarrow{\upsilon_m}) = -\nabla \cdot (a_p \rho_p \vec{u}_{dr,p}) + \sum_{q=1}^{n} (\dot{m}_{qp} - \dot{m}_{pq})$$ [24].

3 Two dimensional project

A description of the simulation done in two dimensions and the parameters used are presented in this chapter. The different tank contents behavior and the effect of insulation thickness are examined using ANYS FLUENT. Finally, the whole procedure and the results for the simulation of LNG evaporation are displayed.

3.1 ANSYS 2D geometry and mesh design issues

Considering that the 53.400 OHS LNG trailer is the only one supplier that provides data about the thickness of insulation, we based our work on this design. The semi-trailer tank specifications are shown in the next figure.

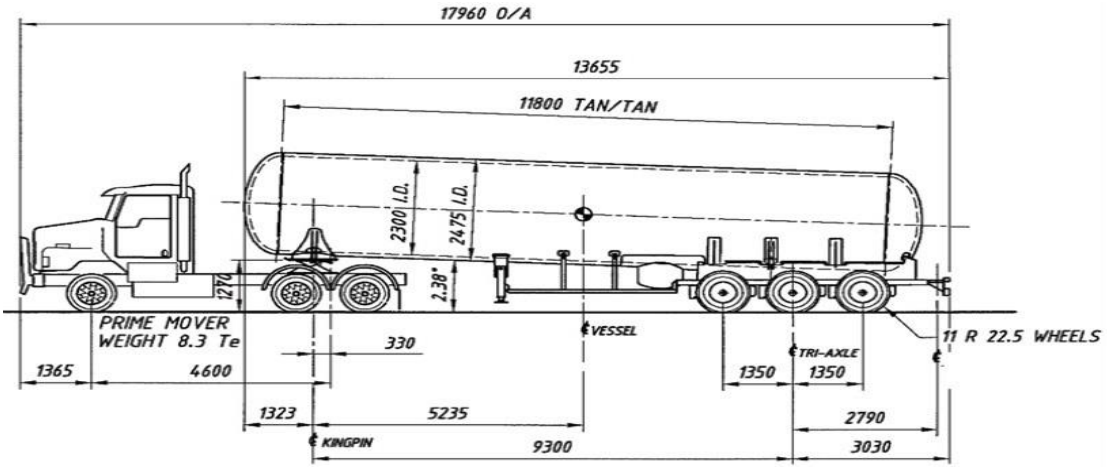

3.1 OHS trailer specifications[14]

The thickness of insulation based on this drawing can be calculated at 87,5mm. However, double size insulation thickness (175mm) is considered for these first experiments in order to compare heat flow dependency on insulation thickness. As a consequence, the first step for our work is to sketch the above drawing using ANYS Design Modeler. The tank of the trailer has been designed inside a rectangle of air (35,4x9m), because our intention is to model the interaction of the tank with the ambient environment. The air rectangle dimensions are chosen carefully in order to simulate the turbulent movement of air outside the tank. Figure 3.2 presents this first model sketch at Design Modeler, where all dimensions are expressed in millimeters.

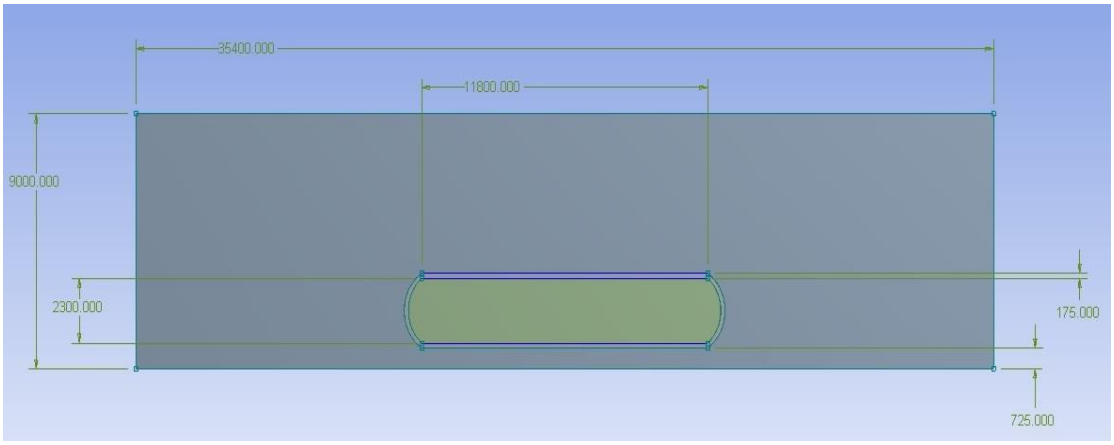

3.2 Design Modeler Sketch

The next step after sketching the tank and the air rectangle is to define the three surfaces of our interest. To separate each surface from the others, we use the Boolean function of the Modeler. The result of this procedure is to create three separate surface bodies for the inner vessel of the tank, the insulation and the ambient air. Another thing that needs attention is to consider the three surface bodies as one part consisting of three surface bodies. In case that we assume three different parts of surface bodies the interaction among surface bodies cannot be simulated because ANSYS recognizes the three bodies isolated from each other. In other words, there is no heat flux from one surface to the other.

The next important step of the simulation is to define the mesh of the model. A dense mesh could be more accurate but would increase the computing requirements. As a consequence, a carefully chosen mesh should balance between these two contradictions. However, the results of the model must be independent from the mesh meaning that a denser mesh should give slightly different results. We can now understand why ANSYS Meshing is an important tool to our simulation.

The appropriate mesh generation using ANSYS Meshing is the next goal of our work. It would be helpful to realize that the temperature differences along insulation surface are so high that it is advisable to condense the mesh locally. Consequently, we use 10mm element size meshing for insulation surface and 500mm for the other two surfaces. In addition, we activate medium relevance center control to smooth the transition among surfaces. Apart from this, it is necessary to name boundaries edges and interior surfaces before importing mesh in FLUENT. The named selections of our case are depicted in figure 1.3.

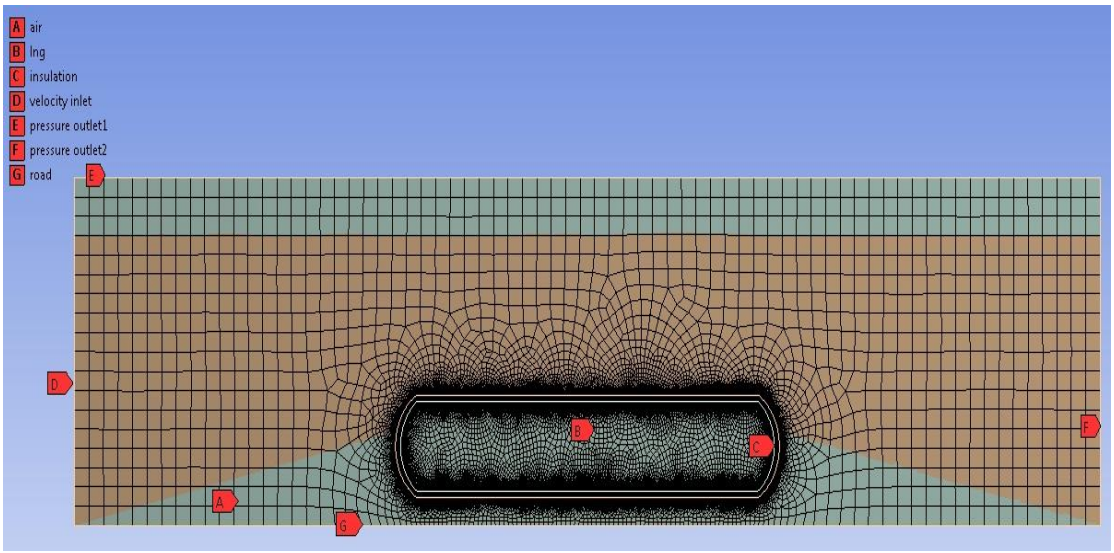

3.3 Mesh details

The left edge of the rectangle is defined as the velocity inlet, while the right one is assumed as the pressure outelet2. The bottom edge is named as road, while the upper one as pressure outlet1. The inner vessel surface is named as lng, while insulation and air surfaces kept their original names. The logic behind this name selection is that air flows from the right edge and exits from the upper and left edges. However, the exit of air from the upper boundary will be re-considered later due to solution convergence problems.

3.2 Initial 2D FLUENT parametric considerations

A series of calculations in FLUENT for different vessel contents are presented in next paragraphs, having completed with the mesh generation. These are initial tests for comparison reasons. They do not correspond to real conditions and do not take into consideration the phase envelope of each component. The behavior of different fluids at different air velocities are going to be checked. Nevertheless, all cases present some common features.

The first step using FLUENT is to import mesh files created according to the previous section. As mentioned before, there are three cell zones (air, insulation, lng) defined in ANSYS Meshing. Air and lng zones are defined as fluids while insulation is defined as solid. Steel is considered as the insulation material for these tests, while the lng zone material will be variable. In addition, steel is also selected as the road and pressure outlet2 material. Finally, the upper edge was transformed from pressure outlet to wall due to air backflow problems while exiting the geometry from the upper boundary that incommode the model convergence.

The solver is selected as pressure-based and transient because our concern is to check heat fluxes during time. A time period of 12 hours or 43.200 seconds is assumed for the simulations. Time step is initially set at 0.01 second in order to facilitate convergence, while it is gradually and carefully increased until 15 seconds. Energy equations are involved in calculations, while standard k-epsilon model is chosen for viscosity modeling. However, gravity effects are not included in calculations. Pressure-velocity coupling is solved using SIMPLE algorithm, while first order upwind spatial discretization is used for energy, momentum and turbulent kinetic energy. The under relaxation factors are the default ones for FLUENT 12.

Another important part of the simulation is the boundaries conditions. As explained in the previous section, velocity inlet, road pressure outlet1 and 2 are the rectangle boundaries. In addition to these, the air-insulation and insulation-lng boundaries are added as the interface boundaries among the three surfaces. The last two are defined as coupled with their shadows (boundaries created from FLUENT) to enable heat flow through the surfaces. On the other hand, road and pressure outlet1 (which is already considered as wall) are set as adiabatic walls with zero heat fluxes. Velocity inlet is set at 400K temperature, 5m/s velocity magnitude, 2% turbulent intensity and 9m hydraulic turbulence diameter (as much as the rectangle height of air). The same turbulence parameters are chosen for pressure outlet2 with the exception that temperature is defined at 300K.

Except from boundary conditions, initial conditions must be determined. Initialization is based on velocity inlet conditions, while different temperatures are patched in insulation and lng surfaces depending on vessel's content. Furthermore, velocity magnitude of the inlet is changed in some cases to examine its effect on heat flows. As a consequence, five different vessel content cases are going to be presented accompanied by their results. The fluids and solids used with their properties are presented in table 3.1, where Prandtl number is calculated from $\mathrm{Pr} = \frac{c_p \mu}{k}$ (c_p specific heat, μ viscosity, k thermal conductivity, ρ density). LNG properties are based on

table 1.2, while all other material properties are found in FLUENT database. In addition all properties are supposed constant and independent.

	$c_p(\frac{j}{kg \cdot K})$	$\mu(Pa \cdot s)$	$k(\frac{W}{m \cdot K})$	$\rho(\frac{kg}{m^3})$	Pr
Air	1006,43	1,79E-05	0,0242	1,225	0,744
Water vapor	2014	1,34E-05	0,0261	0,5542	1,034
Water liquid	4182	1,00E-03	0,6	998,2	6,991
Methane	2222	1,09E-05	0,0332	0,6679	0,728
LNG	3450	1,46E-04	0,193	424,53	2,610
Steel	502,48		16,27	8030	

Table 3.1 Used materials properties [4]

3.3 Examined cases results and comparisons

Seven different simulations are presented in the next paragraphs based on the data and settings mentioned before. The phase of the contents at each temperature is beyond our interest at this early stage. As a consequence, these first results are grounded on material properties. First considerations include the use of air, water liquid and water vapor at 275K consecutively as the content of the inner tank. The same temperature is patched to the insulation. On the other hand, second thoughts include the use of methane and LNG as the vessel content at 113K. In addition, the behavior of methane is more examined by altering velocity magnitude at the inlet. Therefore, three air velocity magnitudes are selected for methane case (5, 10 and 15 m/s).

Time step is manually increased from very low values to higher ones in order to facilitate convergence. However, each case needs different time step treatment. For instance, solution does not converge for time steps higher than 8 seconds in water liquid case. This is the reason why there is no homogeneity in time points and why data FLUENT files are saved for different time points in each case.

In the next figures, temperature contours inside the vessel and air velocity vectors outside the vessel are presented for different time points. In case of temperature contours, figures are zoomed around the vessel in order to present the different temperatures inside insulation. Time is depicted in each case at the left corner of the figure in seconds. Air velocity vectors are almost the same during time and as a result only one time case is presented for each fluid. Figures 3.4-3.10 depict the evolution of temperature inside the vessel for each case due to the tank interface with external air. Four intermediate time points are selected for each case. The windows sequence in each figure is horizontal from the upper left window to the bottom right one (it can be concluded from the time point of each window). Figures 3.11a-b present air velocity vectors of all cases. Sharing the same sequence order with temperature contours figures, air, vapor water, liquid water, methane, methane10, methane15 and LNG cases are depicted. The last one window in figure 3.11b displays the mesh of the model as imported in FLUENT.

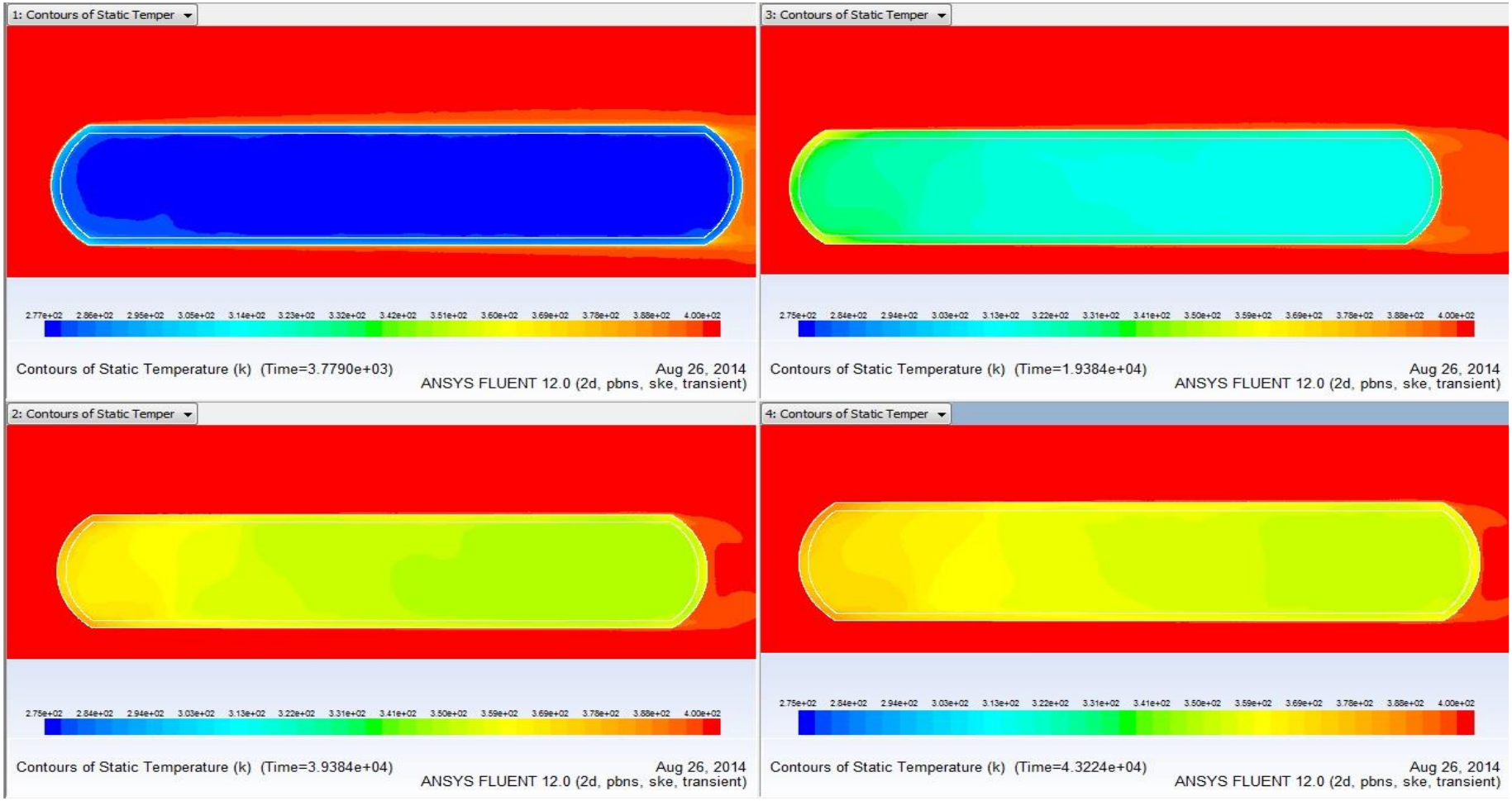

3.4 Air temperature contours

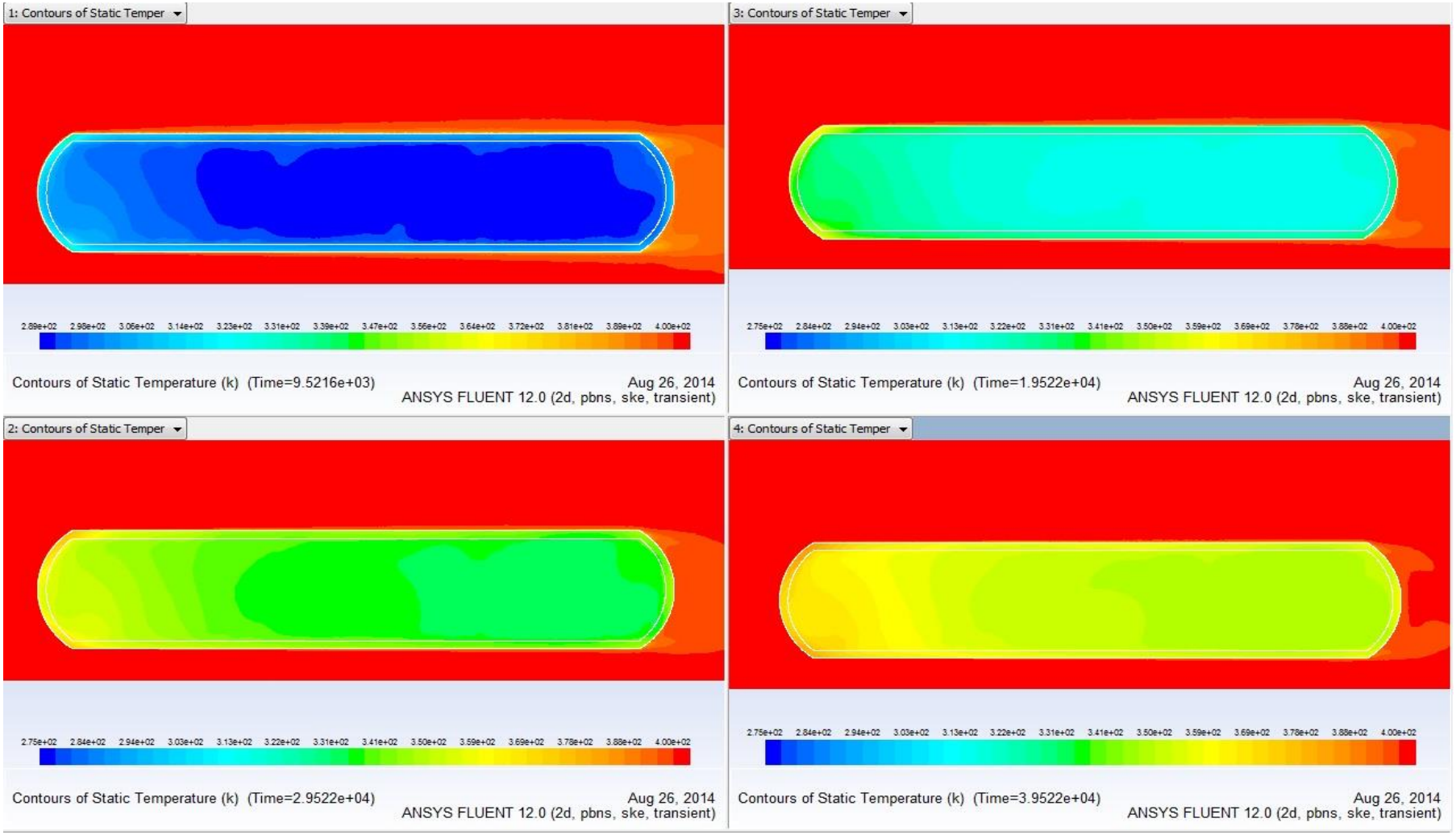

3.5 Water vapor temperature contours

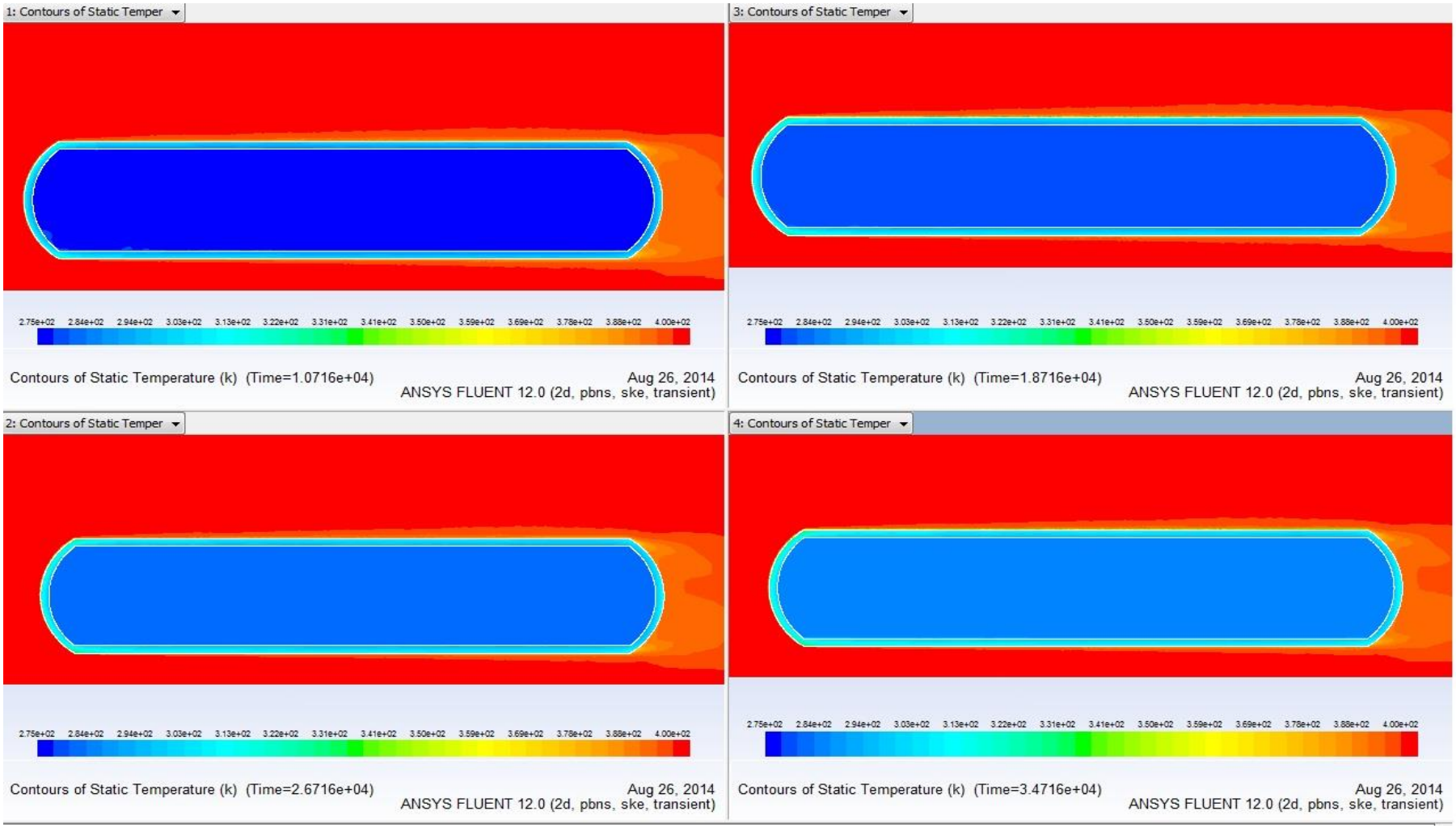

3.6 Water liquid temperature contours

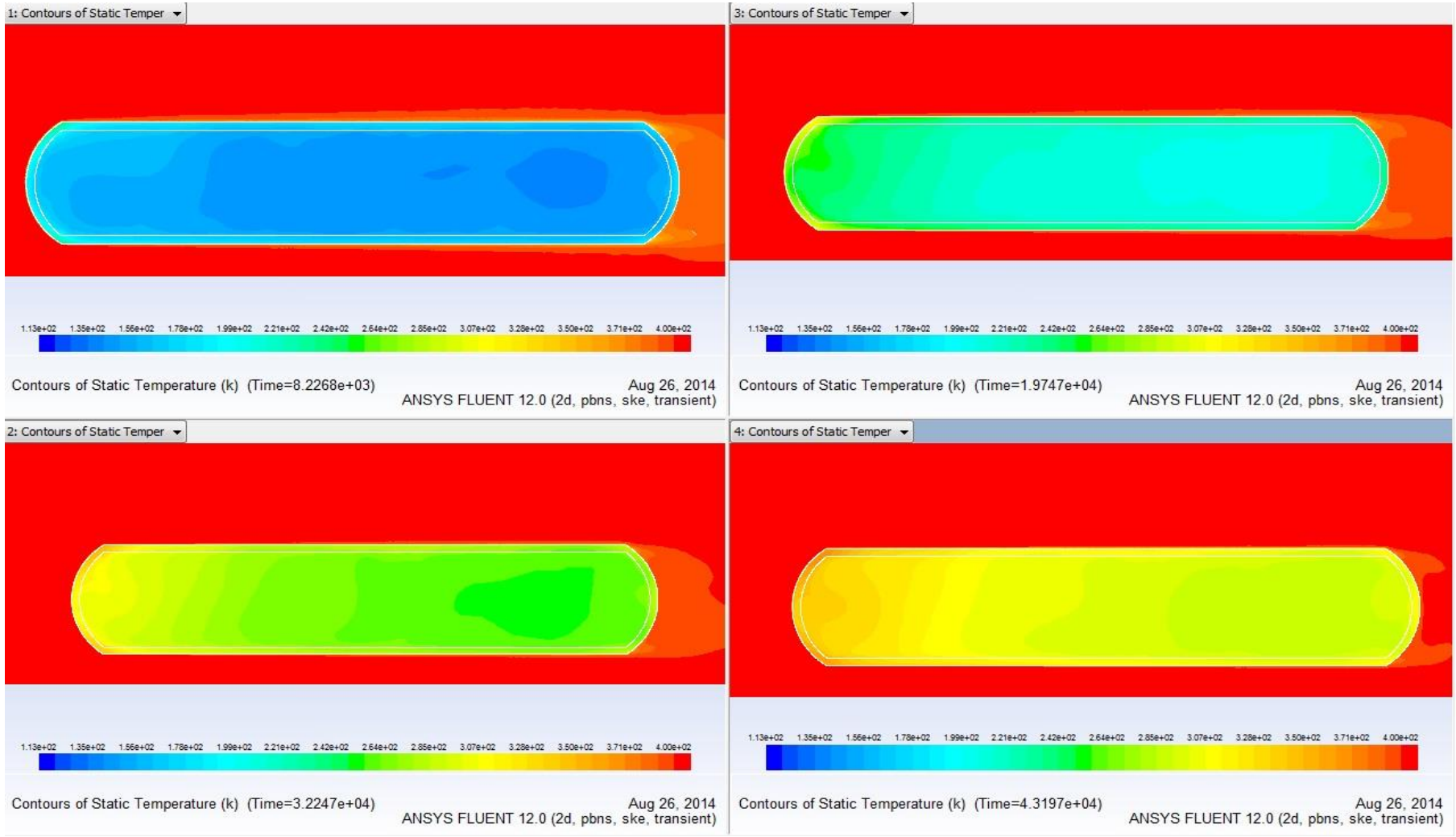

3.7 Methane temperature contours

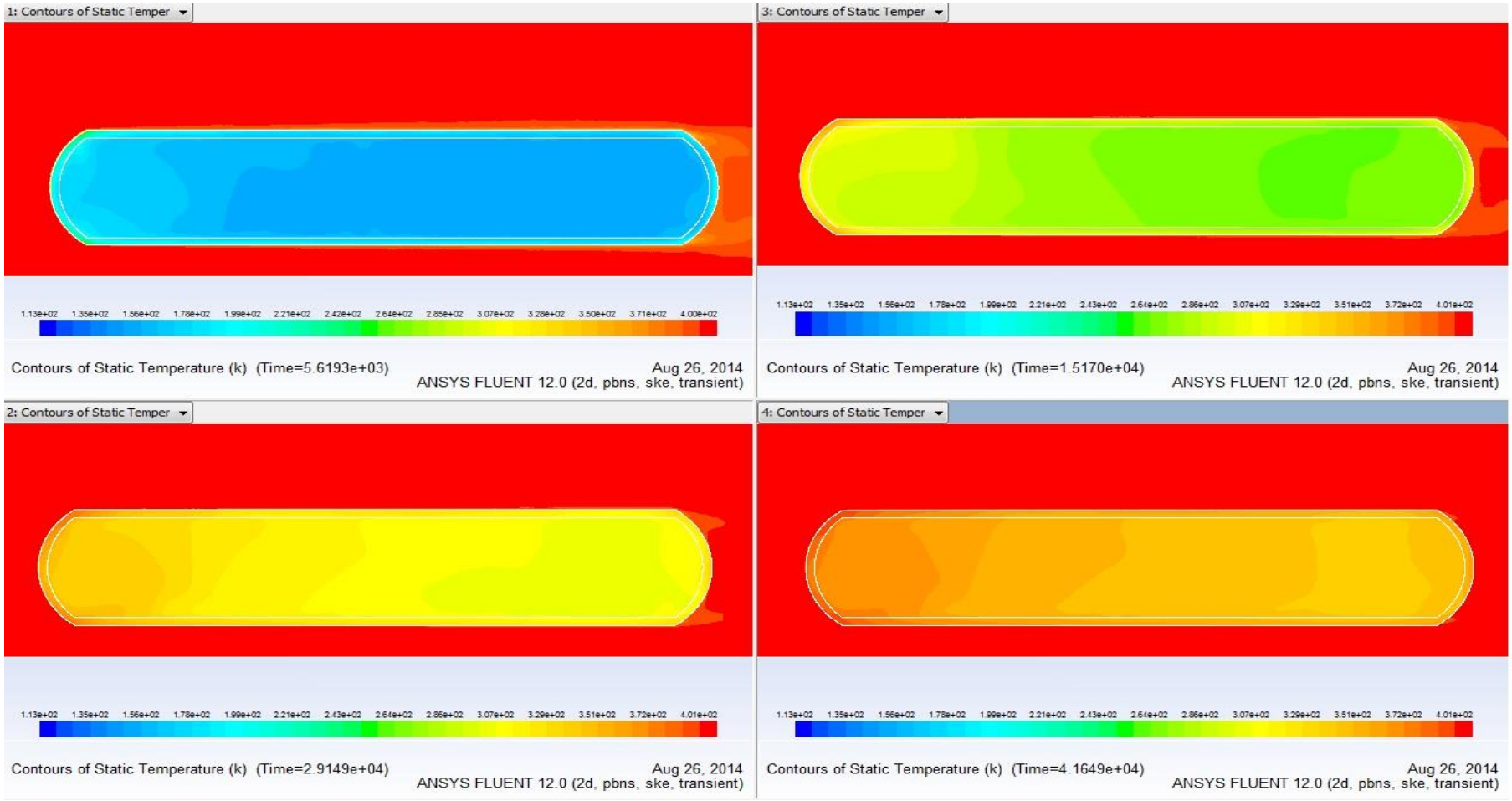

3.8 Methane temperature contours with inlet velocity 10m/s

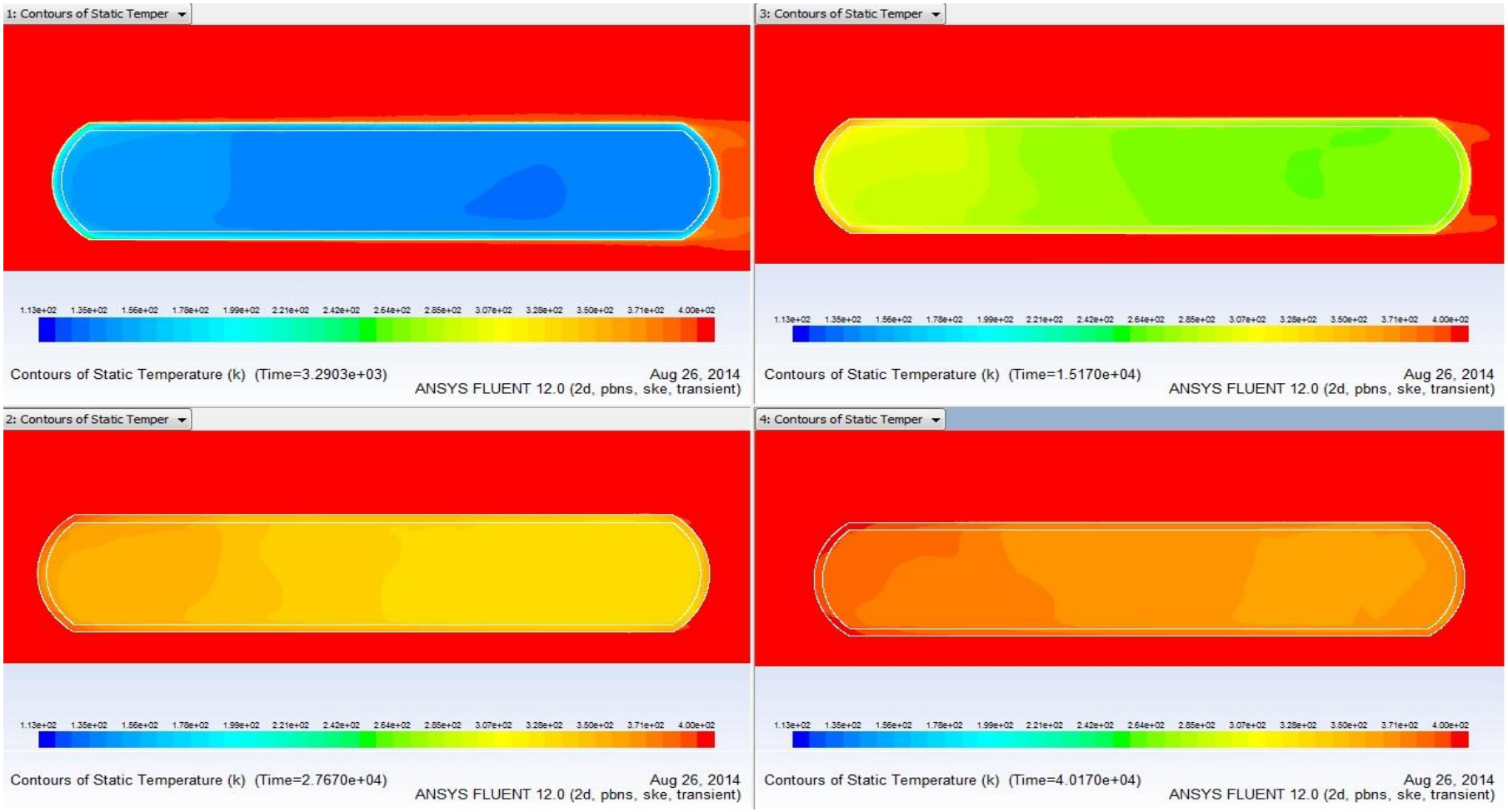

3.9 Methane temperature contours with inlet velocity 15m/s

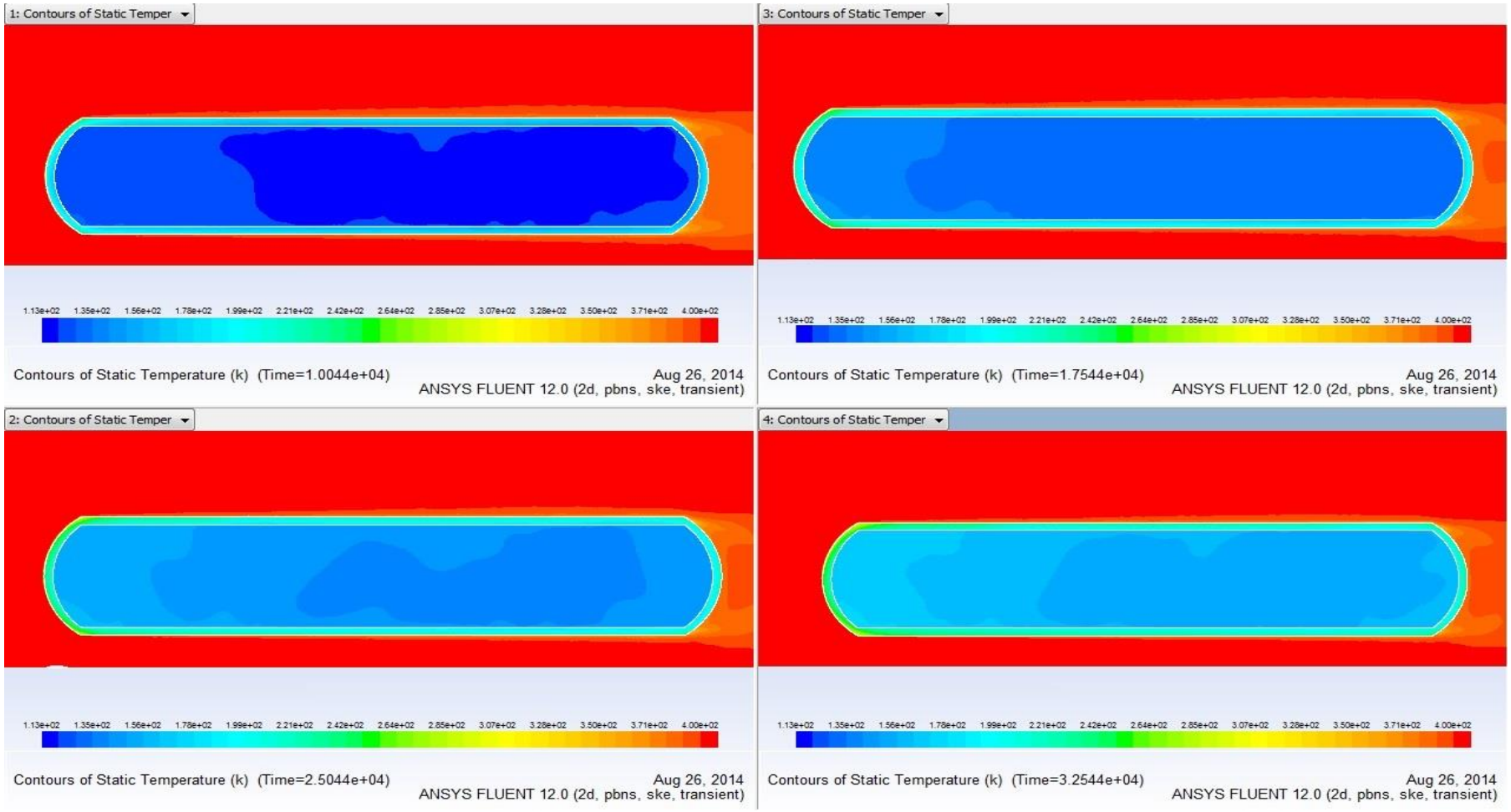

3.10 LNG temperature contours

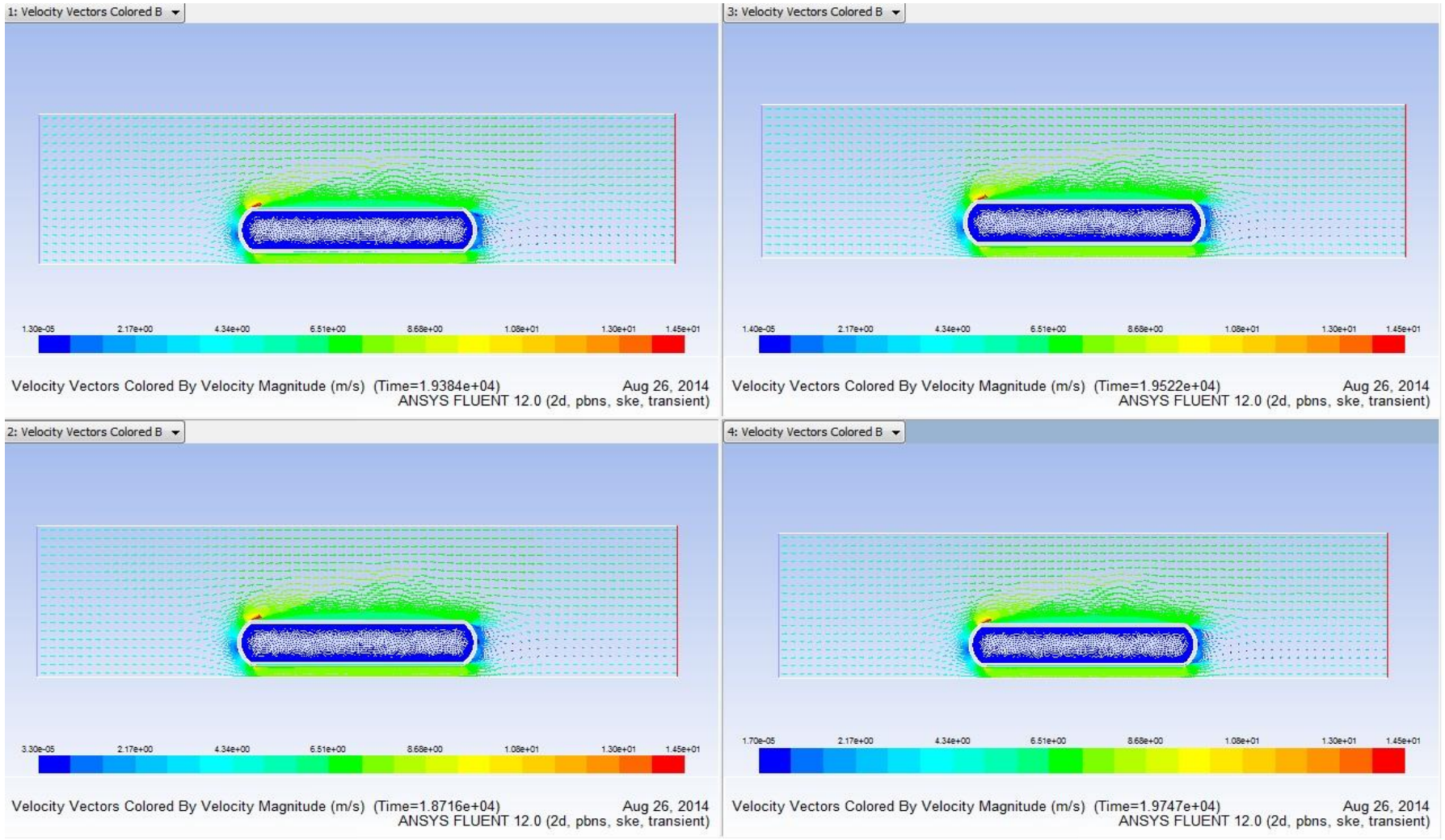

3.11a External air velocity vectors for all cases

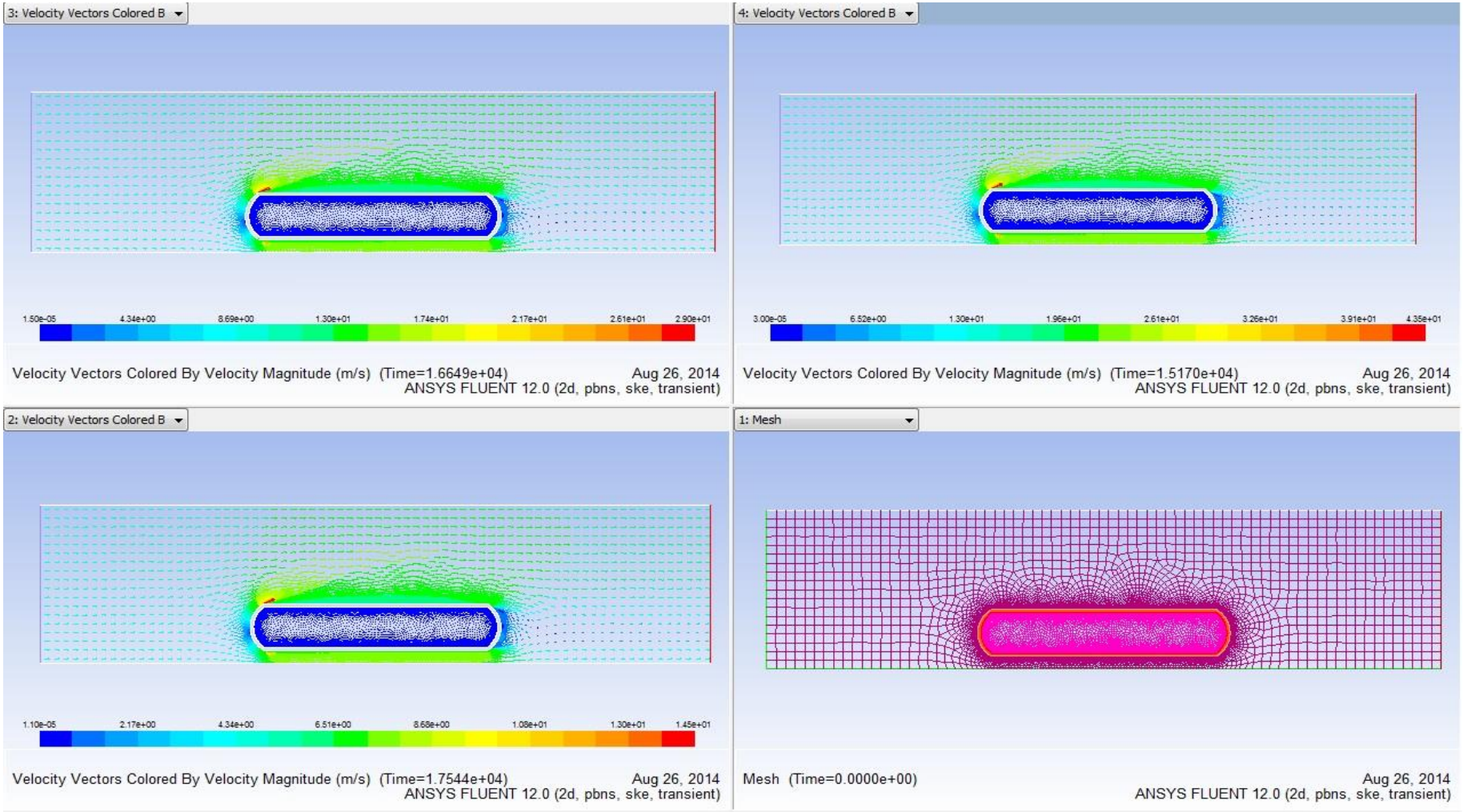

3.11b External air velocity vectors for all cases

Firstly, the left side of the tank is faster heated than the right in all cases, as expected considering that the air inlet is at the left. Comparing the above figures, we can conclude that temperature exhibits the higher increase in methane case. In addition, the higher the air velocity at the inlet the higher the temperature increases. On the other hand, liquid water temperature changes with the slowest pace compared to other materials. Moreover, LNG is slower heated than methane. Finally, vapor water and air display similar behaviors.

The area-weighted average temperature of the lng surface is monitored and recorded in all cases, in an attempt to compare the average temperatures. The result of this procedure is to create a record of average temperatures inside the tank during time for all cases. However, the initial temperature is different in some cases. As a result, the fraction of average temperature to initial temperature is used in order to compare the temperature increases of different cases. Figure 3.12 displays this fraction evolution during time for the seven cases, while table 3.2 presents the final and initial temperatures of all cases. The time point of final temperature is also included for each case.

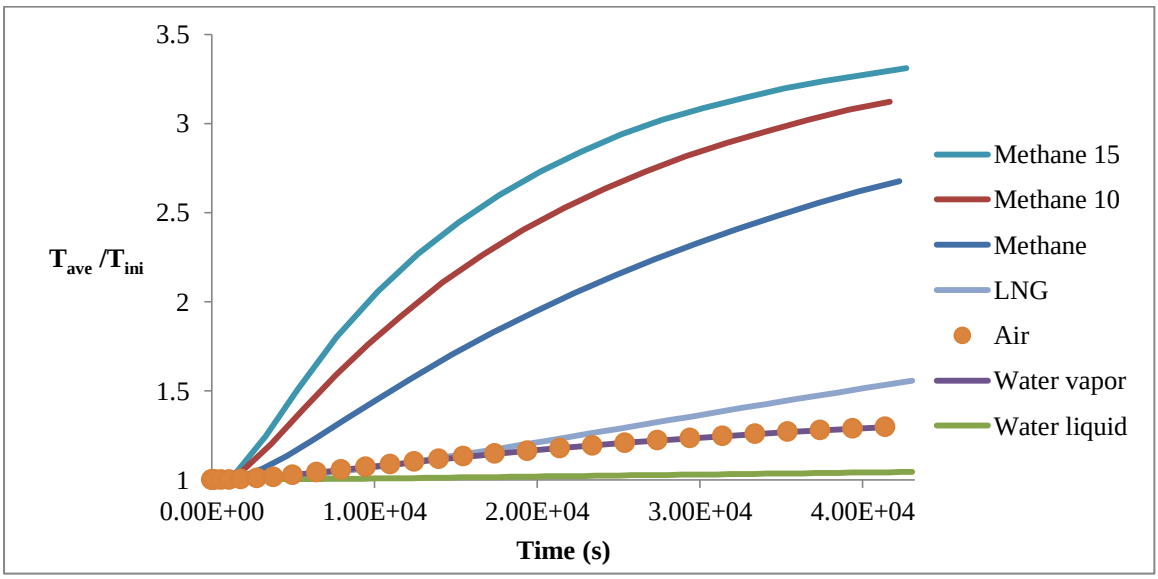

3.12 Area-weighted average temperature inside tank

	$T_{in}(K)$	$T_{fin}(K)$	$Time(s)$
Methane 15	113	374,0	42.670
Methane 10	113	352,7	41.649
Methane	113	302,5	42.247
LNG	113	175,8	43.044
Air	275	356,4	41.384
Water vapor	275	356,6	41.522
Water liquid	275	287,1	43.049

Table 3.2 Initial and final temperatures

On the other hand, external air flows in similar manner in all cases. Air velocity increases at the upper and bottom edge of the tank, while it decreases at the front and back side. The flow is turbulent around the tank and laminar at the inlet and exit.

Highest velocity point is the one at the upper left corner of the tank (almost three times the velocity at the inlet). Naturally, higher velocities are displayed in cases of methane where we use higher velocities at the inlet. However, the same flow characteristics are presented also in these cases (triple velocity at the upper left corner, turbulent flow around tank).

3.4 Insulation thickness effect

The next step to our work is to reduce insulation thickness to its normal size (half of the previous case). The new sketch of the half insulation thickness as designed in Design Modeler is depicted in figure 3.13. The results of this thickness for the area-weighted average lng temperature divided by initial temperature using different tank contents are presented below. In addition, graphs displaying the temperature evolution of the different tank contents in respect to insulation thickness cases are added below. Each material used inside the tank is displayed with the same kind of line for both the case of half insulation and the initial case. Finally, a table which includes the final temperatures and the corresponding time for the two insulation cases is presented.

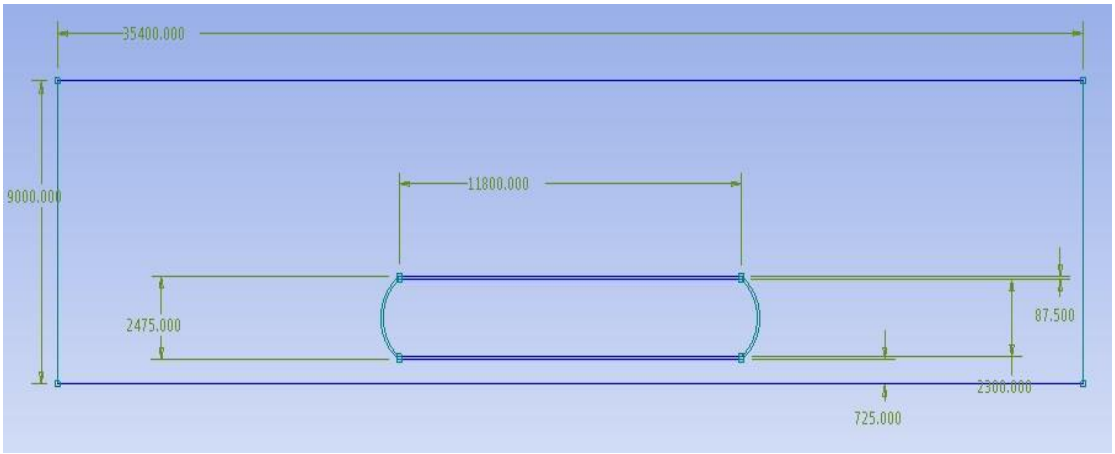

3.13 Half insulation thickness sketch

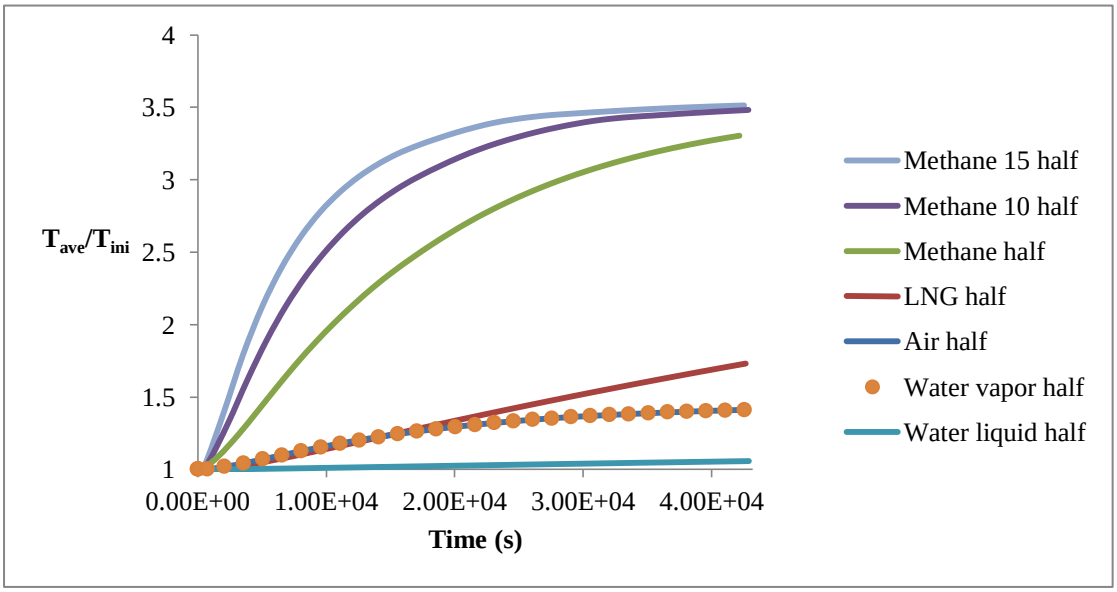

3.14 Area weighted average temperature inside tank for half insulation thickness

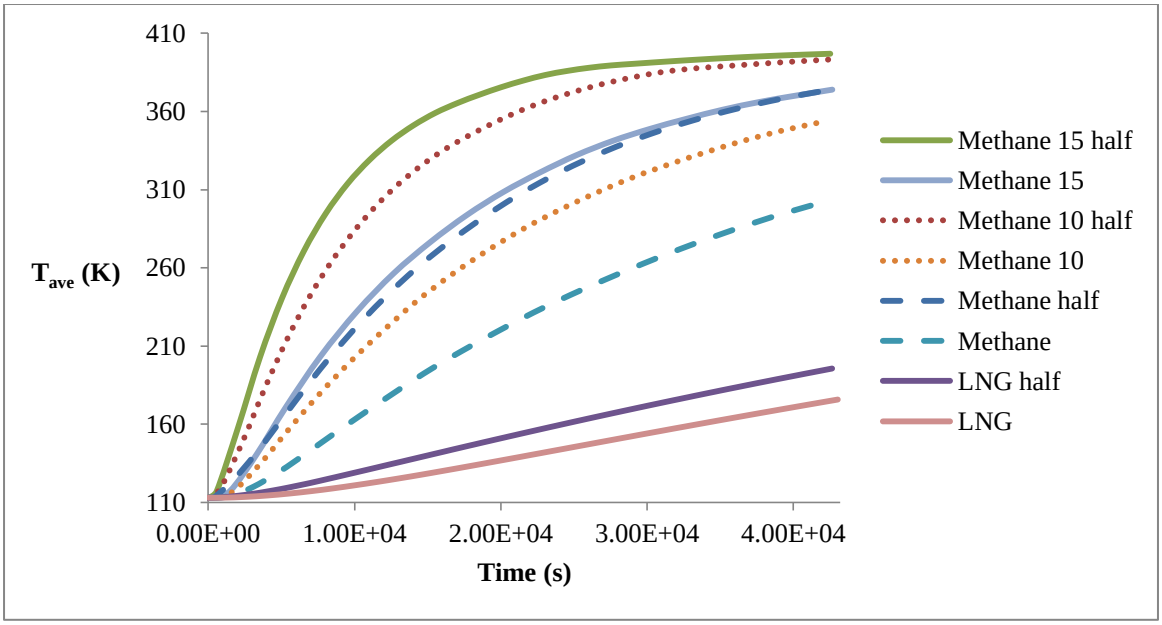

3.15a Temperature evolution for the two insulation cases

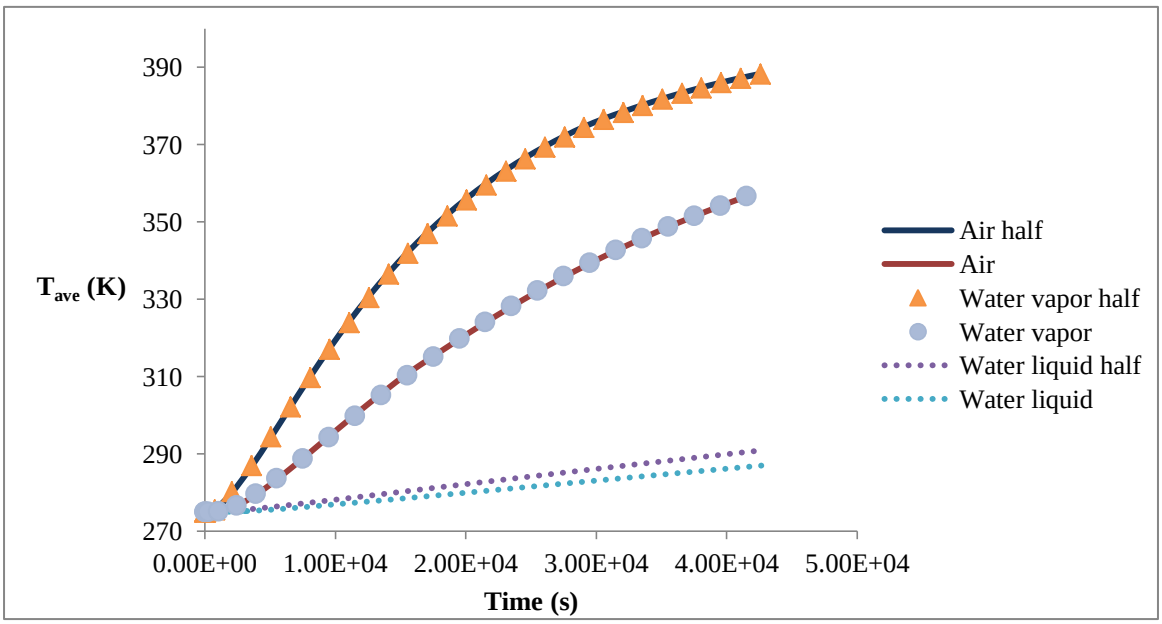

3.15b Temperature evolution for the two insulation cases

	$T_{fin}(K)$	$Time(s)$	$T_{fin}(K)$ Half	$Time(s)$ Half
Methane 15	374,0	42.670	396,9	42.530
Methane 10	352,7	41.649	393,4	42.867
Methane	302,5	42.247	373,3	42.165
LNG	175,8	43.044	195,6	42.655
Air	356,4	41.384	388,3	42.553
Water vapor	356,6	41.522	388,2	42.583
Water liquid	287,1	43.049	291,0	42.903

Table 3.3 Final temperatures for the two insulation cases

Summarizing the above results, we can conclude that the thicker the insulation, the lower the heat added to the tank. As a result, LNG is expected to be heated faster in the case of the tank offered by OHS than the one used at the beginning of this chapter. However, liquids (water and LNG) are less dependent to insulation thickness compared to gases because their temperature increase is apparently lower than gases. Finally, air and vapor water behave in the same manner.

3.5 LNG evaporation

LNG evaporation is based on equation(1): $MassTransferRate = \frac{r \cdot VF_l \cdot \rho_l \cdot (T_l - T_{sat})}{T_{sat}}$,

where r is under relaxation factor (set at 0,1), VF_l is Liquid volume fraction, ρ is Liquid density, T_l is Liquid temperature and T_{sat} is saturated temperature (set at 111K or -162^0C) as mentioned in Chapter 1 according to [4]. However, there are two regions of fluid flows in our work; one region with single phase flow (air) and another one with multiphase flow (inside tank). Nevertheless, FLUENT models cannot be adapted for different regions. As a consequence, the proposed strategy to simulate evaporation includes dividing the problem into two sub-cases. The first one is used to calculate heat fluxes from ambient air to the tank using a single phase model. The second one isolates the tank from air and simulates LNG evaporation inside it using a multiphase model based on heat fluxes calculated before.

3.5.1 Heat fluxes calculation

The scope of this simulation is to calculate the heat absorbed by the tank in order to use this data to the second one. For this purpose, we use sketches and generated mesh of the previous section (87,5mm insulation), while we assume that tank is fully filled with LNG. However, additional models and materials are used to this case. Hence, gravitational acceleration at y-axis is set at 9,81 m/s^2. Moreover, the Boussinesq approximation is also included to simulate natural convection. The specified operating density of air is equal to 1,225 kg/m^3. Furthermore, standard k-e model is enabled for turbulent air flows, while surface to surface model is activated to include radiation heat fluxes.

The FLUENT solar calculator provides information about the solar irradiation at Earth's surface in Thessaloniki (longitude $22^0$58', latitude $40^0$31'). The time of the simulation corresponds to the 21th day of June at 13:00 with good weather conditions. Provided this data, the total solar irradiation at a horizontal plane (direct + diffuse) is calculated at $995W/m^2$. As a consequence, the upper wall heat flux is defined accordingly, assuming that it is constant during this day. FLUENT 2D does not include solar calculator and as result we made this assumption in order to add solar irradiation to this case.

Apart from these, new materials are added to this simulation. Therefore, perlite under vacuum is used as the insulation material, while asphalt is the road material. The properties of these materials are presented in table 3.4. However, perlite thermal conductivity is not constant but temperature-depended, as mentioned in chapter 1. Hofmann suggested the following empirical equation to relate thermal conductivity with temperature $\lambda=a+bT^c$ ($a = 1{,}9112 \cdot 10^{-4}$; $b = 3{,}4757 \cdot 10^{-12}$; $c = 3{,}6783$) for 50 kg/m3 perlite density. As a consequence, a User Defined Function (UDF), presented below, is interpreted to express this correlation.

	Density (kg/m^3)	Specific Heat C_p ($j/kg \cdot K$)	Thermal Conductivity ($W/m \cdot K$)	Emissivity
Perlite	50	387	user-defined	0,55
Asphalt	2360	920	0,75	0,88

Table 3.4 Material properties [25]

```
#include "udf.h"
DEFINE_PROPERTY (cell_thcon, c, t)
{
real thc;
thc=1.9112e-4+pow(C_T(c,t), 3.6783)*3.4757e-12;
return thc;
}
```

3.16 Thermal conductivity UDF [26]

Air and road temperature is assumed to be 40^0C or 313K, while insulation and LNG temperature is fixed at 111K. Moreover, initial tank pressure is 8bar (800.000 Pascal). In addition, vehicle speed is supposed to be around 80km/h (approximately 22 m/s) and as a result this is the velocity magnitude at the inlet. The tank heating is simulated for 15 hours or 54.000 seconds which corresponds to a trip of 1200km. Finally, the upper wall, velocity inlet and pressure outlet are boundaries with unitary emissivity.

Our intention is to calculate the heat fluxes inside the tank and as a result a file containing the total surface heat fluxes at the inner wall of the tank was created. These fluxes refer to the area-weighted average and are recorded with respect to time. Figure 3.17 presents the above fluxes calculated by FLUENT. Furthermore, temperature, pressure and air velocity vectors at the end of time are displayed below. Insulation temperature is increased, while there is a slight temperature rise inside tank above 111K. This result reveals the effectiveness of perlite insulation. In addition, pressure inside tank is raised from 8 to 14bar. Finally, velocity vectors behave in similar manner with previous cases.

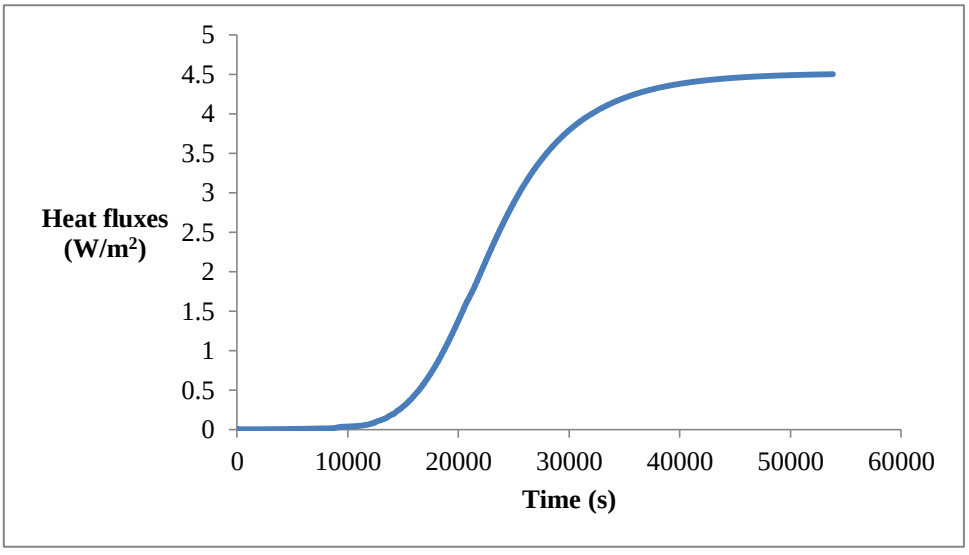

3.17 Inner tank wall heat fluxes

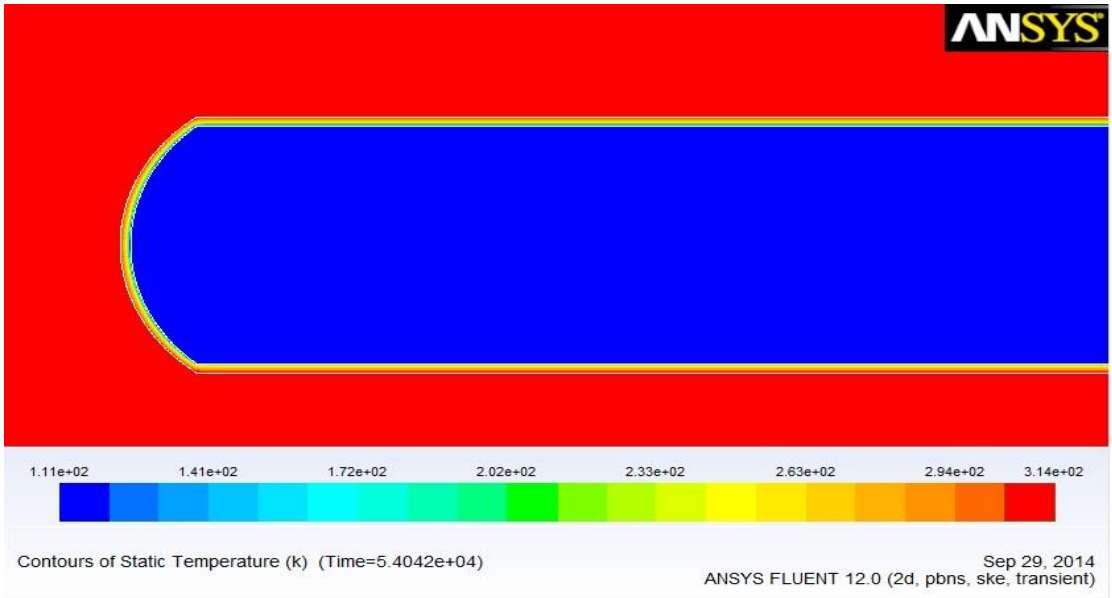

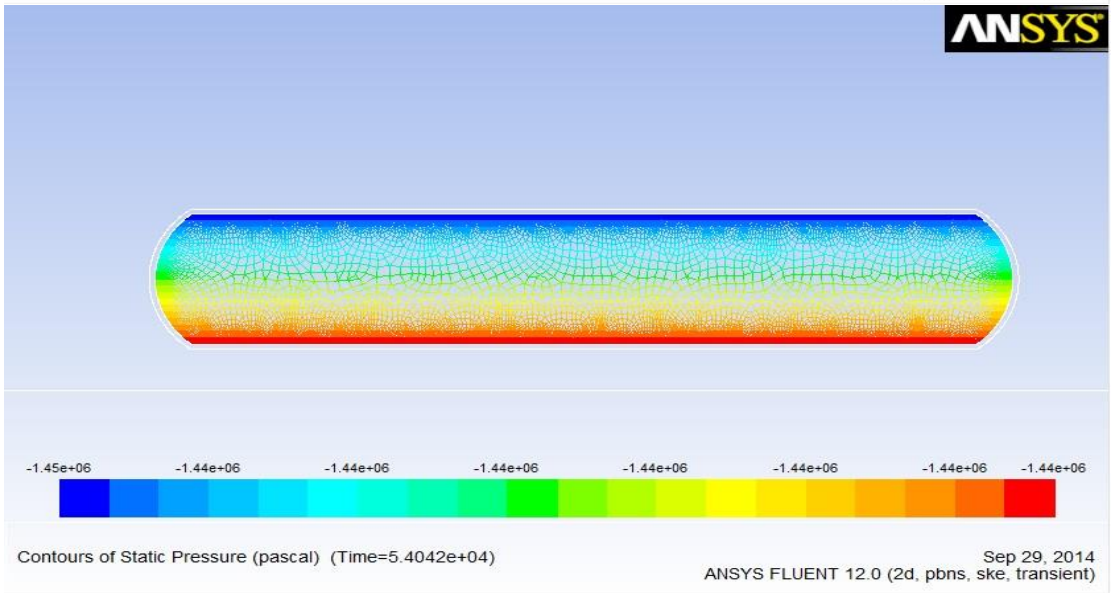

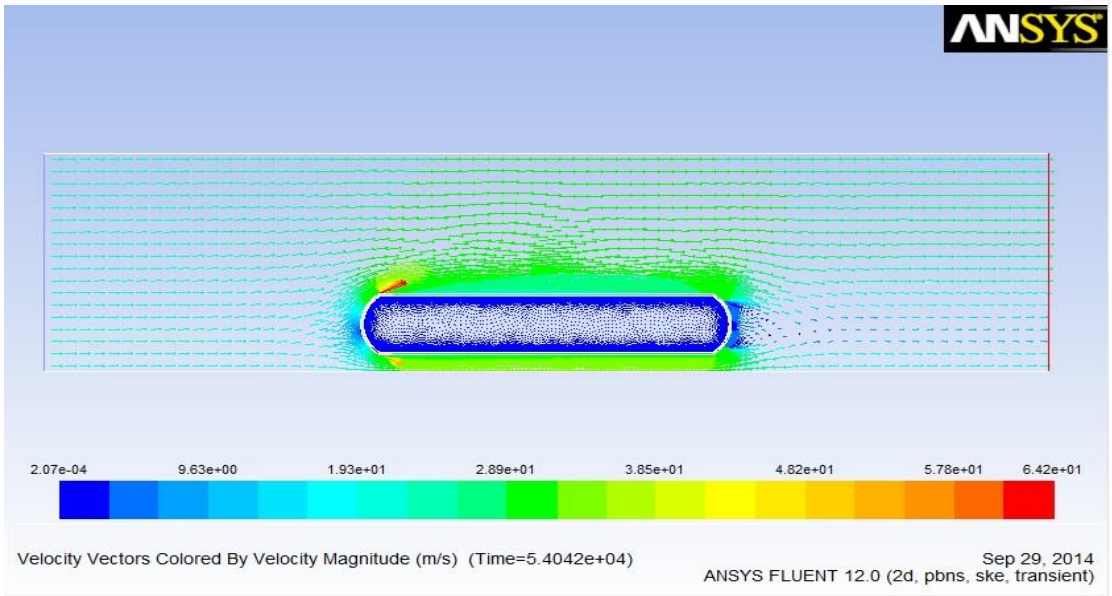

3.18 Temperature, pressure contours and velocity vectors at the end of time

3.5.2 LNG boil-off calculation

The first step for this calculation is to estimate the equation of heat fluxes calculated above with respect to time. If one equation is used for the whole range of time, a low quality approximation of heat fluxes is formed. As a consequence, it is recommended to divide the graph into two sections; the low values section until 10.000s and the high values section after this. Polynomial equations are used in order to estimate the two sections of the graph. E-views can provide us the coefficients of the fifth order equations used for estimation. The estimated equations are two presented below:

$$t \le 10.000s,\ y = 1,73e^{-21} \cdot x^5 - 2,45e^{-17} \cdot x^4 + 9,92e^{-14} \cdot x^3 + 1,16e^{-10} \cdot x^2 - 2,81e^{-7} \cdot x + 0,002161$$

$$t > 10.000s,\ y = -4,67e^{-22} \cdot x^5 + 8,17e^{-17} \cdot x^4 - 6,16e^{-12} \cdot x^3 + 2e^{-7} \cdot x^2 - 0.002727 \cdot x + 12.942$$

Calculated and estimated heat fluxes are presented for both sections below. These equations are going to be used in order to define the evolution of heat fluxes at the inner wall of the tank. Similarly, a new UDF is going to be written to include this evolution of fluxes.

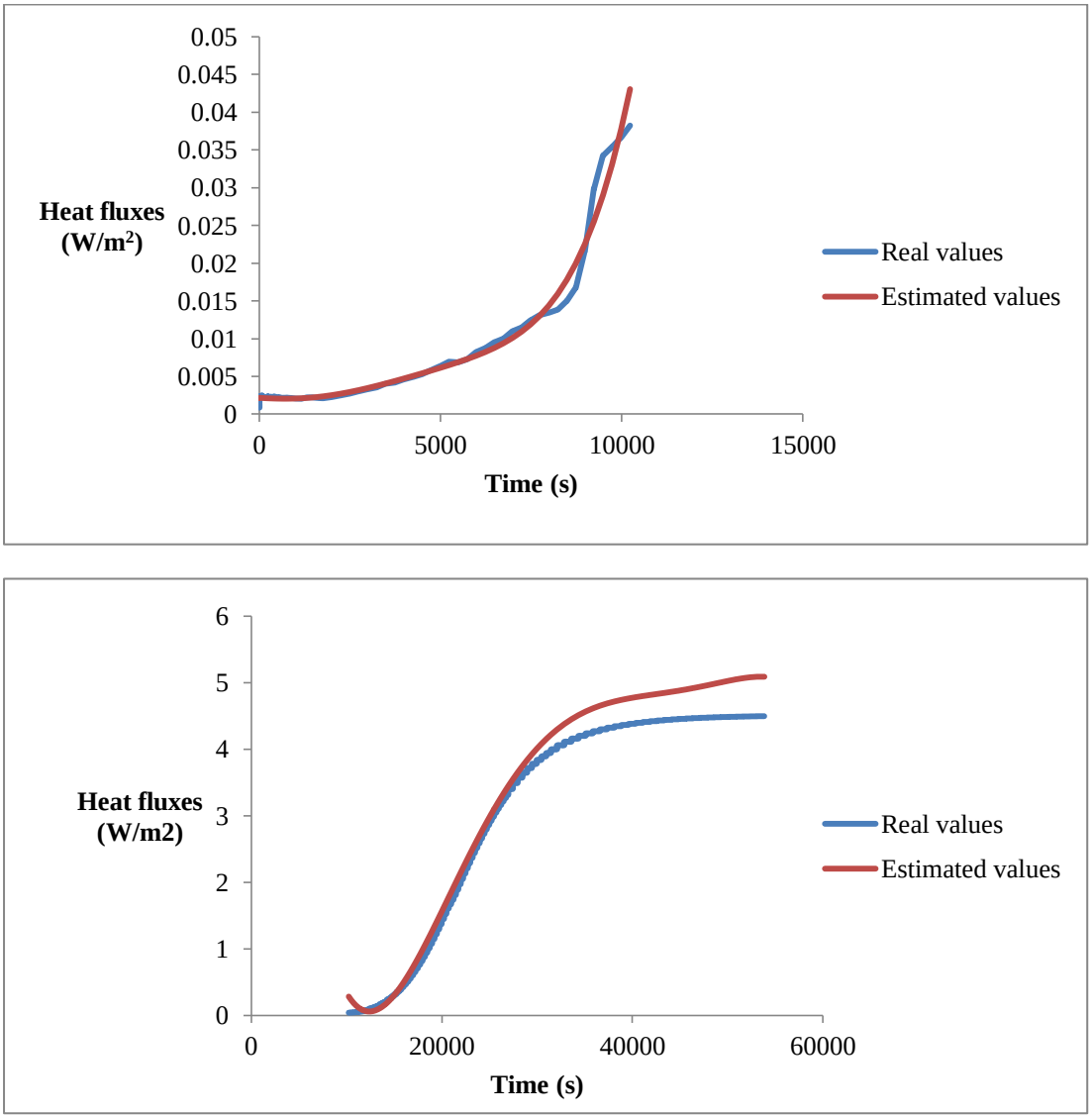

3.19 Real and estimated heat fluxes

Again, gravitational acceleration and Boussinesq approximation are enabled, while mixture model is used for multiphase flow. The number of Eulerian phases is two; LNG is considered as the primary phase and methane as the secondary. Hence, the assumption that LNG evaporates mainly to methane is done at this point. The schiller-naumann drag law for phase interaction was used to describe the drag between the spherical vapor particle (diameter =0.0002m) and surrounding LNG. On the other hand, flow inside tank is considered laminar.

It is mentioned at the beginning of this section that mass transfer will be based on (1). As a consequence the new UDF must consider the mass increase of methane based on (1) and simultaneously decrease LNG with the same amount. In addition, the energy absorbed by this procedure must be determined (E=Latent heat of vaporization*mass transfer). The new UDF including the wall heat fluxes and perlite thermal conductivity is presented below:

```
#include "udf.h"
#include "sg_mphase.h"
#define T_SAT 111
#define LAT_HT 51.03e5

DEFINE_SOURCE(liq_src, cell, pri_th, dS, eqn)
{
 Thread *mix_th, *sec_th;
 real m_dot_l;

 mix_th = THREAD_SUPER_THREAD(pri_th);
 sec_th = THREAD_SUB_THREAD(mix_th, 1);

 if(C_T(cell, mix_th)>=T_SAT){
  m_dot_l = -0.1*C_VOF(cell, pri_th)*C_R(cell, pri_th)*
          fabs(C_T(cell, pri_th) - T_SAT)/T_SAT;
  dS[eqn] = -0.1*C_R(cell, pri_th)*
    fabs(C_T(cell, pri_th) - T_SAT)/T_SAT;
                    }
 else {
  m_dot_l = 0.1*C_VOF(cell, sec_th)*C_R(cell, sec_th)*
          fabs(T_SAT-C_T(cell,mix_th))/T_SAT;

  dS[eqn] = 0.;

    }
 return m_dot_l;
}

DEFINE_SOURCE(vap_src, cell, sec_th, dS, eqn)
{
 Thread * mix_th, *pri_th;
 real m_dot_v;

 mix_th = THREAD_SUPER_THREAD(sec_th);
 pri_th = THREAD_SUB_THREAD(mix_th, 0);

 if(C_T(cell, mix_th)>=T_SAT){
  m_dot_v = 0.1*C_VOF(cell, pri_th)*C_R(cell, pri_th)*
          fabs(C_T(cell, mix_th) - T_SAT)/T_SAT;
  dS[eqn] = 0.;
                    }
```

```
else {
   m_dot_v = -0.1*C_VOF(cell, sec_th)*C_R(cell, sec_th)*
            fabs(T_SAT-C_T(cell,mix_th))/T_SAT;

   dS[eqn] = -0.1*C_R(cell, sec_th)*
     fabs(C_T(cell, sec_th) - T_SAT)/T_SAT;

      }
 return m_dot_v;
}

DEFINE_SOURCE(enrg_src, cell, mix_th, dS, eqn)
{
 Thread *pri_th, *sec_th;
 real m_dot;
 pri_th = THREAD_SUB_THREAD(mix_th, 0);
 sec_th = THREAD_SUB_THREAD(mix_th, 1);

 if(C_T(cell, mix_th)>=T_SAT){
   m_dot = -0.1*C_VOF(cell, pri_th)*C_R(cell, pri_th)*
            fabs(C_T(cell, pri_th) - T_SAT)/T_SAT;

   dS[eqn] =  -0.1*C_VOF(cell, pri_th)*C_R(cell, pri_th)/T_SAT;
                        }

 else {
   m_dot = 0.1*C_VOF(cell, sec_th)*C_R(cell, sec_th)*
            fabs(T_SAT-C_T(cell,mix_th))/T_SAT;

   dS[eqn] = -0.1*C_VOF(cell, sec_th)*C_R(cell, sec_th)/T_SAT;}

 return LAT_HT*m_dot;
}

DEFINE_PROFILE(heat_flux,t,i)
{
real y;
face_t f;
begin_f_loop(f,t)
{
y = CURRENT_TIME;
if (y<=10000){
F_PROFILE(f,t,i) = 1.73e-21*pow(y,5) -2.45e-17*pow(y,4)+9.92e-14*pow(y,3)+1.16e-10*pow(y,2)-
2.81e-07*y+0.002161;
}
else {
F_PROFILE(f,t,i) = -4.67e-22*pow(y,5) +8.71e-17*pow(y,4)-6.16e-12*pow(y,3)+2.00e-07*pow(y,2)-
0.002727*y+12.942;
}}
end_f_loop(f,t)
}
DEFINE_PROPERTY (cell_thcon, c, t)
{
real thc;
thc=1.9112e-4+pow(C_T(c,t), 3.6783)*3.4757e-12;
return thc;
}
```

3.20 Evaporation UDF [26]

First of all, under-relaxation factors are set at 0,5 for pressure, 0,2 for momentum and 0,4 for volume fraction. Concerning calculation methods; Body Forced Weighted is selected for pressure and QUICK method for momentum, volume fraction and energy. Simulation is done for 54.000 seconds, while LNG is initialized at 110.999K and 8bar. Additionally, the area-weighted averages for pressure, temperature and volume fraction inside the tank are recorded. However, average temperatures and pressures are almost constant considering that most portions of the tank are slightly affected. As a consequence, volume fraction graph of methane inside tank (presented below) is the most interesting one. Moreover, temperature, volume fractions, pressure and velocity vectors at the end of time are presented in the next figures.

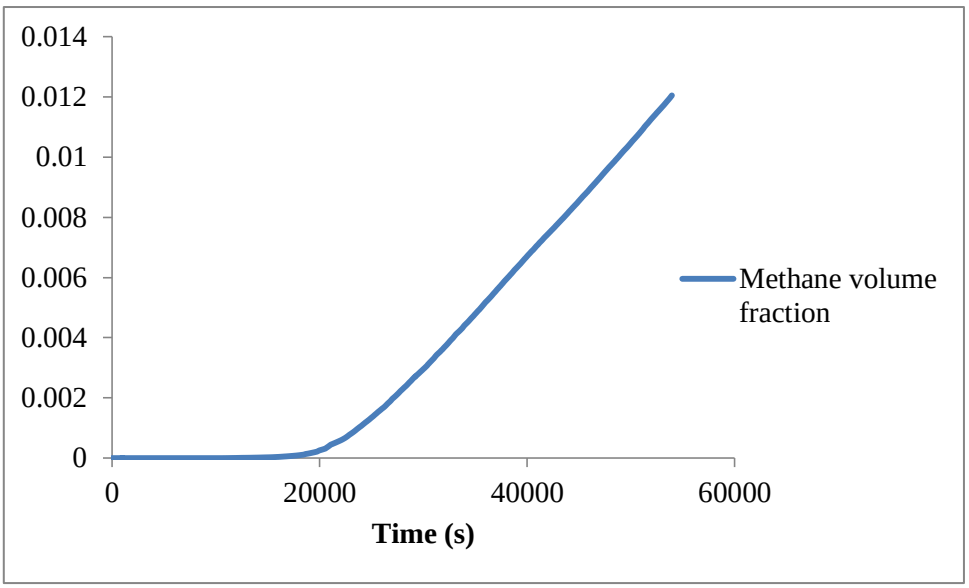

3.21 Methane volume fraction

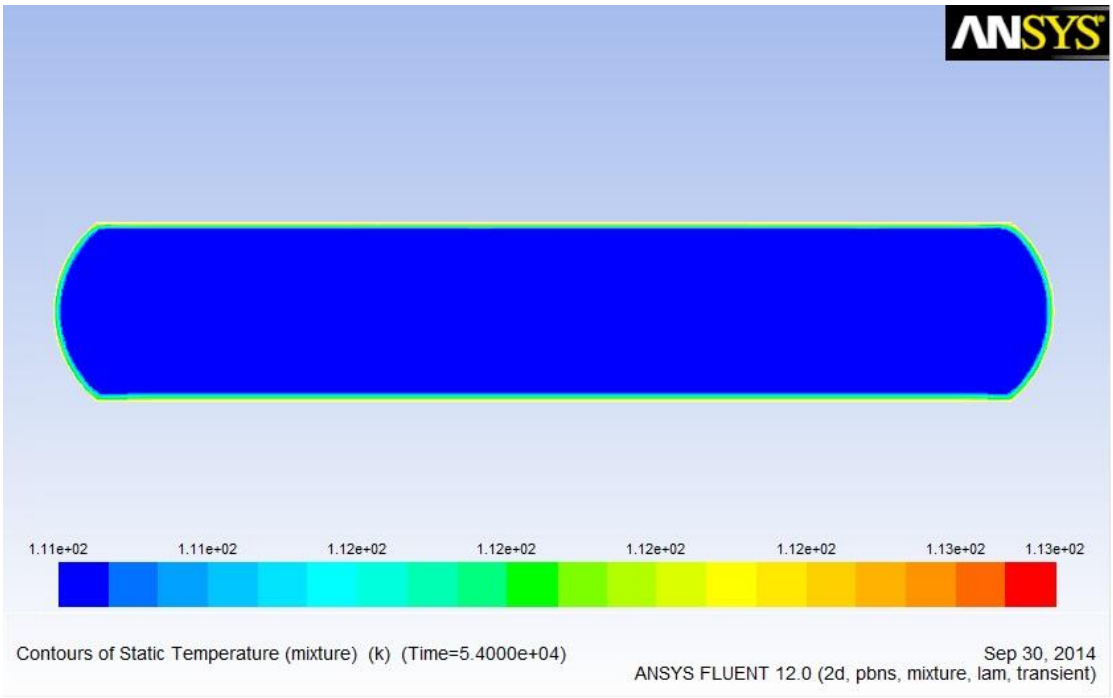

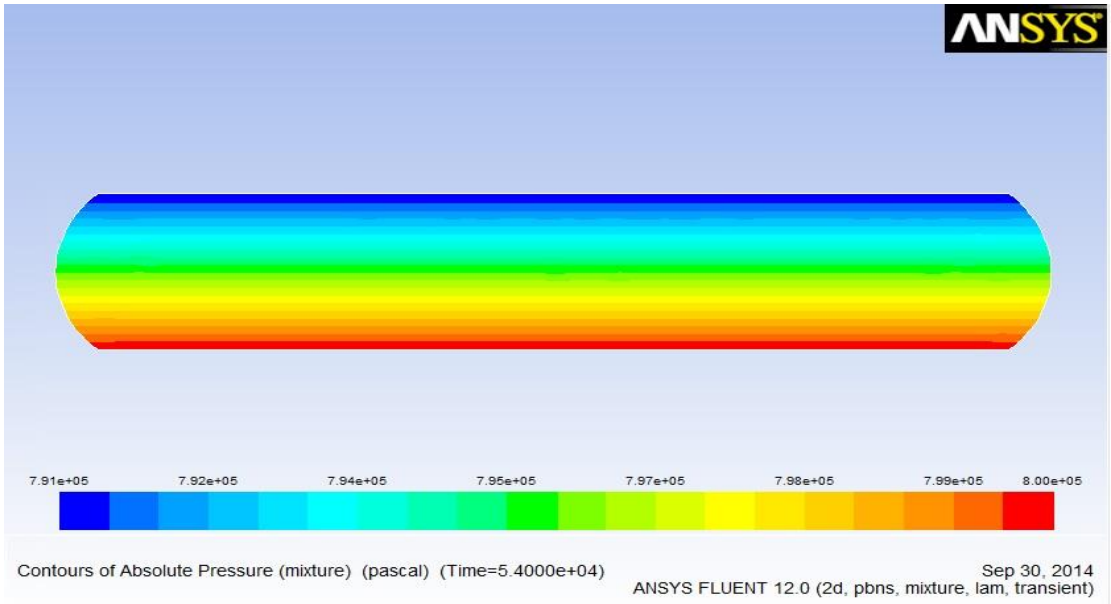

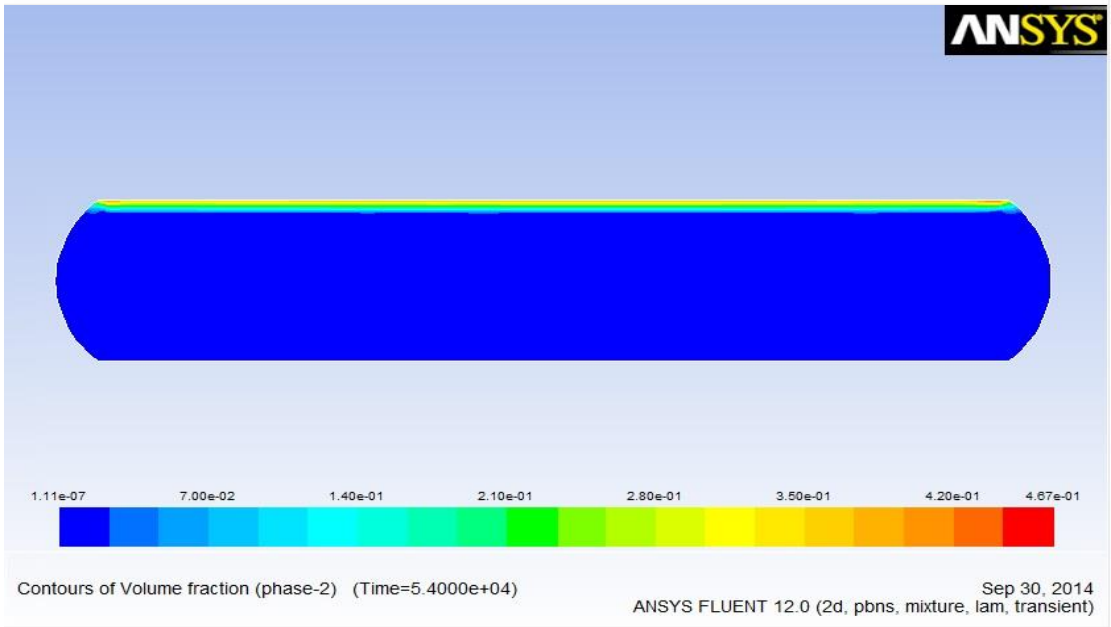

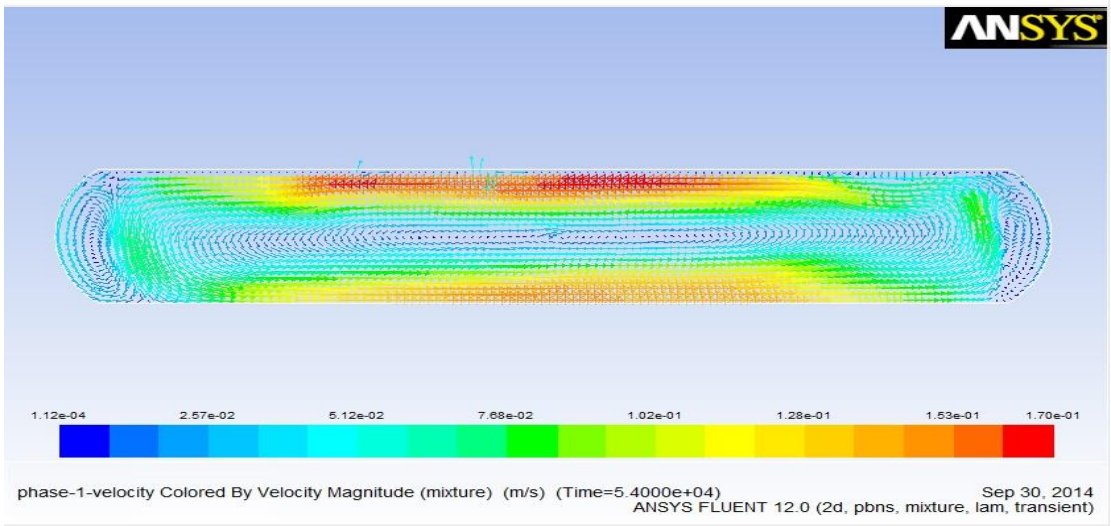

3.22 Temperature, pressure, volume fraction contours and velocity vectors

4 Three dimensional project

This chapter extends the problem described in the previous one into three dimensions. As a consequence, it shares the same format, while it contains further issues resulting from the additional dimension.

4.1 ANSYS 3D geometry and mesh design issues

Geometry of the tank is based again on the 53.400 OHS LNG trailer presented in previous sections. However, the three dimensional design is our concern at this chapter following the two dimensional model presented before. Sketches and modeling of the geometry are designed again in ANSYS Design Modeler. The concept is the same with the two dimensional one, where the tank is placed inside ambient air. Nevertheless, the design procedure is slightly different.

The first step of the three dimensional geometry is to create the two dimensional XY plane sketch (XY coordinates). This would be the same as the two dimensional model. However, the axis at the center of the tank is assumed as symmetry axis because sketch is going to be revolved. As a result, half of the two dimensional model is going to be sketched. Figure 4.1 displays the XY plane sketch of the three dimensional model, where all dimensions are expressed in millimeters. Double size insulation thickness (175mm) is used again for comparison reasons, while all dimensions have been kept constant compared to the two dimensional model.

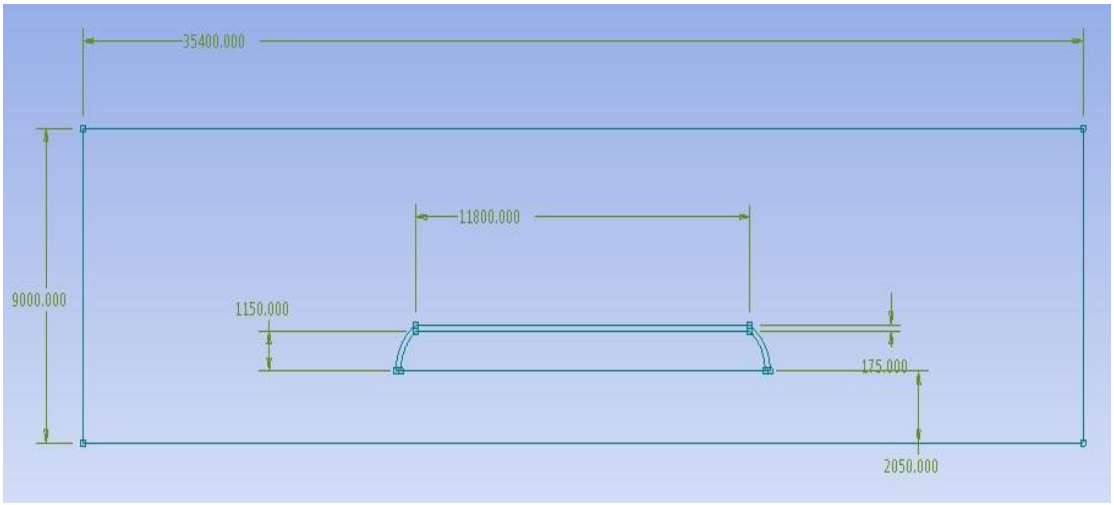

4.1 XY plane sketch of the 3D geometry

The next step includes the addition of Z-coordinate data. For this reason, we revolve the outer vessel of the tank by 360^0. Nevertheless, this command creates a compact cylindrical solid, which is not desired as the tank is empty at the inner vessel. As a consequence, we revolve the inner vessel by 360^0 using cut material operation instead of the add material one used in the first rotation. The sectional view at the center of tank is depicted in figure 4.2, while the whole tank is displayed in figure 4.3. Except from the tank, ambient air box must be created. For this reason, we extrude symmetrically the air rectangle for 5m. As a result the box dimensions are $35,4 \times 9 \times 10\,\mathrm{m}^3$. One important thing when drawing these solids is to freeze the tank in order to distinguish tank from the air box. Another thing that needs attention is to consider the two solid bodies as one part in order to study the interaction between

them. Figure 4.4 presents the whole model design. Figures 4.5-7 depict the generated meshes accompanied with bodies and faces designation, as described in the next paragraph

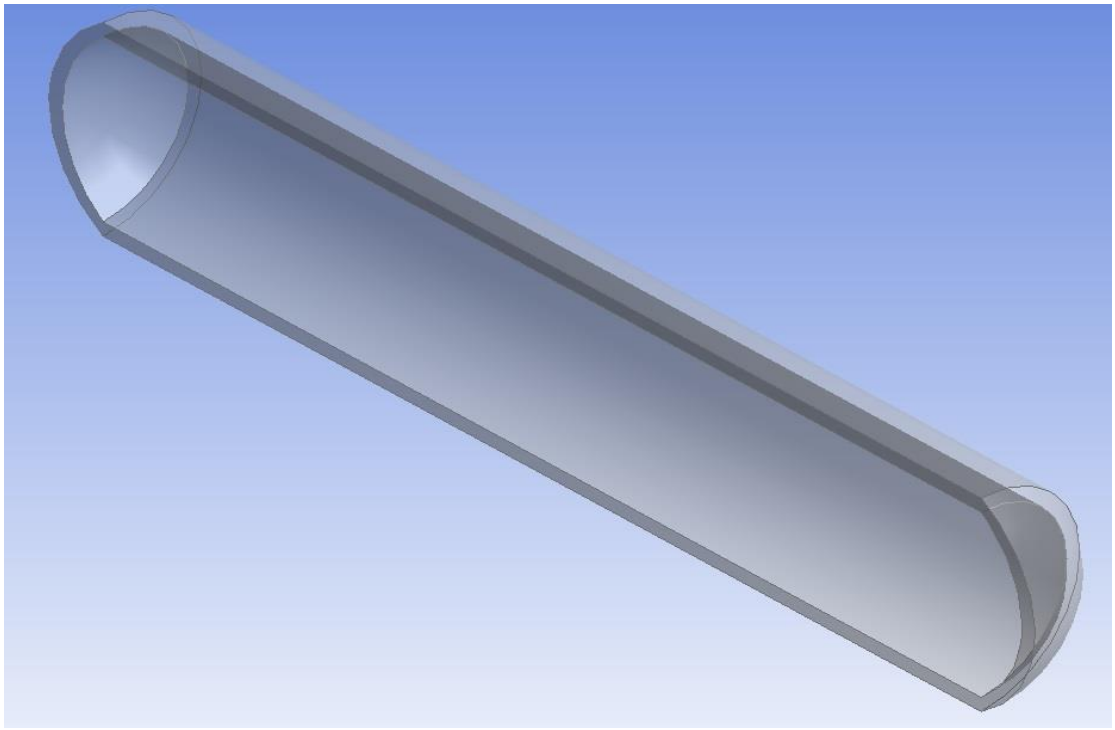

4.2 Sectional view of the tank

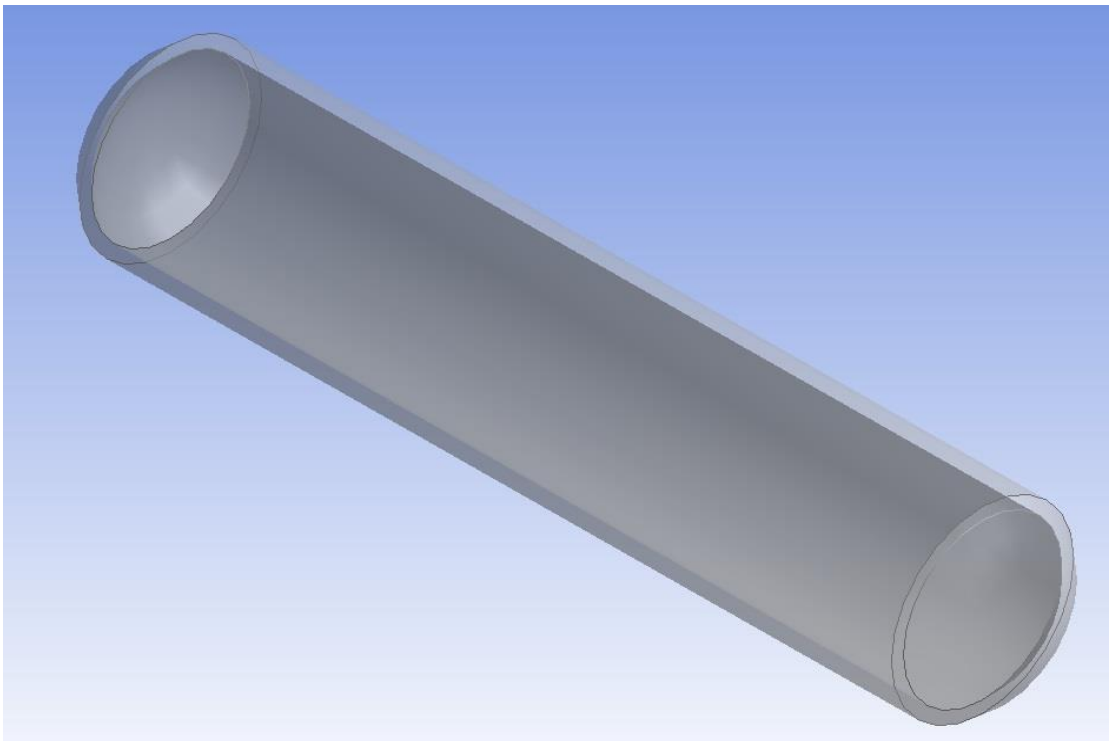

4.3 Whole tank view

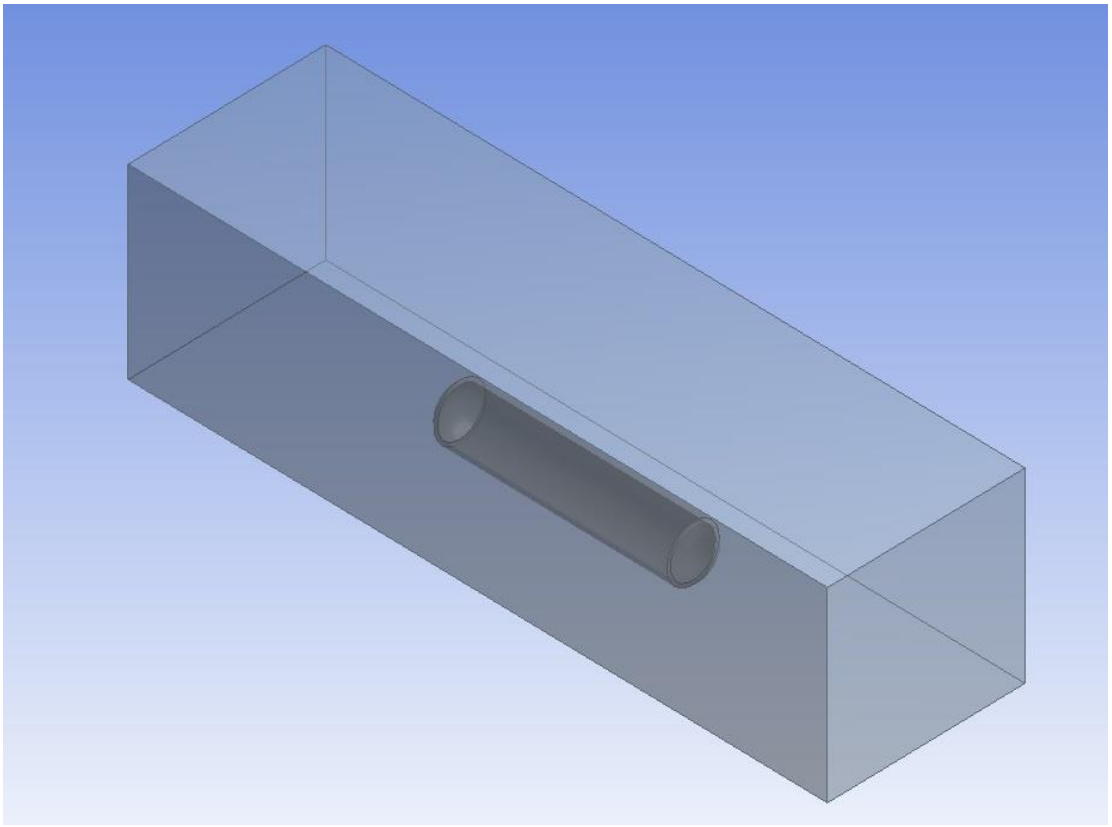

4.4 Whole 3D model

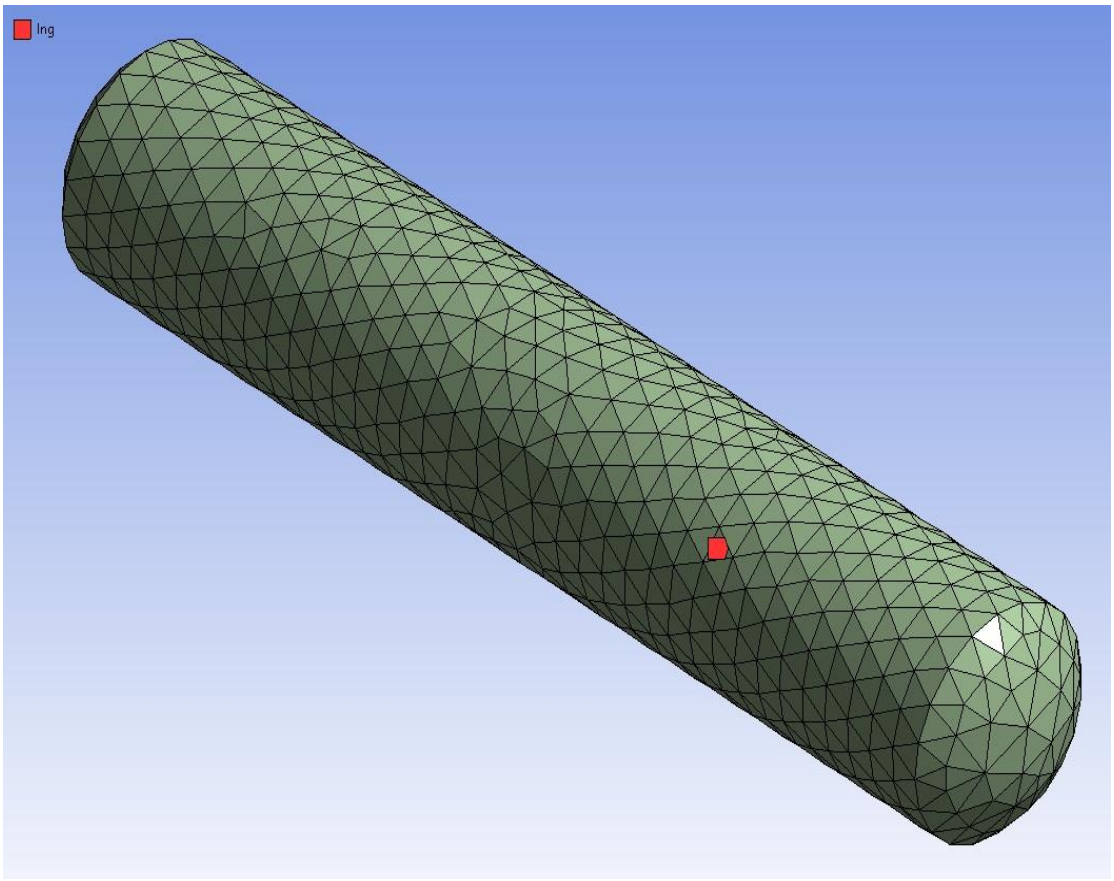

4.5 Inner vessel mesh

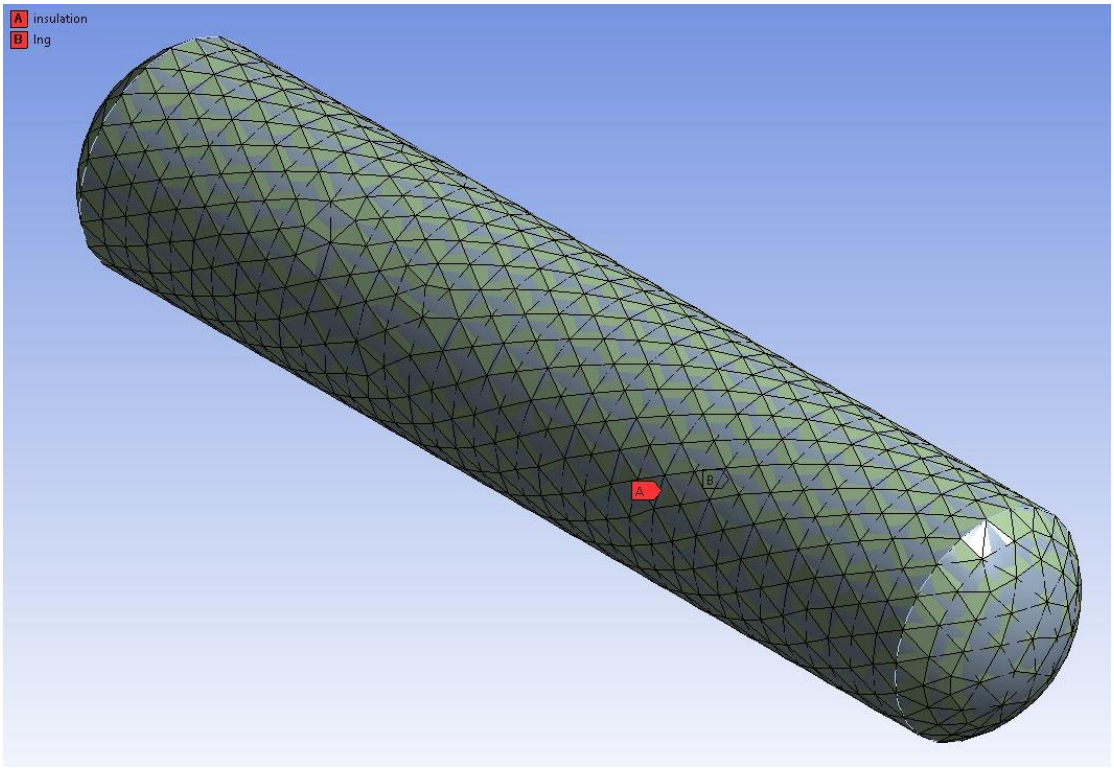

4.6 Outer Vessel mesh

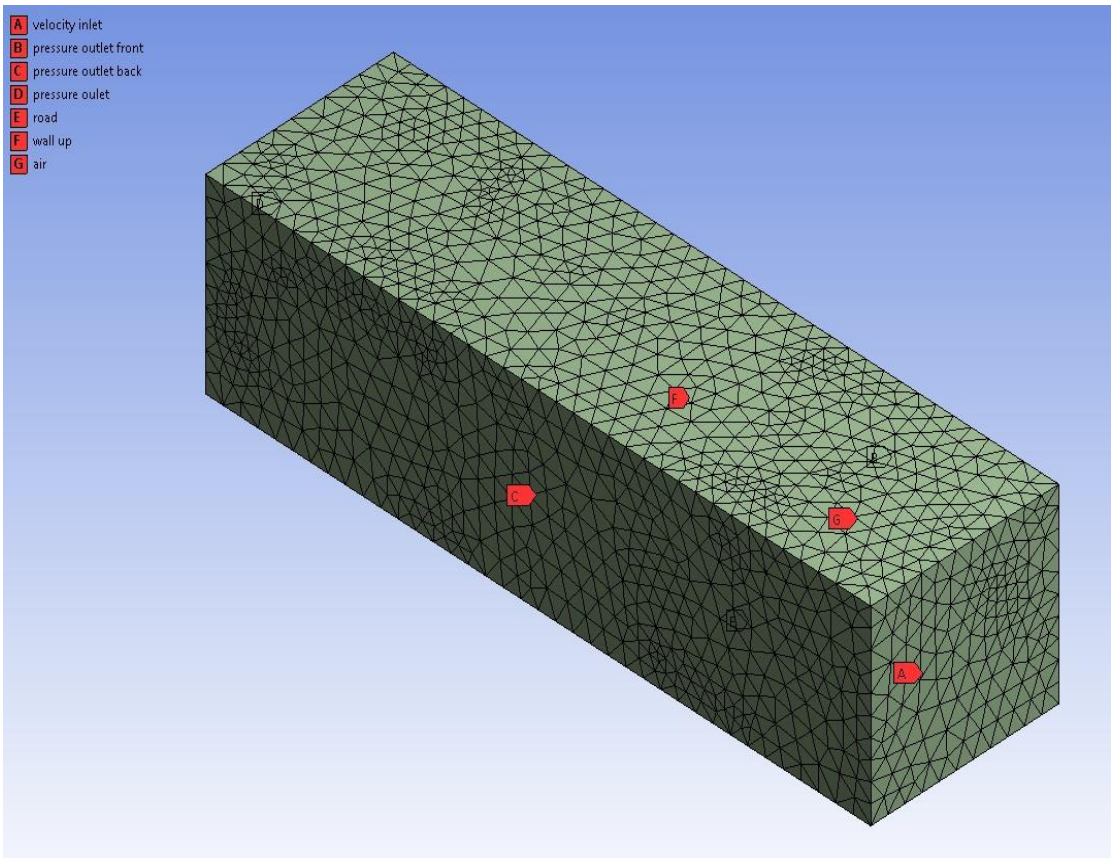

4.7 Air box mesh

Mesh generation and parts designation is done using ANSYS Meshing. Fluent solver preference and medium relevance center are selected for mesh generation. The three bodies and the six box faces are named accordingly to the two dimensions model. Air box, outer vessel and inner vessel are represented as air, insulation and lng bodies in the model. In addition, the small rectangle of the box is assumed to be the velocity inlet, while the opposite one is the pressure outlet. The lateral faces are displayed as pressure outlet front and pressure outlet back. However, these boundaries selection as pressure outlets will be re-considered later due to solution convergence problems as done in the two dimensions case. Finally, the bottom face is the road, while the upper one is symbolized as wall up.

4.2 Initial 3D FLUENT parametric considerations

The seven cases examined in the two dimensions section are going to be re-considered for the three dimensions case. Similarly, these are initial tests for comparison reasons, while they do not take into consideration the phase envelope of each material. The material properties used are the same with those presented in table 3.1.The three cell zone conditions created in ANSYS Meshing are air, insulation and lng. Air and lng zones are defined as fluids while insulation is defined as solid. Steel is considered as the insulation material for these tests, while the lng zone material will be variable.

The solver is selected as pressure-based and transient because our concern is to check heat fluxes during time. A time period of 12 hours or 43.200 seconds is assumed for the simulations. Time step is initially set at 0.01 second in order to facilitate convergence, while it is gradually and carefully increased. Energy equations are involved in calculations, while standard k-epsilon model is chosen for viscosity modeling. However, gravity effects are not included in calculations. Pressure-velocity coupling is solved using SIMPLE algorithm, while first order upwind spatial discretization is used for energy, momentum and turbulent kinetic energy. The under relaxation factors are the default ones for FLUENT 12.

On the other hand, eight boundaries are created from FLUENT (the six box faces and the two interface boundaries). Again, the air-insulation and insulation-lng boundaries are defined as coupled with their shadows to enable heat flow through the surfaces. Lateral box boundaries (pressure outlet front, pressure outlet back) are transformed from pressure outlets to steel walls, as the road and wall up boundaries, due to air backflow problems. All walls are considered adiabatic with zero heat fluxes. Velocity inlet is set at 400K temperature, 5m/s velocity magnitude, 2% turbulent intensity and 9m hydraulic turbulence diameter. The same turbulence parameters are chosen for pressure outlet with the exception that temperature is defined at 300K.

4.3 Examined cases results and comparisons

The results of the seven cases are presented in the next figures. Initial temperature of the tank at 275K is assumed for the first three cases and 113K for the rest. Figures 4.8-4.14 display the temperature contours of two different time points, one at the half time and another at the end of time (approximately after 6 hours and after 12 hours). In each time case the temperature contours at the perpendicular plane in the middle of the tank are presented at the right window. Figures 4.15-16 present air velocity vectors at planes x=0 (the point of maximum air velocity) and z=0 for methane cases.

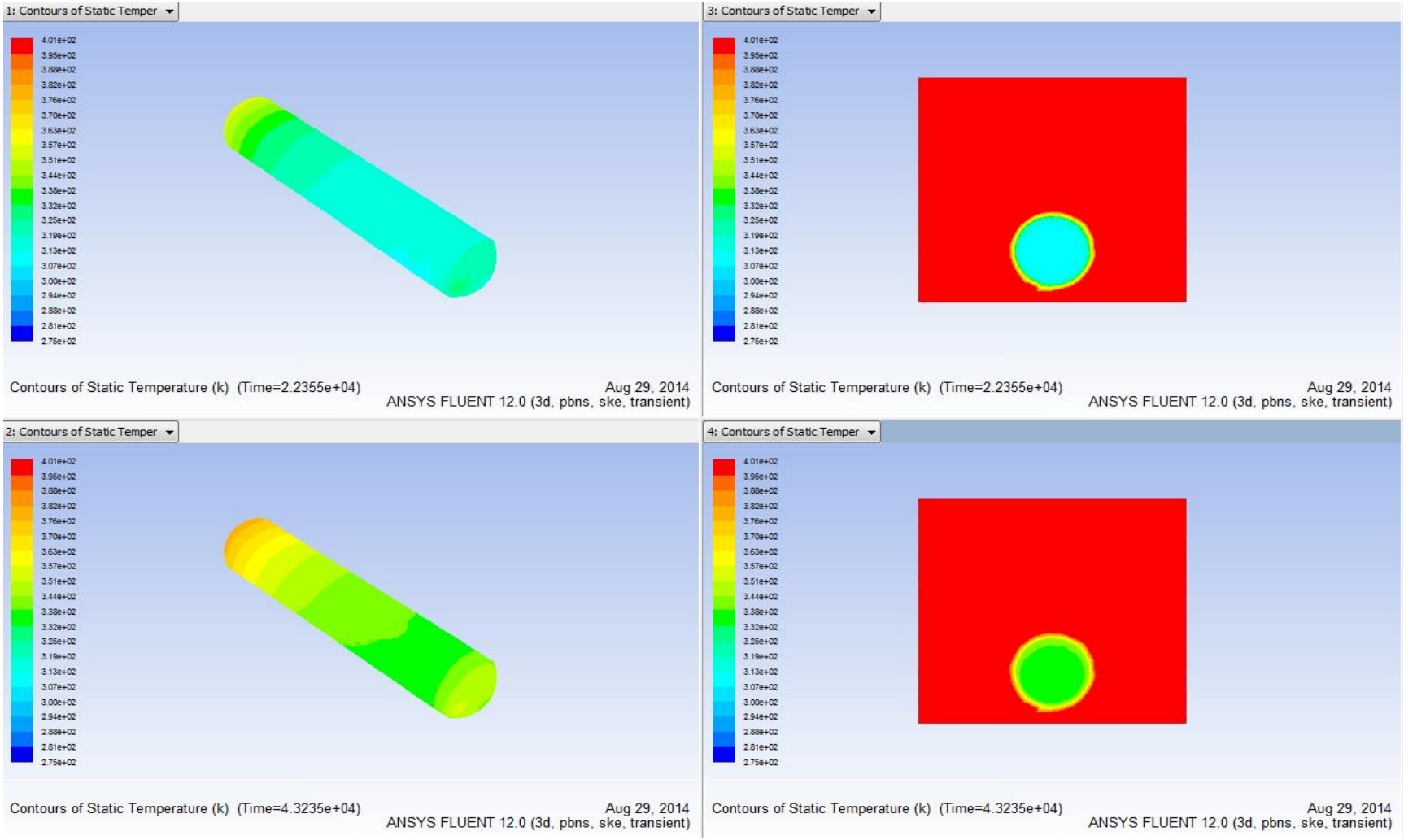

4.8 Air temperature contours

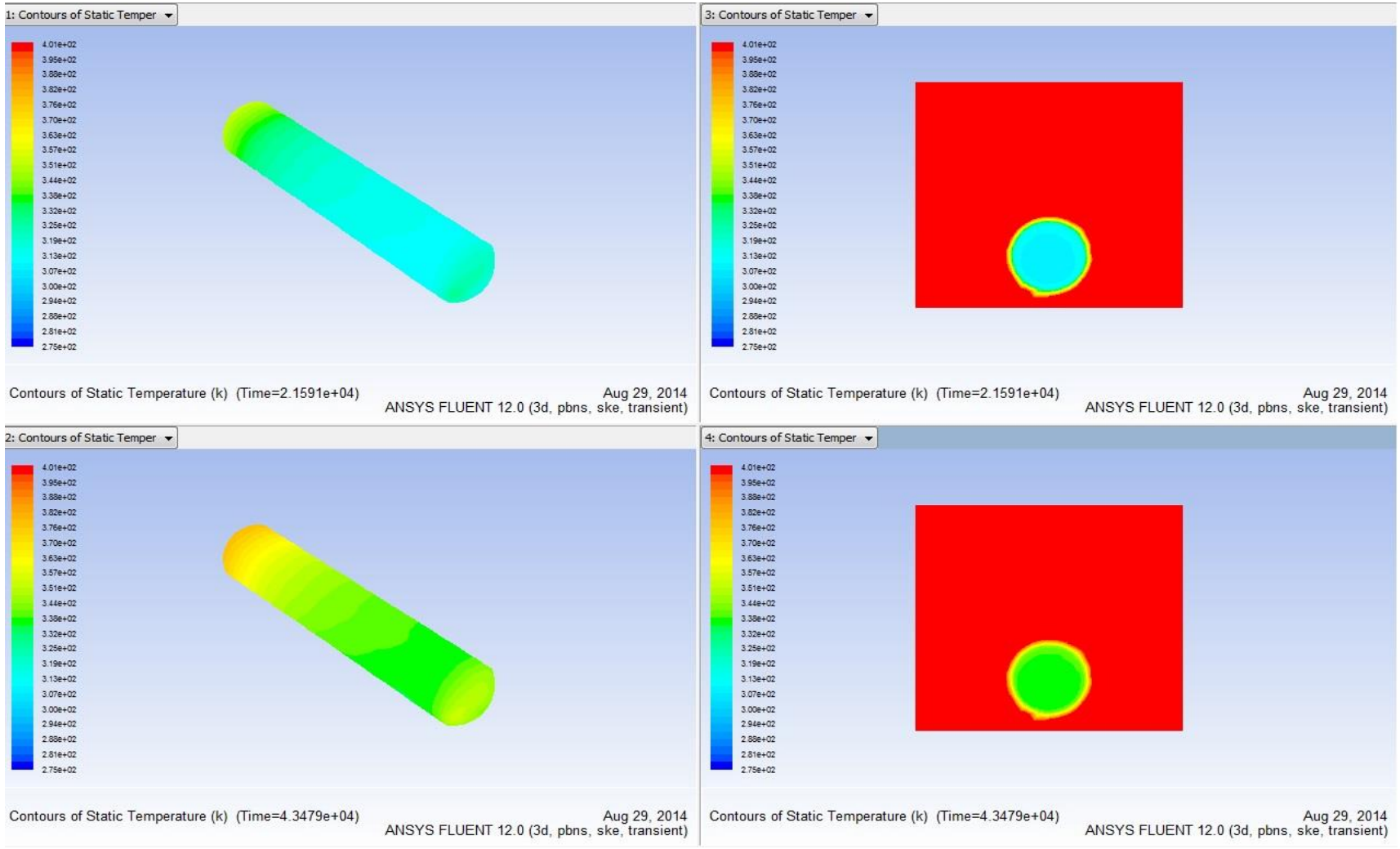

4.9 Water vapor temperature contours

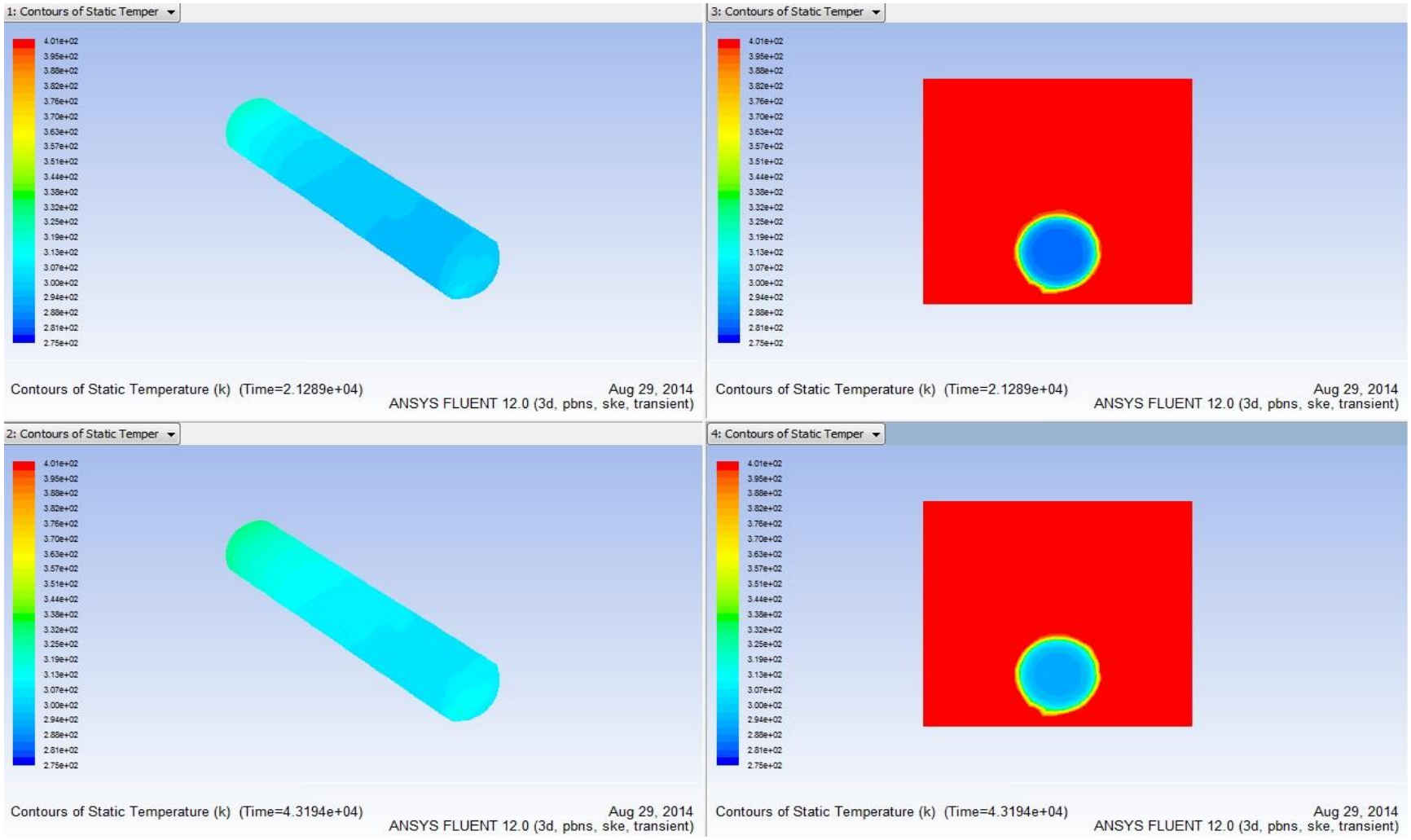

4.10 Water liquid temperature contours

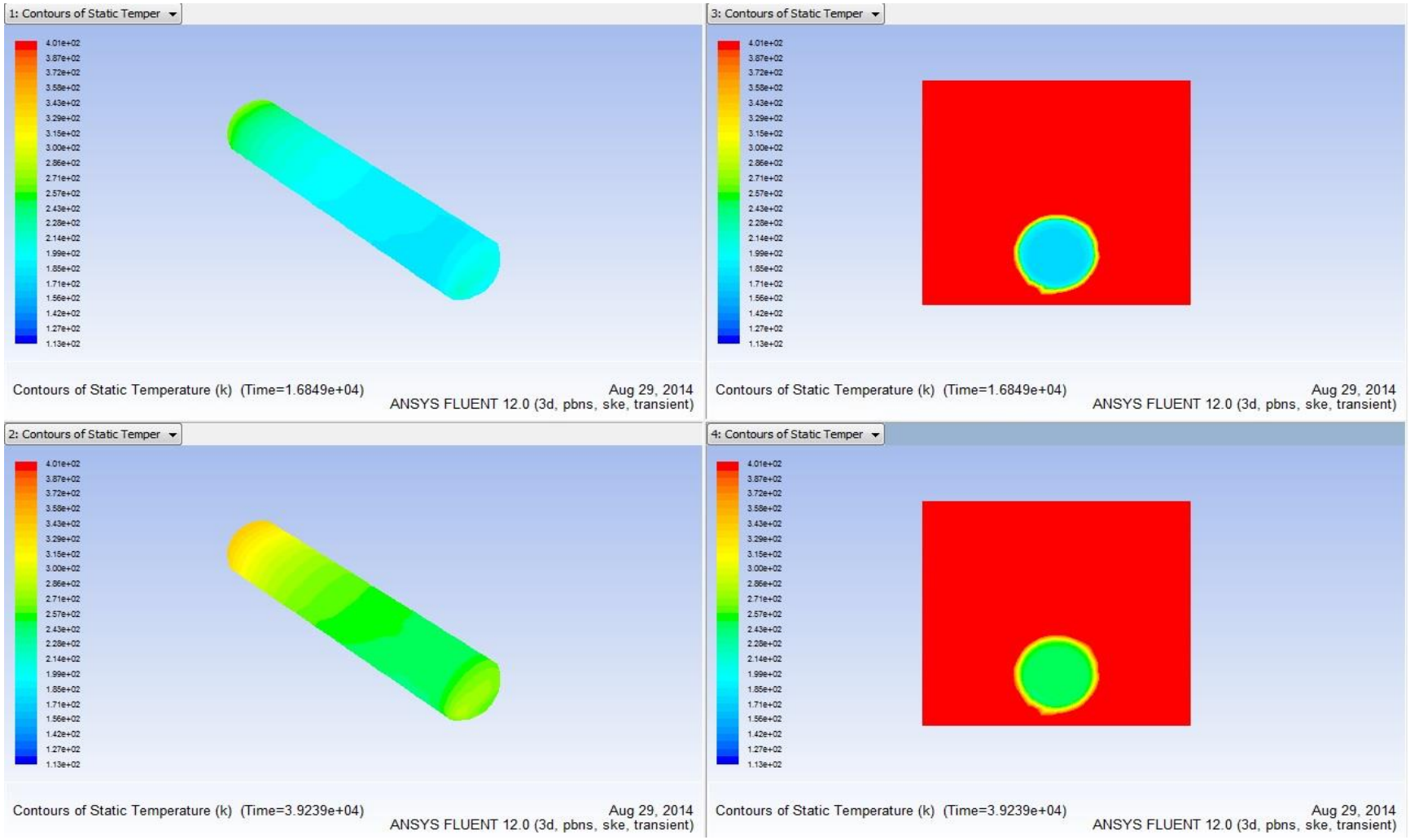

4.11 Methane temperature contours

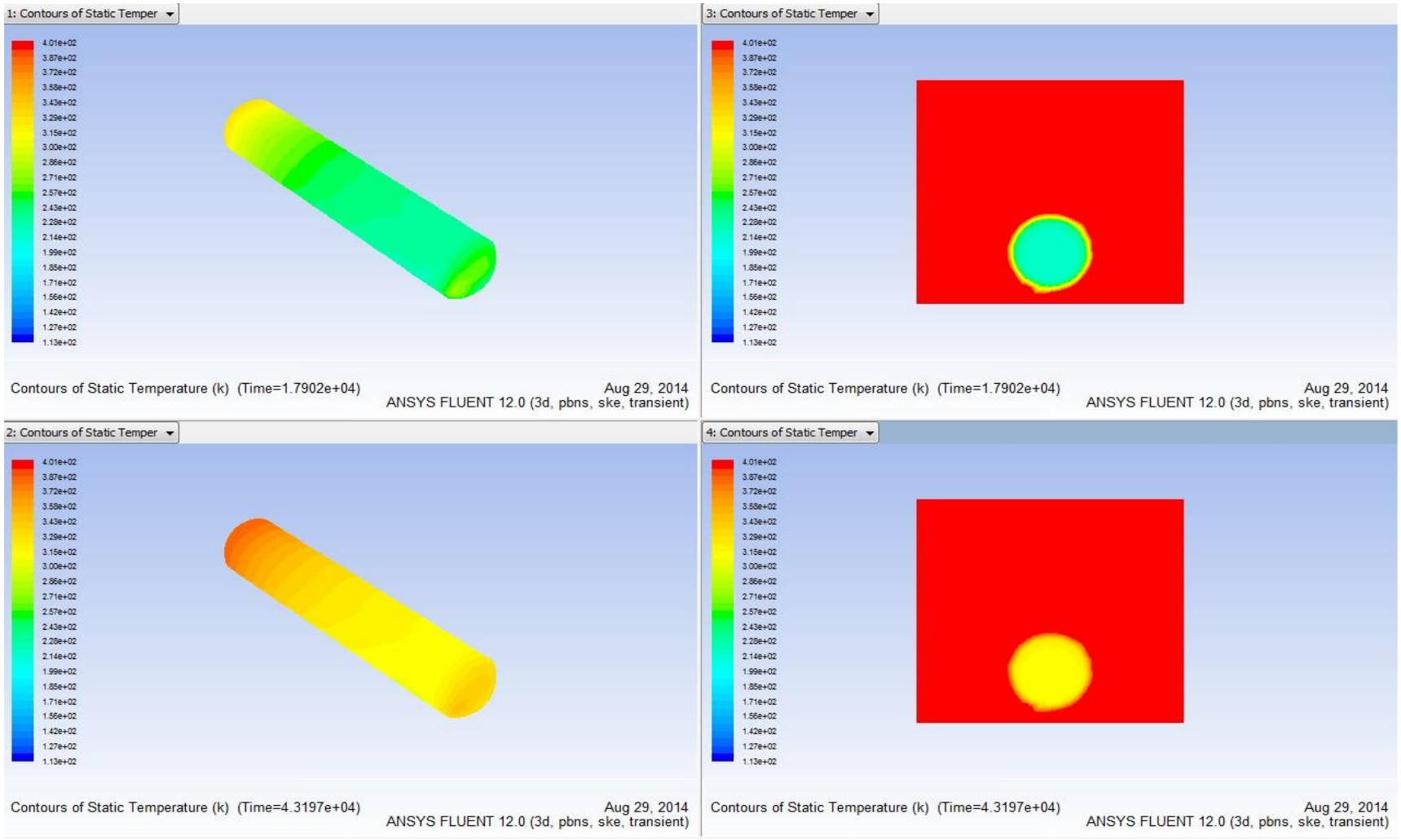

4.12 Methane temperature contours with inlet velocity 10m/s

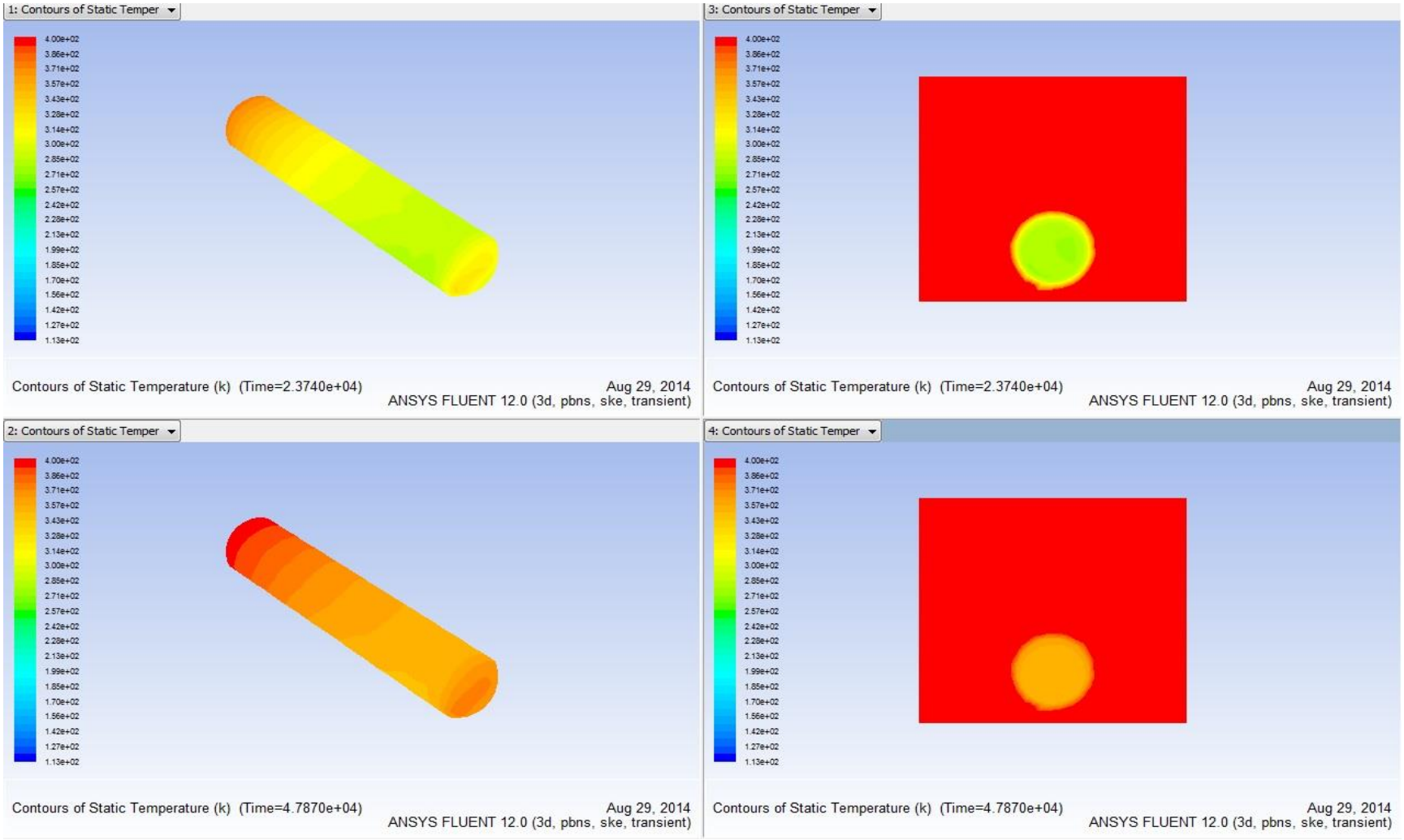

4.13 Methane temperature contours with inlet velocity 15m/s

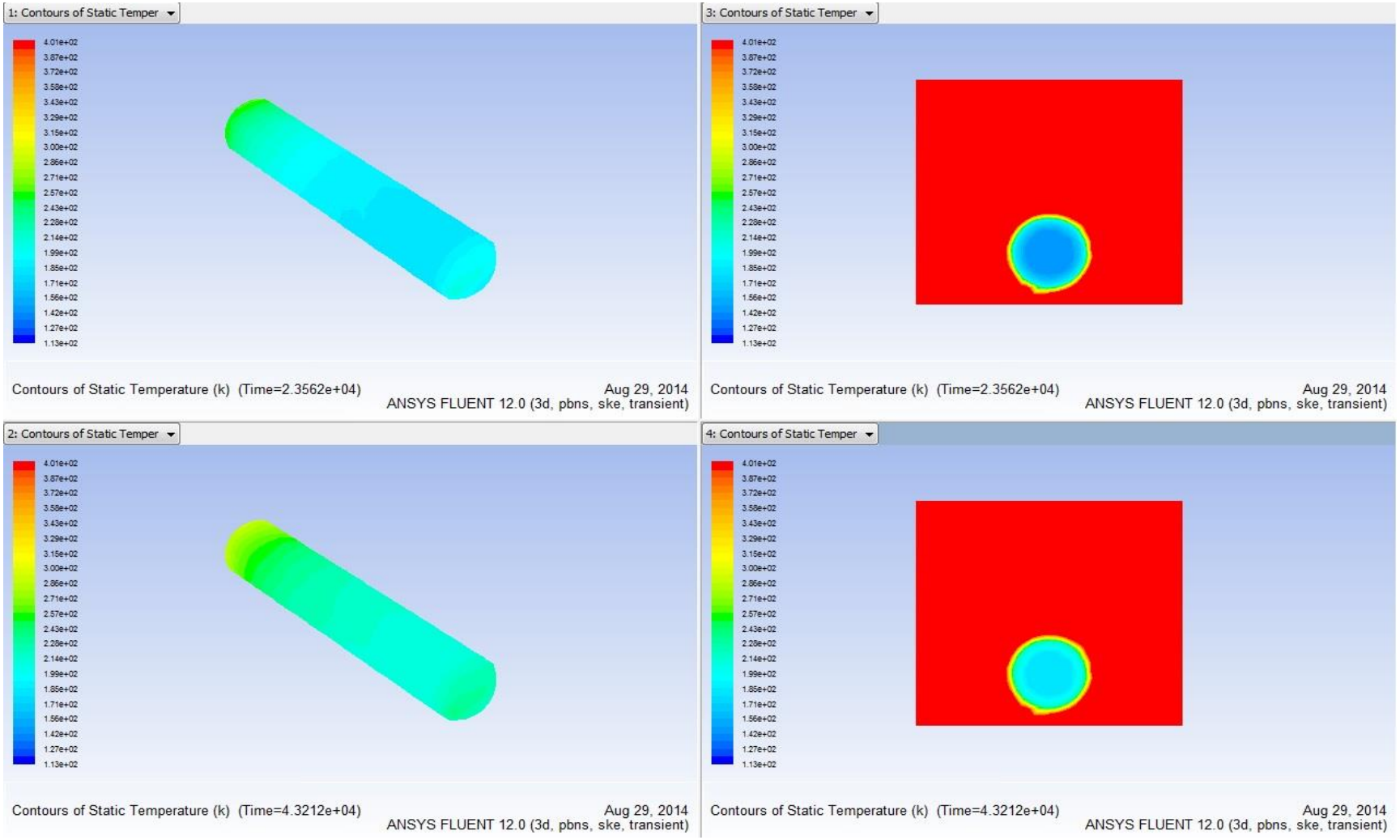

4.14 LNG temperature contours

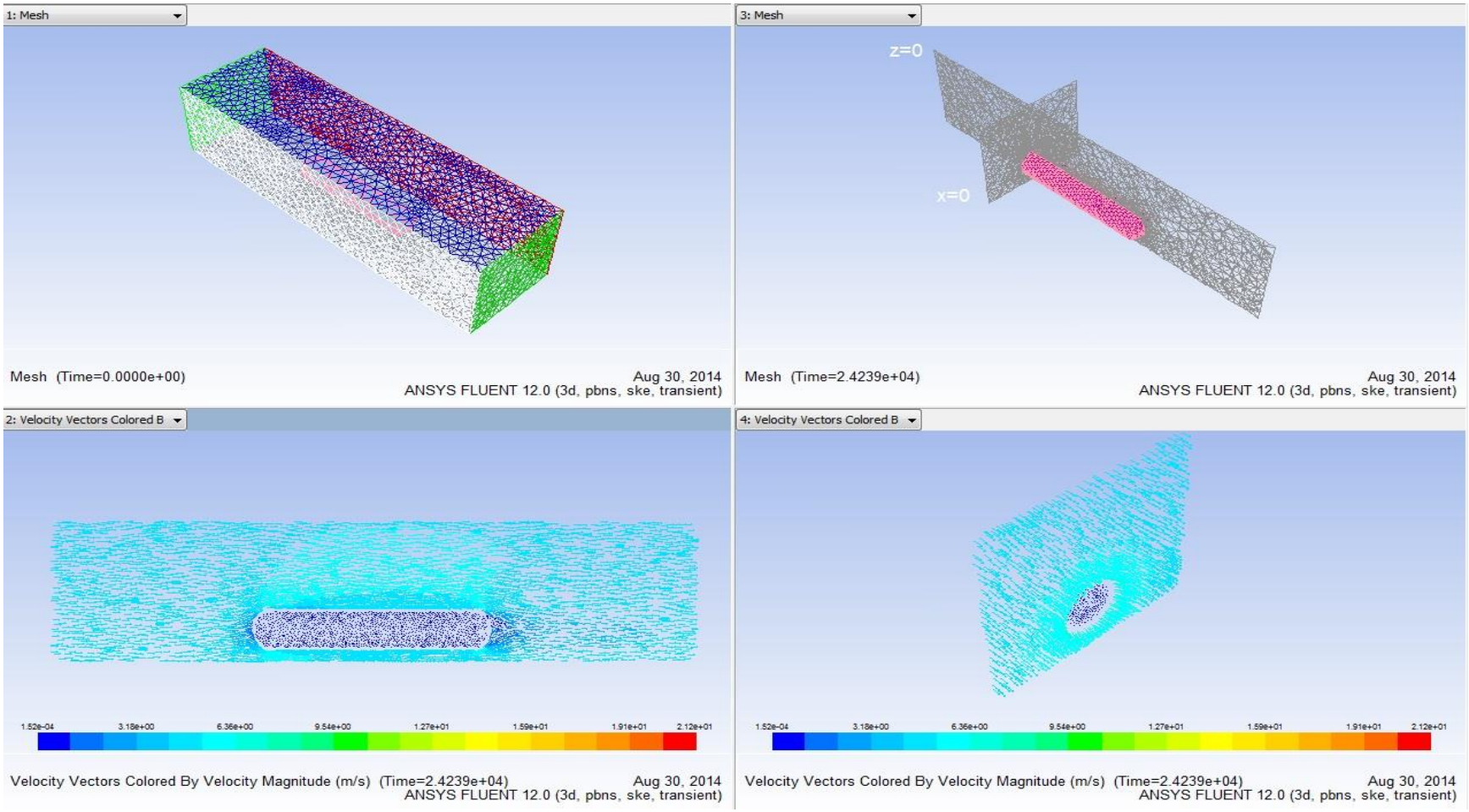

4.15 FLUENT mesh, examined planes and methane air velocities

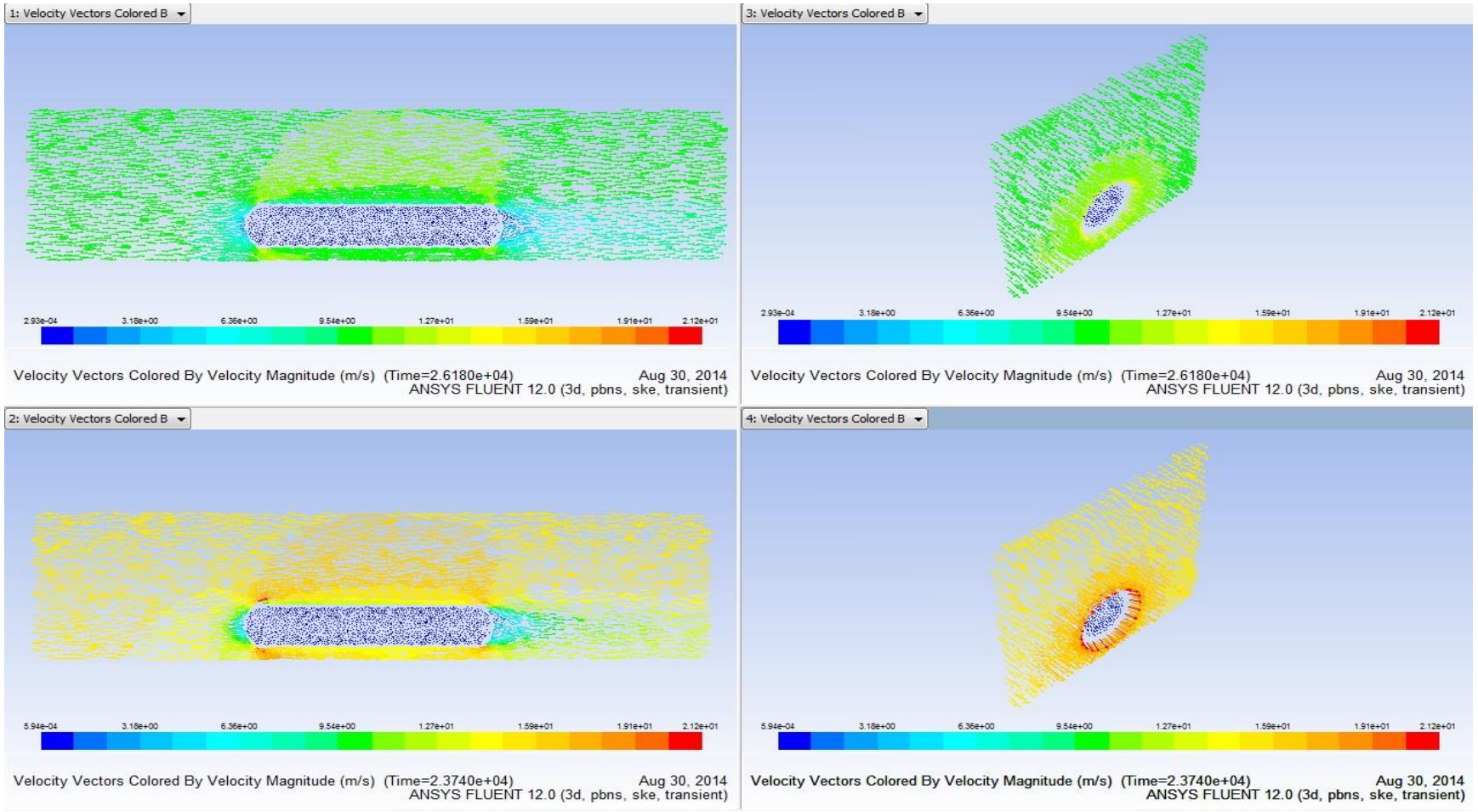

4.16 Air velocities vectors for methane10 (up) and methane15 (down) cases

Comparing the above figures, we can conclude that methane is faster heated compared to LNG. In addition, the higher the inlet velocity, the higher the temperature increases. Air has similar behavior with vapor water, which is slower heated than LNG and faster heated than liquid water. The area-weighted average temperature of the lng body is monitored and recorded in all cases, in an attempt to compare the average temperatures. Figure 4.17 displays the temperature evolution compared to initial temperature of lng body during time, while table 4.1 depicts initial and final temperatures for all cases. The time point of final temperature is also included for each case.

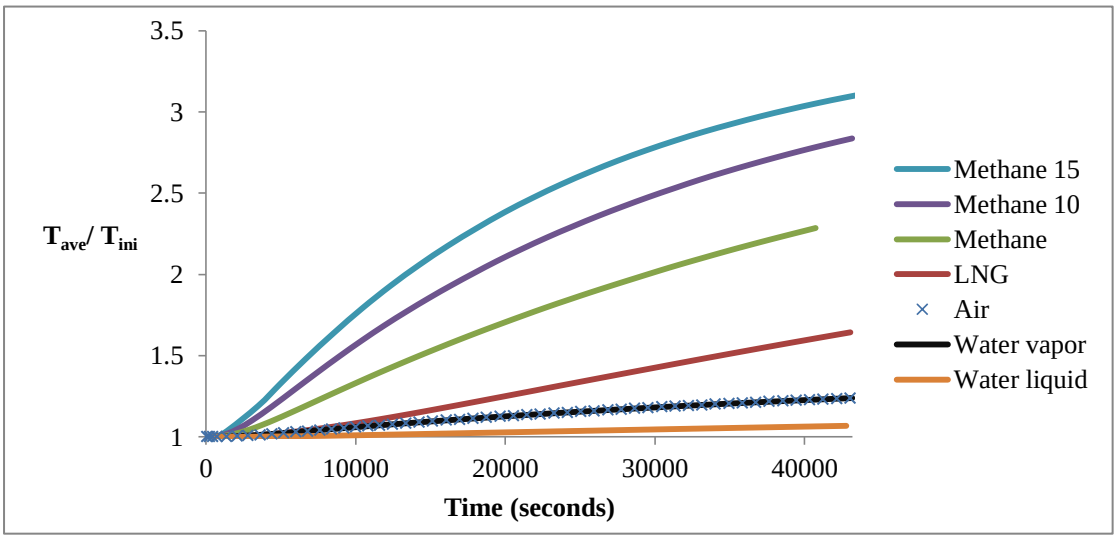

4.17 Area-weighted average temperature inside tank

	$T_{in}(K)$	$T_{fin}(K)$	$Time(s)$
Methane 15	113	356,4	46.540
Methane 10	113	320,6	43.180
Methane	113	258,3	40.739
LNG	113	185,7	43.062
Air	275	340,7	43.055
Water liquid	275	340,8	43.191
Water vapor	275	293,8	42.789

Table 4.1 Initial and final temperatures

Comparing air velocity vectors, we can conclude that air velocity magnitude at the inlet is the most important factor. All cases with 5 m/s inlet velocity share the same results. This is the reason why only methane case is presented. Air velocities are higher at the front face and reach their peak at the left corners of the tank (x=0 plane). On the other hand, velocities are decreased at the side behind the tank. The highest velocity magnitudes are 21, 14 and 7 m/s for inlet velocities of 15, 10, 5 m/s respectively. Finally, the mesh as imported in FLUENT and the two planes used are depicted in figure 4.15.

4.4 Insulation thickness effect

Our consideration in this section is to examine the impact of the insulation thickness on the temperature increase of the tank content. As mentioned at the beginning, the insulation thickness of the OHS trailer tank is half the one used already. As a result, the real one is depicted in figure 4.18 sketched at Design Modeler. The sectional view of the tank after revolving the previous sketch is presented in figure 4.18. The results of this thickness for the area-weighted average lng temperature divided by initial temperature using different tank contents are presented below. In addition, graphs displaying the temperature evolution of the different tank contents in respect to insulation thickness cases are added below. Each material used inside the tank is displayed with the same kind of line for both the case of half insulation and the initial case. Furthermore, tank temperature is examined for the OHS trailer when air temperature at velocity inlet is 300K instead of 400K. Again, temperature evolution for both inlet cases is presented in one graph. Finally, a table which includes the final temperatures and the corresponding time for the above examined cases is presented.

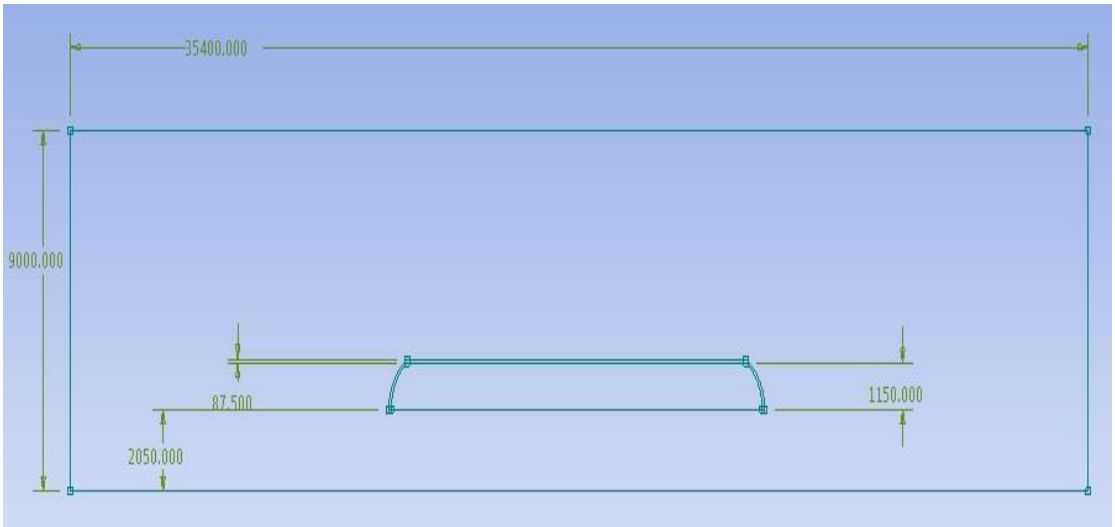

4.18 XY plane sketch of the half insulation tank

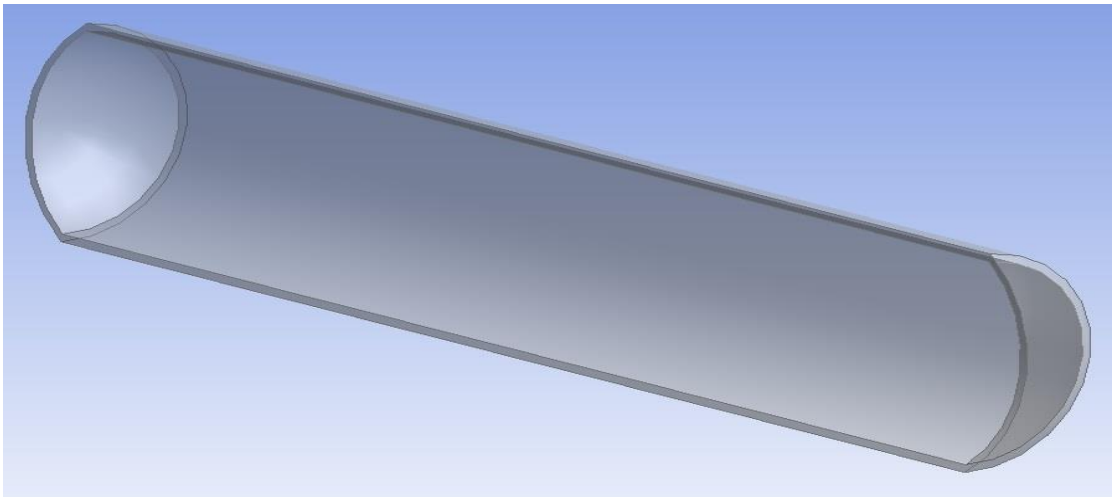

4.19 Sectional view of the half insulation tank

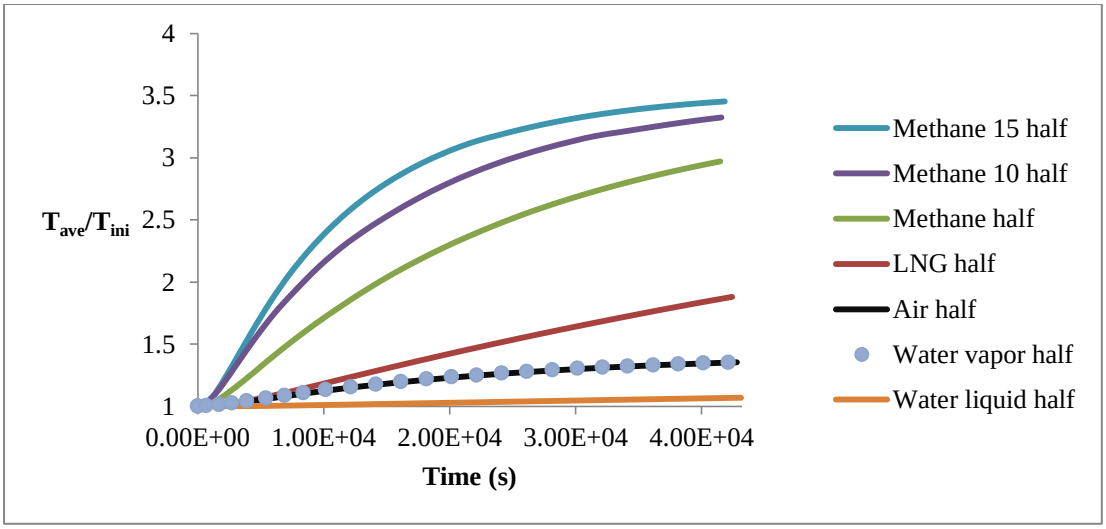

4.20 Area-weighted average temperature for the half insulation tank

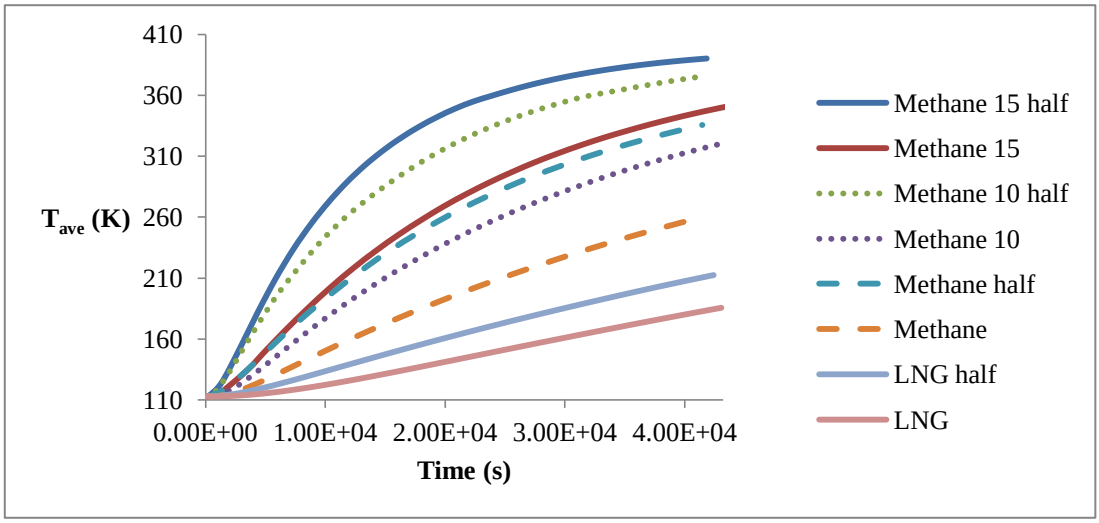

4.21a Temperature evolution for the two insulation cases

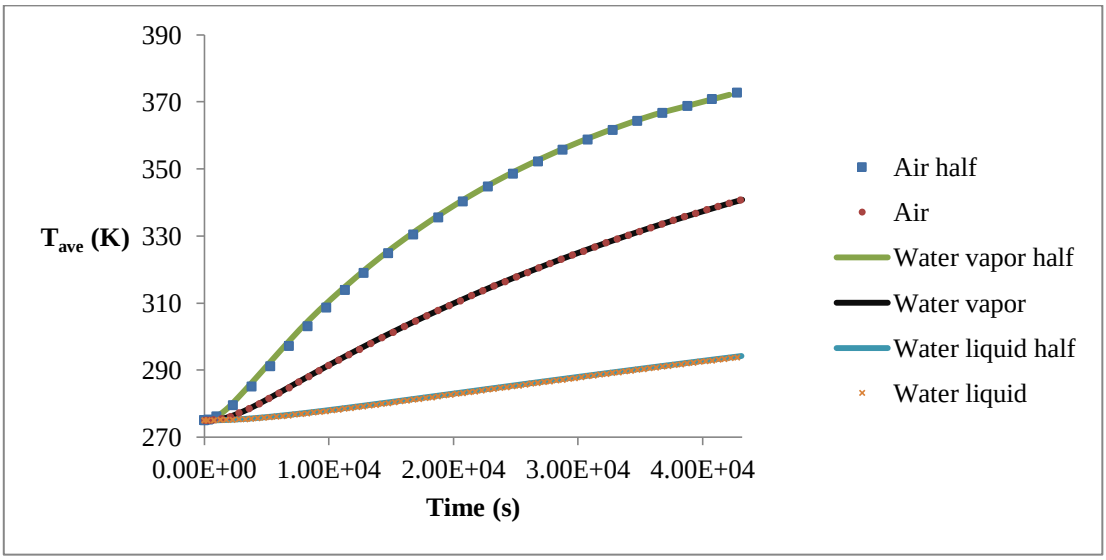

4.21b Temperature evolution for the two insulation cases

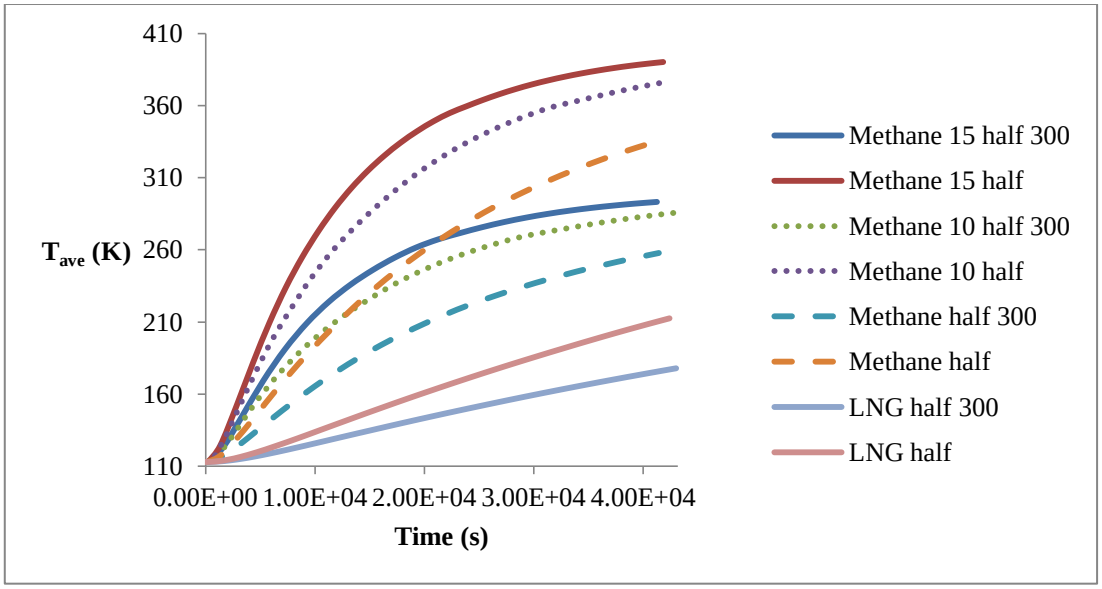

4.22a Temperature evolution for velocity inlet cases

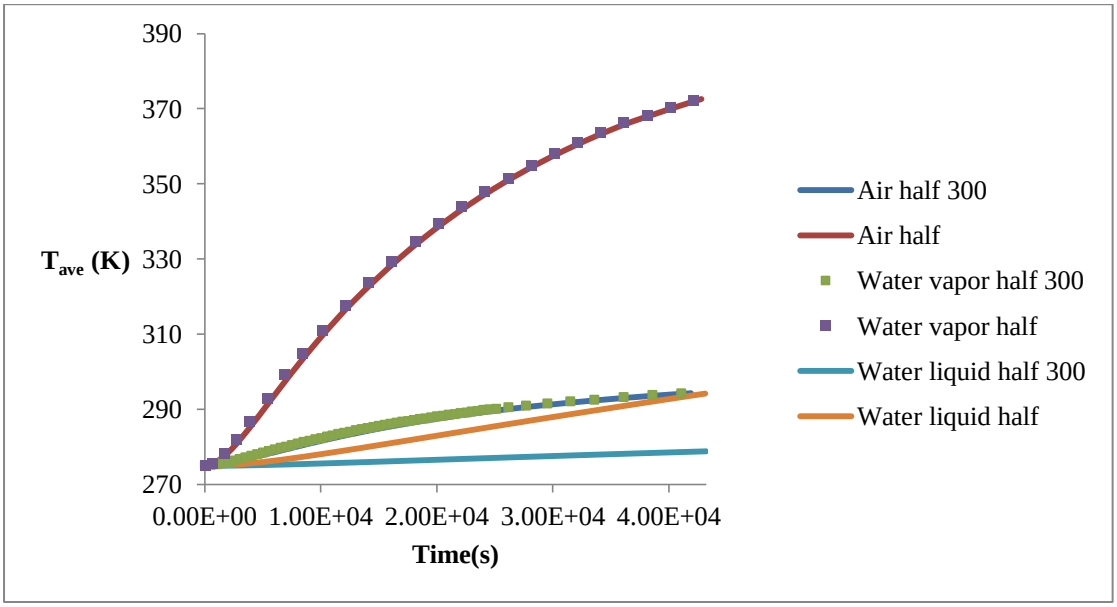

4.22b Temperature evolution for velocity inlet cases

	$T_{fin}(K)$	$Time(s)$	$T_{fin}(K)$ Half	$Time(s)$ Half	$T_{fin}(K)$ Half 300	$Time(s)$ Half 300
Methane 15	356,4	46.540	390,1	41.840	293,2	41.270
Methane 10	320,6	43.180	375,6	41.575	285,5	42.774
Methane	258,3	40.739	335,6	41.475	257,8	41.449
LNG	185,7	43.062	212,5	42.420	177,9	43.026
Air	340,7	43.055	372,6	42.804	294,3	41.901
Water vapor	340,8	43.191	372,1	42.161	294,2	41.122
Water liquid	293,8	42.789	294,2	43.133	278,9	43.207

Table 4.2 Final temperatures for the examined cases

Summarizing the above results, we can conclude that the thickness of the insulation is an important parameter for the tank added heat. Reduced insulation results in higher temperature increases. Again, gases are more dependent to insulation thickness compared to liquids (water, LNG). Another important parameter of the tank temperature increase is the temperature of the ambient air. Higher temperatures heat faster the tank content.

4.5 LNG evaporation

The calculation is based again on the procedure described on chapter 3. For this reason, two sub-calculations are going to be presented; one for the heat fluxes from ambient air to the tank and another one for the multiphase flow in the isolated tank. However, the three dimensional model provides more calculation options like the solar calculator making the simulation more realistic. On the other hand, the higher the amount of nodes the more complicated the problem resulting in slower calculation times. The above issues are presented below.

4.5.1 Heat fluxes calculation

The scope of this simulation is to calculate the heat absorbed by the tank in order to use this data to the second one. For this purpose, we use sketches and generated mesh of the previous section (87,5mm insulation), while we assume that tank is fully filled with LNG. However, additional models and materials are used to this case. Hence, gravitational acceleration at y-axis is set at 9,81 m/s2. Moreover, the Boussinesq approximation is also included to simulate natural convection. The specified operating density of air is equal to 1,225 kg/m3. Furthermore, standard k-e model is enabled for turbulent air flows, while surface to surface model is activated to include radiation heat fluxes.

In contrast with the two dimensional model, this simulation offers the solar ray tracing model in order to calculate the solar irradiation at the Earth's surface. As a consequence, we set the longitude and latitude of Thessaloniki to the solver and time is set at the 21th of June at 08:00. In addition, perlite under vacuum and asphalt are used in this simulation (properties of these materials are presented in chapter 3). The thermal conductivity of perlite is calculated with the same UDF used in the previous chapter.

Air and road temperature is assumed to be 400C or 313K, while insulation and LNG temperature is fixed at 111K. Moreover, initial tank pressure is 8bar (800.000 Pascal). In addition, vehicle speed is supposed to be around 80km/h (approximately 22 m/s) and as a result this is the velocity magnitude at the inlet. The tank heating is simulated for 15 hours or 54.000 seconds which corresponds to a trip of 1200km. Finally, the upper, left and right walls, velocity inlet and pressure outlet are boundaries with unitary emissivity.

The area-weighted average heat fluxes at the inner surface of the insulation are recorded with respect to time. The figure below displays this relation. In addition, pressure and temperature contours and air velocity vectors at the end of time are presented.

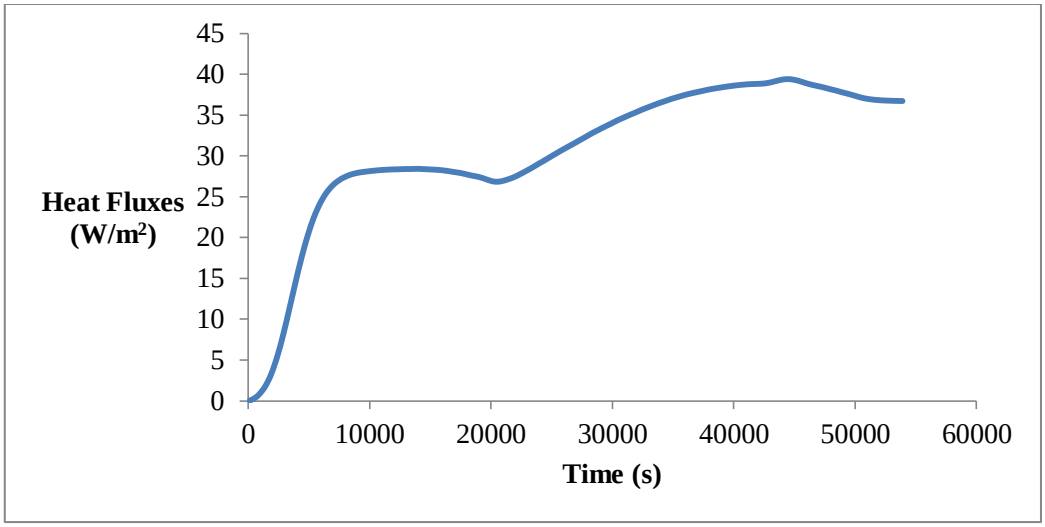

4.23 Inner tank wall heat fluxes

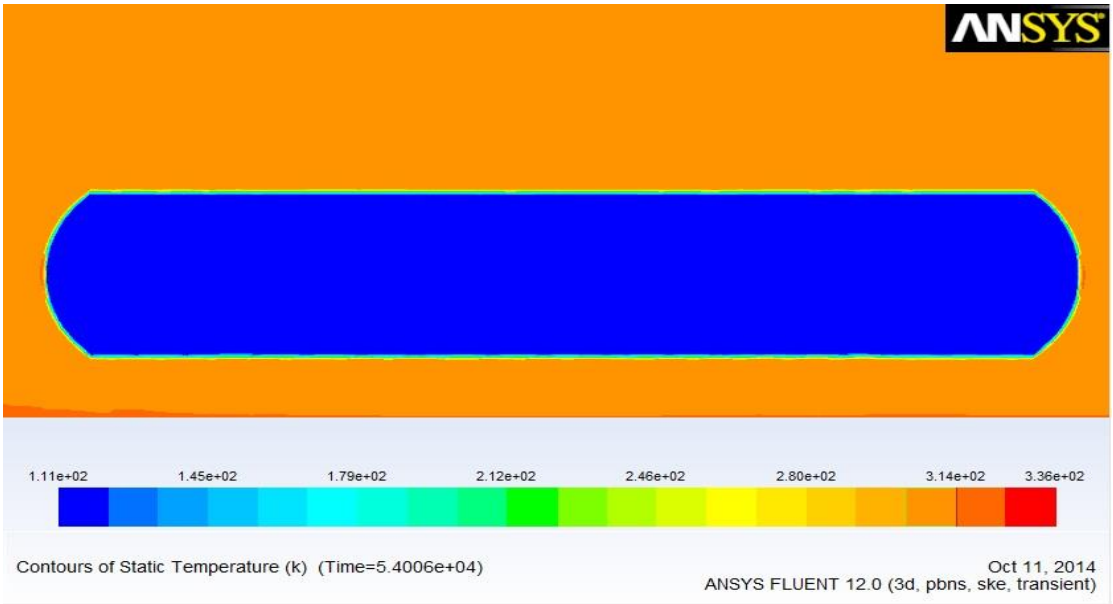

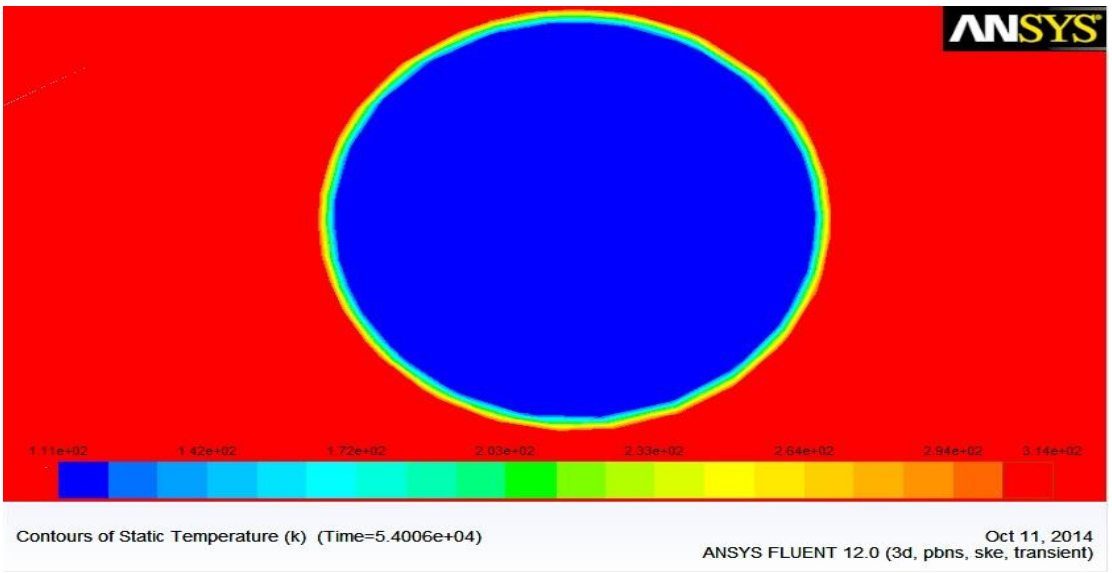

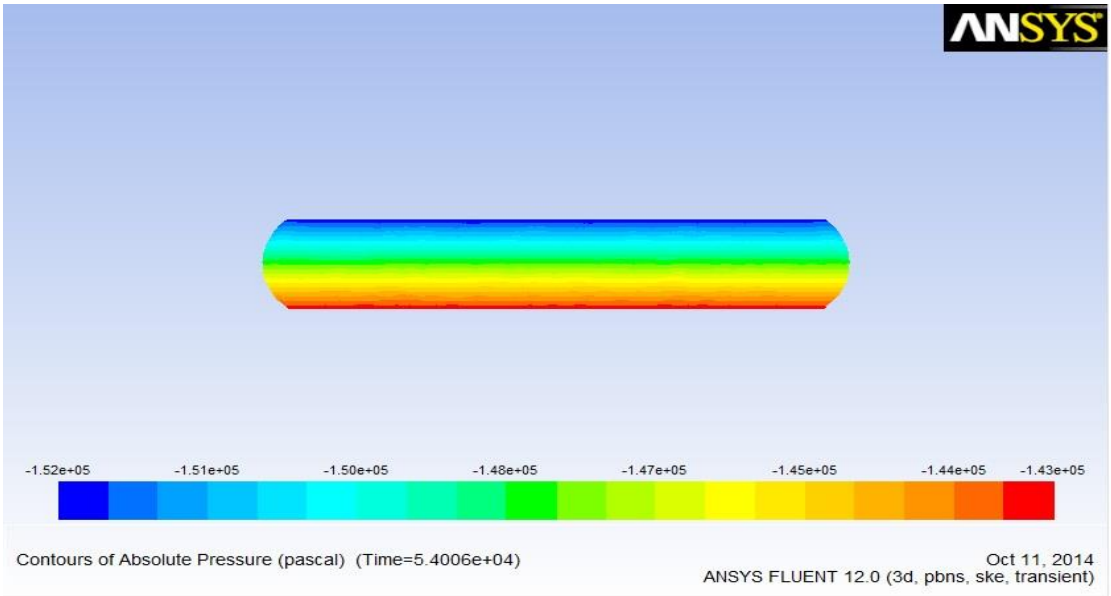
ANSYS
-1.52e+05
-1.51e+05
-1.50e+05
-1.48e+05
-1.47e+05
-1.45e+05
-1.44e+05
-1.43e+05
Contours of Absolute Pressure (pascal) (Time=5.4006e+04)
Oct 11, 2014
ANSYS FLUENT 12.0 (3d, pbns, ske, transient)

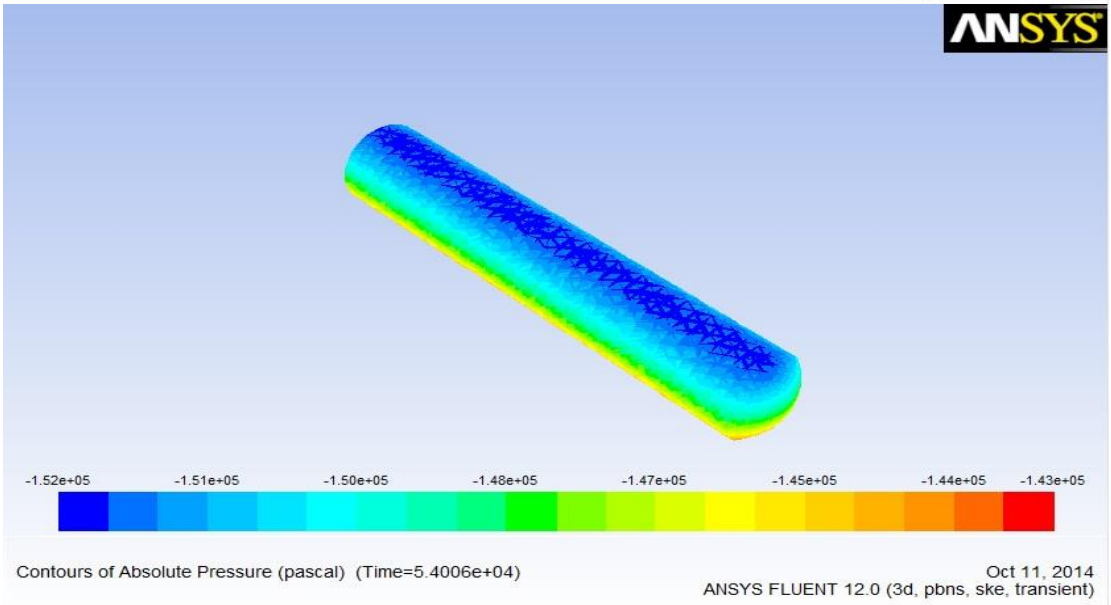
ANSYS
-1.52e+05
-1.51e+05
-1.50e+05
-1.48e+05
-1.47e+05
-1.45e+05
-1.44e+05
-1.43e+05
Contours of Absolute Pressure (pascal) (Time=5.4006e+04)
Oct 11, 2014
ANSYS FLUENT 12.0 (3d, pbns, ske, transient)

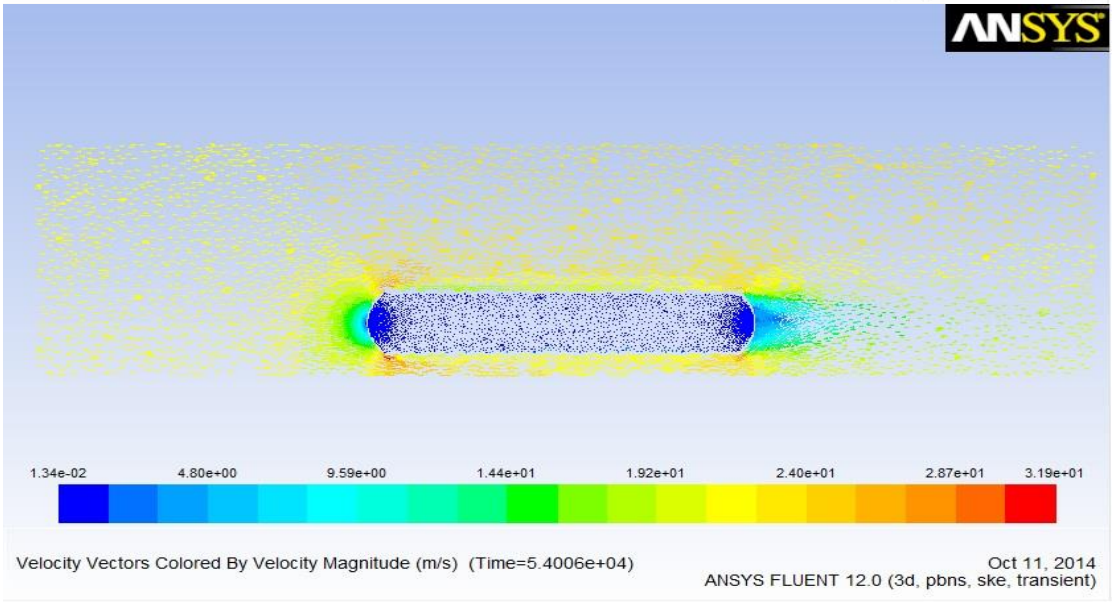
ANSYS
1.34e-02
4.80e+00
9.59e+00
1.44e+01
1.92e+01
2.40e+01
2.87e+01
3.19e+01
Velocity Vectors Colored By Velocity Magnitude (m/s) (Time=5.4006e+04)
Oct 11, 2014
ANSYS FLUENT 12.0 (3d, pbns, ske, transient)

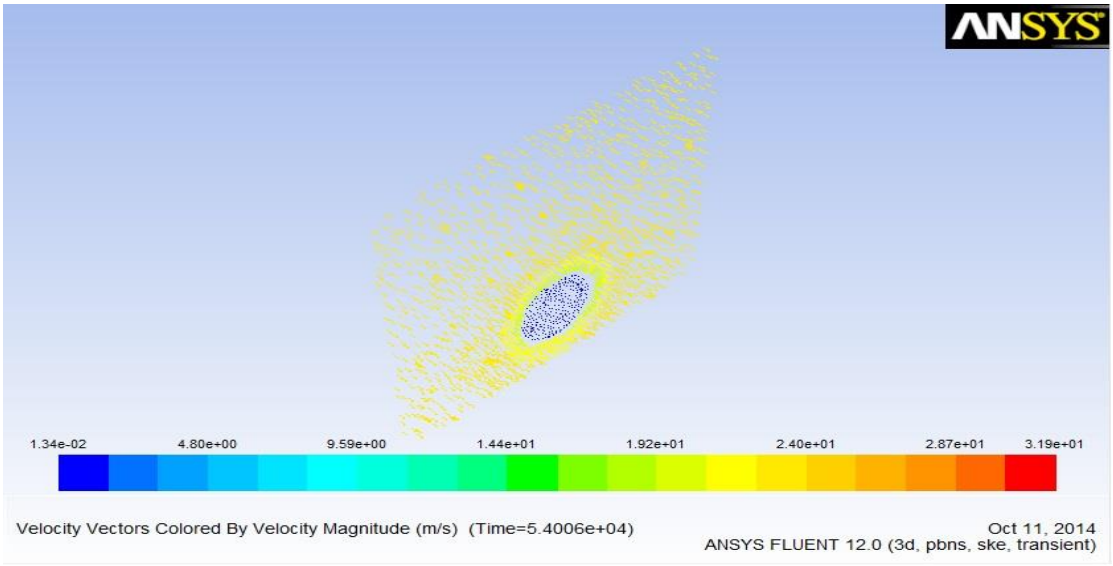

4.24 Temperature, pressure contours and velocity vectors at the end of time

4.5.2 LNG boil-off calculation

The wall heat fluxes are divided again into two regions in order to estimate the polynomial equations that describe these relations more accurately. One region includes observations until 18.000 seconds and the other one the rest. As a consequence, the two estimated equations are the following:

$t \leq 18.000s$, $y = 3{,}97e^{-23} \cdot x^6 - 2{,}63e^{-18} \cdot x^5 + 6{,}74e^{-14} \cdot x^4 - 8{,}21e^{-10} \cdot x^3 + 4{,}46e^{-6} \cdot x^2$
$-0{,}004881 \cdot x + 1{,}292144$

$t > 18.000s$, $y = 5{,}20e^{-17} \cdot x^4 - 8{,}08e^{-12} \cdot x^3 + 4{,}32e^{-7} \cdot x^2 - 0{,}008997 \cdot x + 90{,}35014$

However, simulation includes results until 7.200 seconds (2 hours) due to convergence issues and low calculation speed (time step=0.5s). As a result, only the first equation is practically used. Calculated and estimated heat fluxes are presented for both regions below. Hence, the interpreted UDF should include this data.

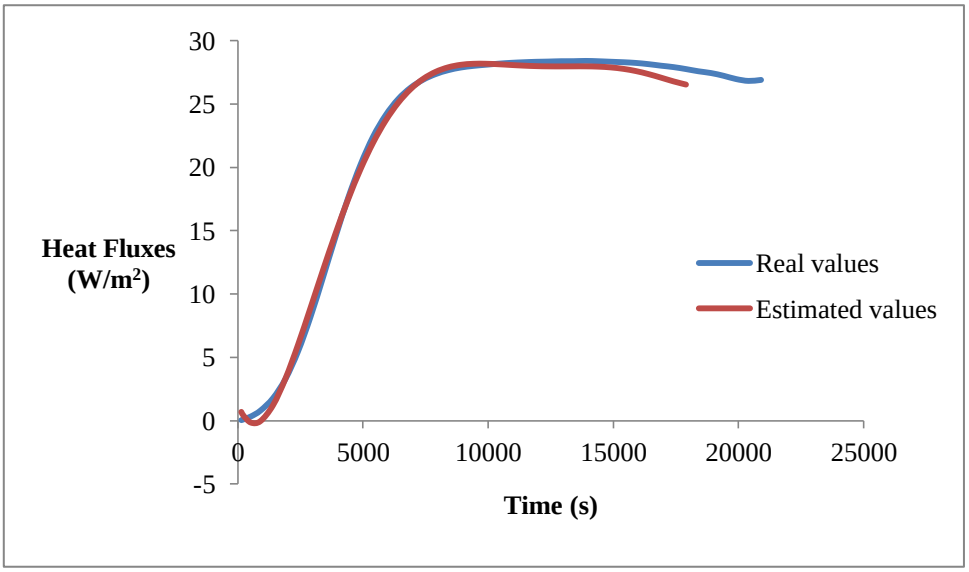

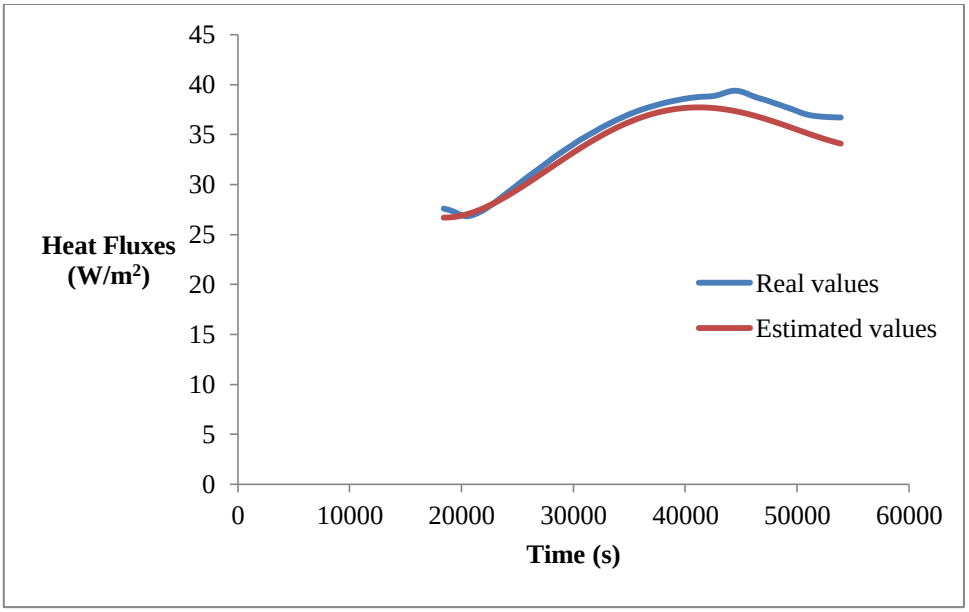

4.25 Real and estimated heat fluxes

The same model specifications with the two dimensional case are used. However, mixture model is substituted with VOF model for multiphase flows due to convergence problems. The assumption that LNG evaporates to methane is done again. The area-weighted average volume fraction of methane inside the tank is displayed below. Moreover, the part of the UDF with the new heat fluxes equations is presented below. In addition, temperature, pressure and volume fraction contours and velocity vectors at the end of time are presented in the next figures.

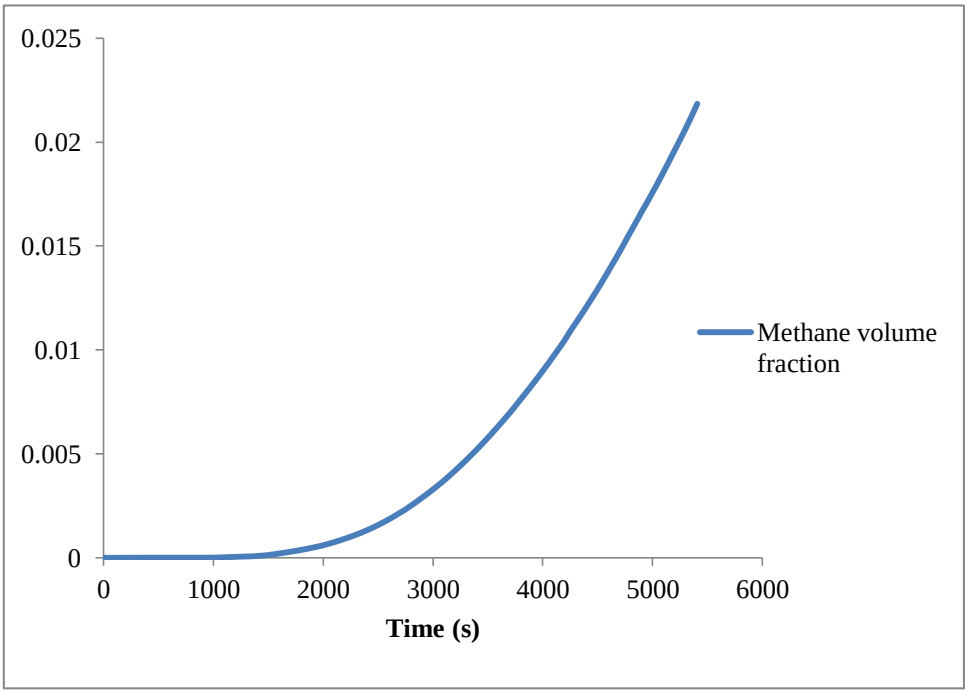

4.26 Methane volume fraction

```
DEFINE_PROFILE(heat_flux,t,i)
{
real y;
face_t f;
begin_f_loop(f,t)
{
y = CURRENT_TIME;
if (y<=18000){
F_PROFILE(f,t,i) =3.97e-23*pow(y,6)-2.63e-18*pow(y,5)+ 6.74e-14*pow(y,4)-
8.21e-10*pow(y,3)+4.46e-06*pow(y,2)-0.004881*y+1.292144;
}
else {
F_PROFILE(f,t,i) = 5.20e-17*pow(y,4)-8.08e-12*pow(y,3)+4.32e-07*pow(y,2)-
0.008997*y+90.35014;
}}
end_f_loop(f,t)
}
```

4.27 Heat fluxes UDF [26]

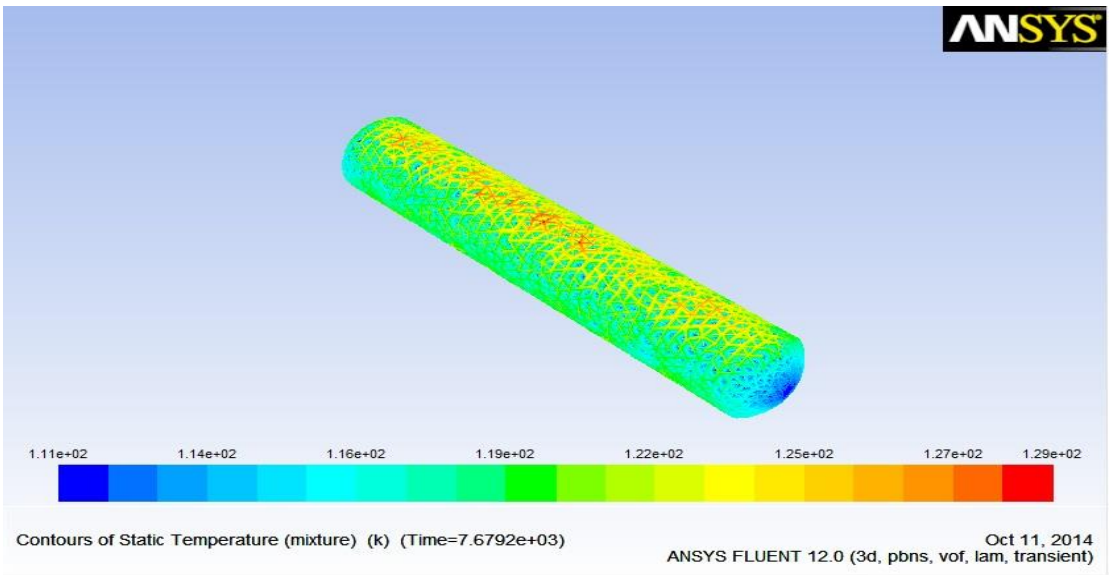

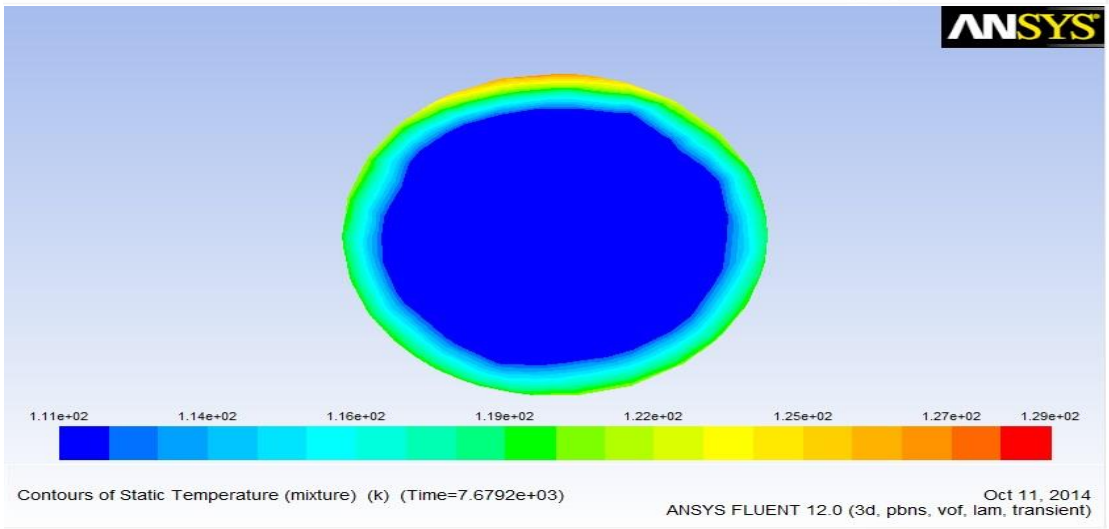

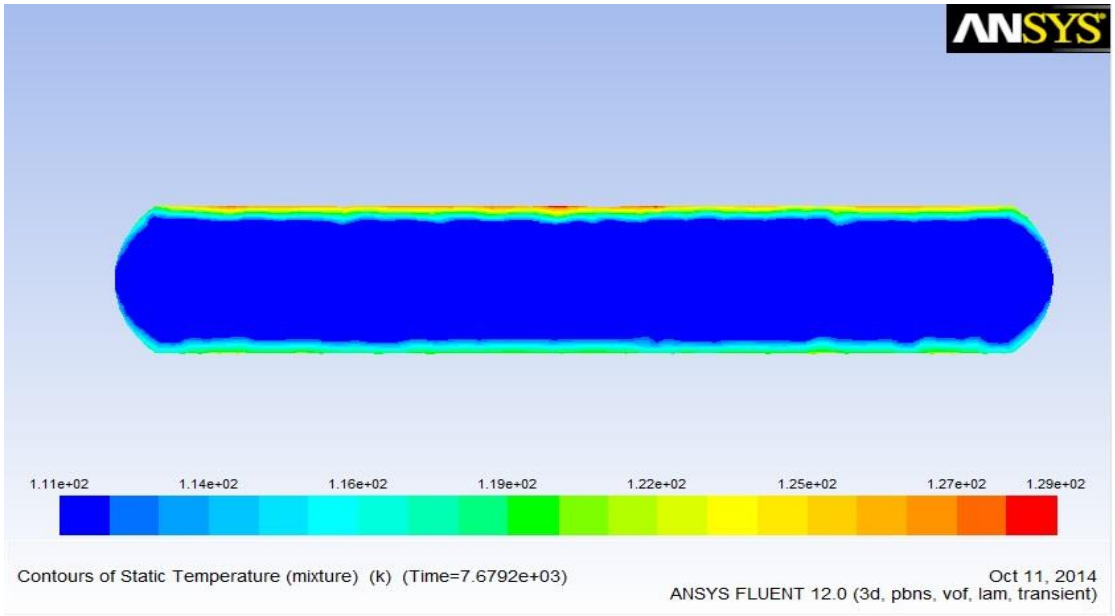
ANSYS
1.11e+02
1.14e+02
1.16e+02
1.19e+02
1.22e+02
1.25e+02
1.27e+02
1.29e+02
Contours of Static Temperature (mixture) (k) (Time=7.6792e+03)
Oct 11, 2014
ANSYS FLUENT 12.0 (3d, pbns, vof, lam, transient)

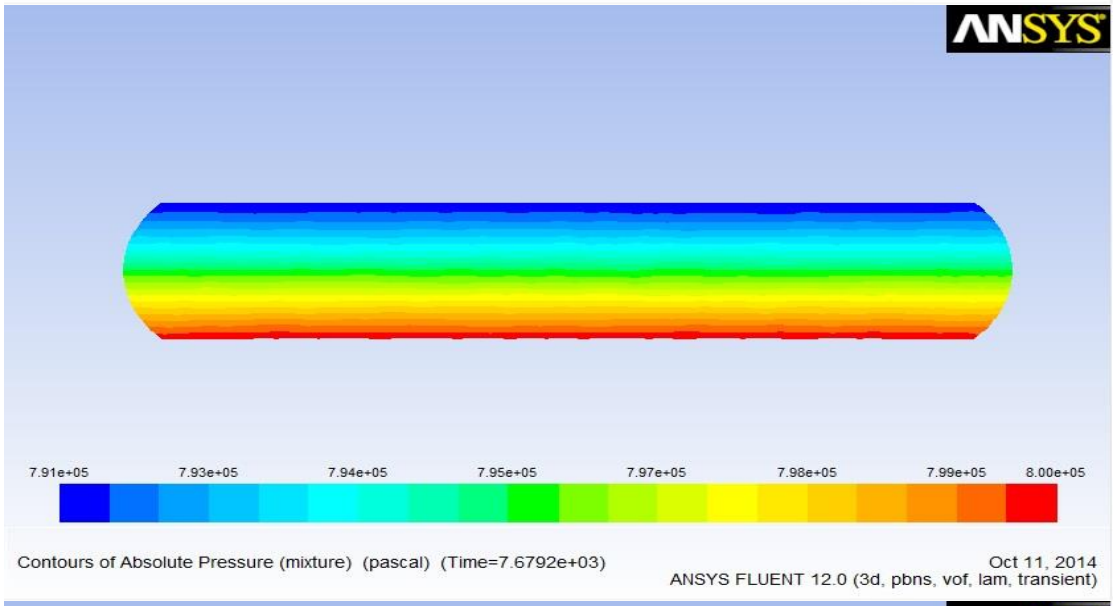
ANSYS
7.91e+05
7.93e+05
7.94e+05
7.95e+05
7.97e+05
7.98e+05
7.99e+05
8.00e+05
Contours of Absolute Pressure (mixture) (pascal) (Time=7.6792e+03)
Oct 11, 2014
ANSYS FLUENT 12.0 (3d, pbns, vof, lam, transient)

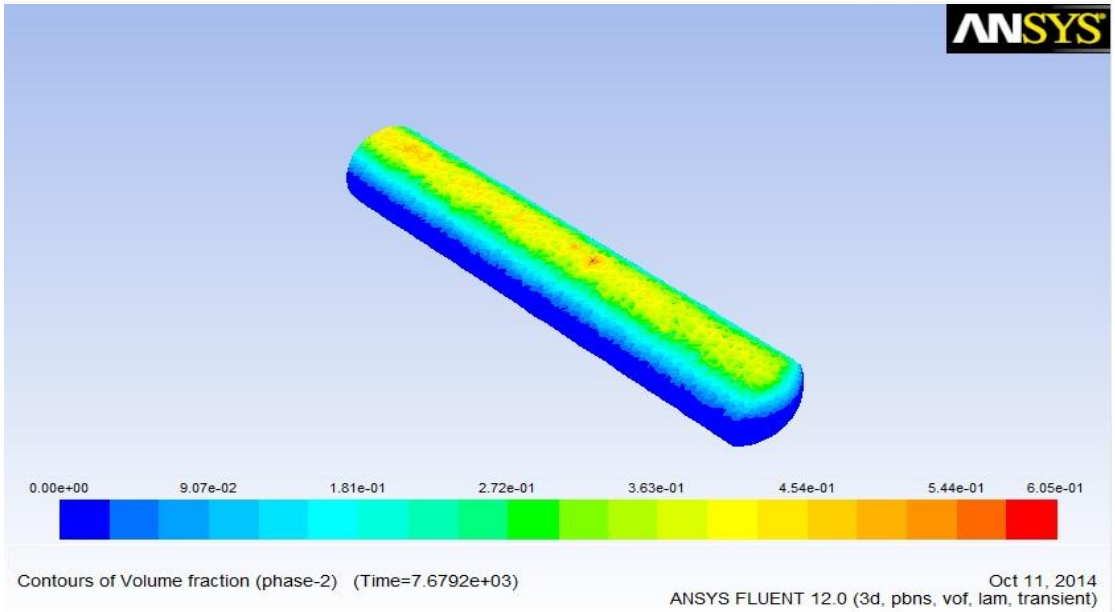
ANSYS
0.00e+00
9.07e-02
1.81e-01
2.72e-01
3.63e-01
4.54e-01
5.44e-01
6.05e-01
Contours of Volume fraction (phase-2) (Time=7.6792e+03)
Oct 11, 2014
ANSYS FLUENT 12.0 (3d, pbns, vof, lam, transient)

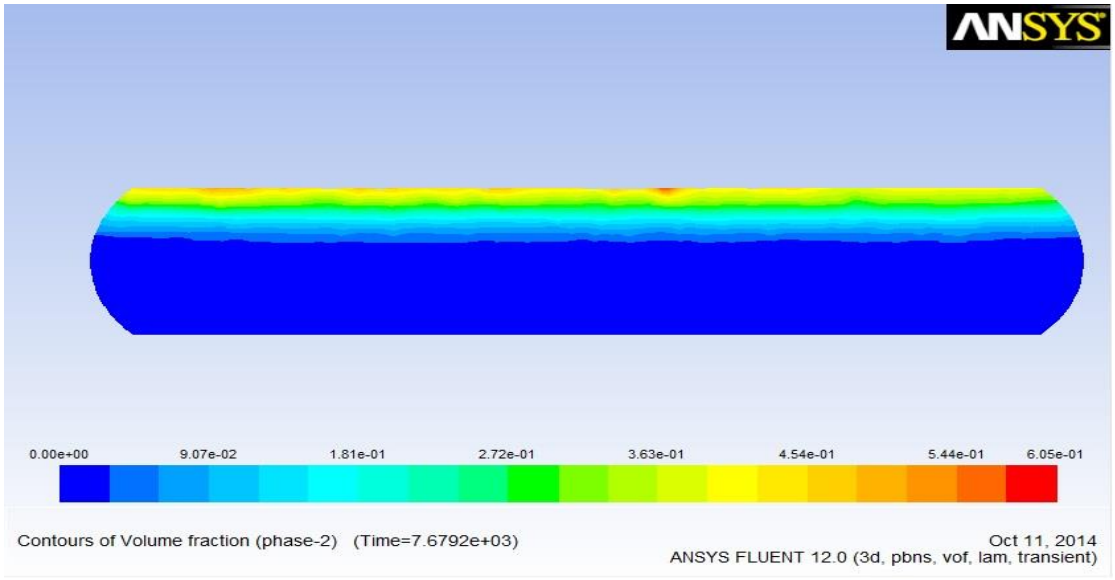

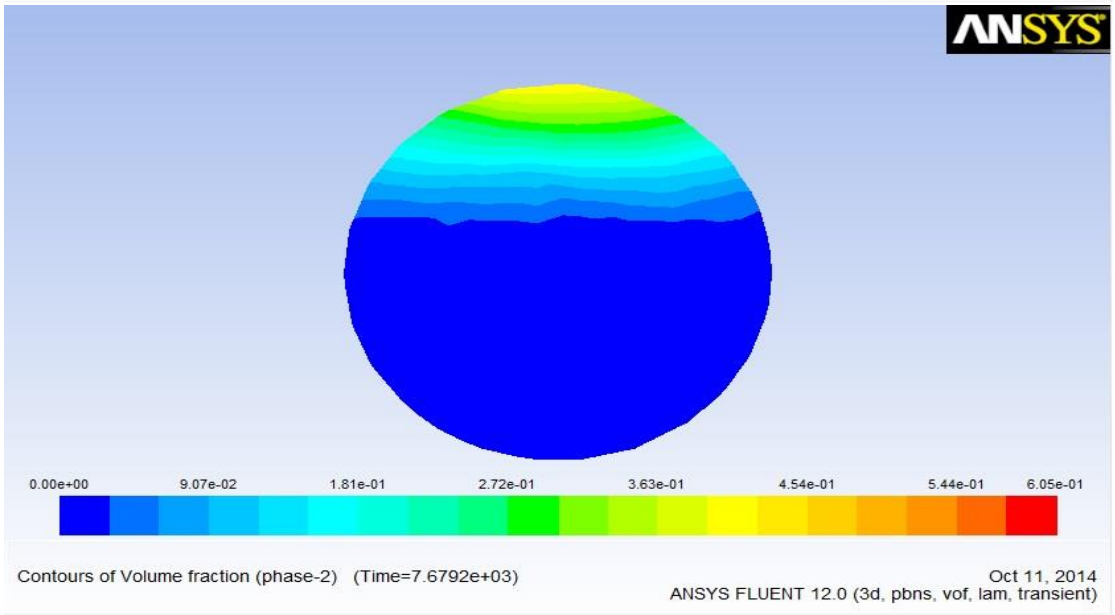

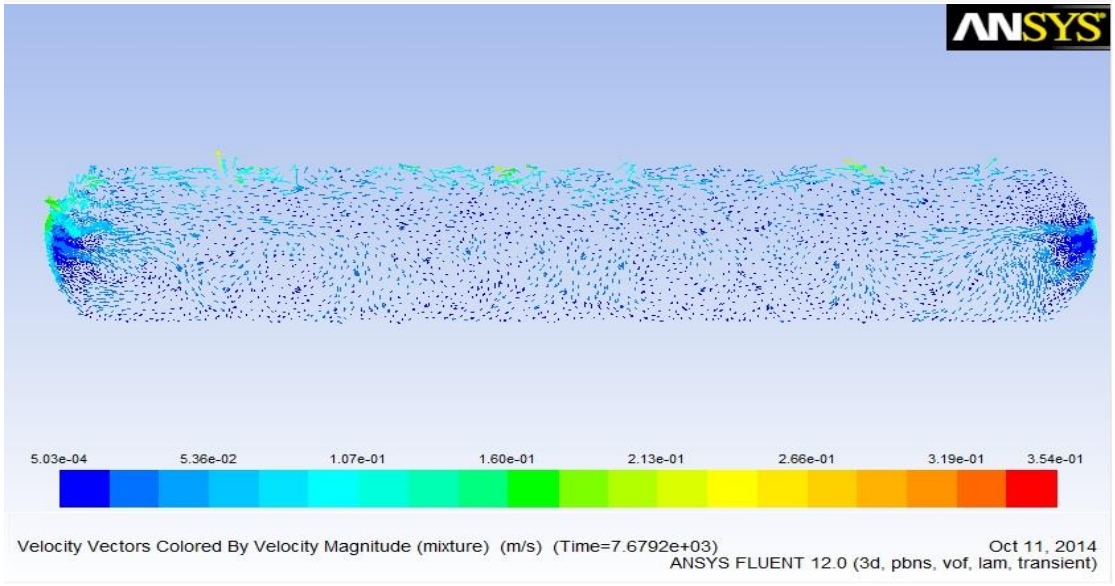

4.28 Temperature, pressure, volume fraction contours and velocity vectors

5. Conclusions

It is clear that the intention of the European policy is the establishment of alternative fuel infrastructure including facilities for Liquefied Natural Gas. For this purpose, it is proposed that publicly accessible LNG refueling stations should be placed every 400km on the Trans-European Transport Core Network. As a result, small scale LNG transport is expected to concern Europe the upcoming years.

Following the above trend, the subject of this dissertation is LNG road transport and especially LNG semi-trailer trucks. There are many firms around the world offering cryogenic trailers for LNG transport and as a consequence different trailer trucks are available. However, the transport capacity ranges from 40 to 60 thousands liters at an operating pressure of 4 to 8 bar. The mean length of the trailers is about 15m. Nevertheless, the most important trailer characteristic is the insulation material and its thermal conductivity. Evacuated perlite is the most common insulation material used with thermal conductivity up to 40 times less than 0,029 $W/m \cdot K$ depending on vacuum and temperature. This fact is extremely important considering the previous results of steel insulation, where temperature increase of the tank was many degrees higher than the initial one. Taking into consideration that just one degree of temperature increase can change the liquid phase of natural gas, we can understand the importance of using perlite as insulation material.

Other important characteristics are the insulation thickness, the air velocity and the air temperature. Different cases of tank contents and their behavior are examined for comparison reasons. It is shown that double insulation results in much lower temperature increases, even at 70K lower in methane case. However, this result of insulation thickness is dependent on the tank content. Indeed, high viscosity fluids are less influenced and as a result liquids are less affected than gases. In addition, the higher the air velocity at the inlet, the higher the temperature increases. Finally, high air temperature at the inlet accelerates temperature growth.

On other hand, the most important result refers to the fraction of liquid transformed to gas. It is calculated that the volume fraction of evaporated LNG is 0,022 after 5.400s (1,5h) for the three dimensional case and 0.012 after 54.000s (15h) for the two dimensional case. This deflection is normal if we think that the second case is just a part of the first one. The importance of this result could be emerged if the released natural gas is priced. For this reason, we assume that the whole evaporated LNG is lost to the environment and that there is no re-liquefaction system to the truck. The EEX spot price for TTF natural gas at 22/11/2014 is 23,5 €/MWh. The truck capacity is 53.000ltrs and the evaporated LNG is 1.166ltrs, which corresponds to 699.600lts of natural gas. The energy content of one liter of natural gas is approximately 10^{-5} MWh. As a consequence, there is a loss of 157€ after a trip of one hour and a half. Finally, it is worth mentioning that the two dimensional case does not support the solar tractor, in contrast to the three dimensional one. However, the last one presents lower convergence speed due to more complex structure.

Bibliography

[1] http://ec.europa.eu/transport/infrastructure/tentec/tentec-portal/site/maps_upload/09_01_2014SchematicA0_EUcorridor_map_outlined.pdf

[2] http://eur-lex.europa.eu/legal-content/EN/TXT/PDF/?uri=CELEX:52013PC0018&from=EN

[3] S. Mokhatab, J. Y. Mak, J. V Valappil, and D. A. Wood, *Handbook of Liquefied Natural Gas*, Elsevier,2014.

[4] M. S. Zakaria, K. Osman, M. N. A. Saadun, M. Z. A. Manaf, and M. H. Mohd Hanafi, "Computational Simulation of Boil-Off Gas Formation inside Liquefied Natural Gas Tank Using Evaporation Model in ANSYS Fluent," *Appl. Mech. Mater.*, vol. 393, pp. 839–844, Sep. 2013.

[5] J. P. Misra, "Design , Operation & Safety Aspects of LNG Road Transportation and LNG satellite stations LNG at Doorstep System."

[6] Đ. Dobrota, B. Lalić, and I. Komar, "Problem of Boil - off in LNG Supply Chain," *Trans. Marit. Sci.*, vol. 02, no. 02, pp. 91–100, Oct. 2013.

[7] C. Emmer, "LNG DIRECTLY TO CUSTOMER STATIONS," pp. 1–16.

[8] M. Edgar, M. Udaeta, J. Luiz, D. O. Bernal, L. Claudio, R. Galvão, J. Aquiles, and B. Grimoni, "Natural Gas Virtual-Pipeline for Alternative Energy Distribution,"*INTECH,* 2012.

[9] E. Lisowski and W. Czyzycki, "TRANSPORT AND STORAGE OF LNG IN CONTAINER TANKS," *Krakow University of Technology*, vol. 18, no. 3, 2011.

[10] http://literature.chart-ind.com/getproductfile.ashx?id=637

[11] http://www.cryolor.com/file/otherelement/pj/4d/54/f8/1f/brochure%20lng%20sr%2050000l%207bar%20uk5224647217114071242.pdf

[12] http://www.dragonproductsltd.com/wp-content/uploads/2014/07/LNGTRANSPORT.pdf

[13] http://ohsuk.com/wp-content/uploads/2014/01/58KL-LNG-TRAILER-GOFA-OHS.pdf

[14] http://www.ohsuk.com/wp-content/uploads/2014/01/53kl-Australian-tanker.pdf

[15] A. Bahadori, “Thermal Insulation Handbook for the oil, gas and petrochemical Industries”, *Elsevier*, 2014.

[16] http://www.europerl.at/fileadmin/downloads/Europerl /Allgemein/Andere_Sprachen/English_2009/Super_insulating_perlite_for_evacuated_cryogenic_servicepdf.pdf

[17] A. Hofmann, “The thermal conductivity of cryogenic insulation materials and its temperature dependence,” *Cryogenics (Guildf).*, vol. 46, no. 11, pp. 815–824, Nov. 2006.

[18] Rafał Sedlaczek, “ BOIL-OFF IN LARGE- AND SMALL-SCALE LNG CHAINS” *Faculty of Engineering Science and Technology Department of Petroleum Engineering and Applied Geophysics*, no.May, 2008.

[19] S. Roh, G. Son, G. Song, and J. Bae, “Numerical study of transient natural convection in a pressurized LNG storage tank,” *Appl. Therm. Eng.*, vol. 52, no. 1, pp. 209–220, Apr. 2013.

[20] Q.-S. Chen, J. Wegrzyn, and V. Prasad, “Analysis of temperature and pressure changes in liquefied natural gas (LNG) cryogenic tanks,” *Cryogenics (Guildf).*, vol. 44, no. 10, pp. 701–709, Oct. 2004.

[21] M. S. Zakaria, K. Osman, and M. N. Musa, “Boil-Off Gas Formation inside Large Scale Liquefied Natural Gas (LNG) Tank Based on Specific Parameters,” *Appl. Mech. Mater.*, vol. 229–231, pp. 690–694, Nov. 2012.

[22] E. Adom, S. Z. Islam, and X. Ji, “Modelling of Boil-Off Gas in LNG Tanks : A Case Study,” vol. 2, no. 4, pp. 292–296, 2010.

[23] E. Querol, B. Gonzalez-Regueral, J. García-Torrent, and M. J. García-Martínez, “Boil off gas (BOG) management in Spanish liquid natural gas (LNG) terminals,” *Appl. Energy*, vol. 87, no. 11, pp. 3384–3392, Nov. 2010.

[24] http://orange.engr.ucdavis.edu/Documentation12.0/120/FLUENT/flth.pdf

[25] P. M. Angelopoulos, D. I. Gerogiorgis, and I. Paspaliaris, “MODELING EXPANDED PERLITE PRODUCTION IN A VERTICAL ELECTRICAL FURNACE.” *School of Mining and Metallurgical Engineering, National Technical University of Athens.*

[26] http://orange.engr.ucdavis.edu/Documentation12.1/121/FLUENT/fludf.pdf